Technical Memorandum WHOI-01-98

Woods Hole Oceanographic Institution

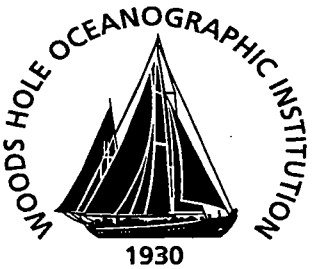

Late Cenozoic Geology of the Central Persian (Arabian) Gulf from Industry Well Data and Seismic Profiles

by

Stephen A. Swift, Elazar Uchupi and David A. Ross

April, 1998

Technical Memorandum

Department of Geology and Geophysics, Woods Hole Oceanographic Institution, Woods Hole, MA

TABLE OF CONTENTS

Late Cenozoic Geology of the Central Persian (Arabian) Gulf from Industry Well Data and Seismic Profiles

Stephen A. Swift, Elazar Uchupi and David A. Ross
Woods Hole Oceanographic Institution

ABSTRACT

Industry seismic reflection profiles shot in the 60's and early 70's in the central Persian (Arabian) Gulf are used to map two late Tertiary unconformities, and velocity data from a centrally located well is used to convert travel time to depth to the unconformities. The deeper horizon correlates with a regional unconformity at the end of the Eocene in most wells and dips monotonically to the northeast, whereas the shallower horizon is flatter and correlates with the mid-upper Miocene section in one well. Isopach maps based on wells indicate that sedimentation was relatively uniform across the region until the middle to late Miocene. Sediments deposited since the late Miocene thicken from 100-200 m on the Arabian side of the Gulf to >1000 m near Iran reflecting deposition of sediments eroded from the rapidly uplifting Zagros fold-belt. As a result of the rapid deposition, the velocity gradient in the upper 1 km decreases from ~4 km/sec per km near Arabia to about 2 km/sec per km on the Iranian side of the Gulf.

INTRODUCTION

The Persian (Arabian) Gulf (the Gulf, hereafter) is an epicontinental sea connected to the Indian Ocean through the Straits of Hormuz (Fig. 1). The basin covers an area of 226,000 km^2 and is elongate to the northwest being about 800 km long and 185 to 115 km wide. Water depths are less than 20 m near Arabia on the southwest side and deepen to 70-100 m in a shallow trough along Iran on the northeast side. Surface sediments range from carbonate sands off Arabia to detrital marly silts off Iran (Hartmann et al., 1971; Uchupi et al., 1996).

The Gulf lies on the Arabian plate and is underlain entirely by continental crust of pre-Cambrian age (Ross et al., 1986). The Mesozoic and Cenozoic strata indicate that until a few million years ago the region was the site of shallow sea carbonate and marl deposition, a sedimentary regime interrupted episodically by erosional events associated with eustatic sealevel changes and tectonics of the surrounding plate edges (Murris, 1980; Koop and Stoneley, 1982). In Late Cretaceous subduction along the northeast edge of the Arabian plate, the region of the present Zagros suture zone, led to an orogeny that produced nappes, formation of foredeeps filled with coarse flysch sediments, emplacement of ophiolites, and a change to a more varied sedimentary environment throughout the region. Shallow water sedimentation continued until late Miocene when two microplates and the Arabian plate collided with Eurasia along the Zagros suture zone raising mountains 2-3 km high (Falcon, 1961; Berberian and King, 1981; Beydoun, 1991). In late Miocene and Pliocene, this mountain building was followed by shedding of large quantities of silt, sands and coarser debris to the southwest (the Agha Jari and Bakhtyari formations in Fig. 2; James and Wynd, 1965). In late Pliocene the Phanerozoic stratigraphic section in southwest Iran responded to uplift of the suture zone by sliding on mobile evaporite and shale layers producing the elongate 'whale-back' folds of the Zagros Mountains (Ross et al., 1986). This deformation propagated progressively from the suture towards the southwest and continues to the present time. The present Persian Gulf region is a flooded asymmetric basin formed by the depression of crust under southwest Iran due to the shifting load of the Zagros mobile fold belt and to warping of the Arabian plate in response to spreading in the Red Sea.

STATEMENT OF PROBLEM

The post-middle Miocene clastic formations in the Persian (Arabian) Gulf are thicker than any of the deeper formations (James and Wynd, 1965; Koop and Stoneley, 1982). Despite its pronounced affect on the geography and stratigraphy in the Gulf region, this section is poorly studied. For example, in a regional investigation of Gulf well stratigraphy, Mina et al. (1967) display only pre-Oligocene sections. Also, the Neogene section is too young to be a target of reservoir exploration, and most industry wells wash through the upper portions as part of the spudding process. Dating of the youngest Bakhtyari Formation is difficult because the sediments are coarse-grained, non-marine, and lack adequate fossils for fine-scale stratigraphic subdivision. In addition, the only publicly-available seismic reflection profiles imaging this clastic wedge were obtained on the southwest flank of the Neogene syncline in the Gulf with a short, six-channel array from the *R/V Atlantis II* in 1977 (Ross et al., 1986). These data show the depression of the Mesozoic and early Cenozoic strata by the Neogene wedge of sediments, but details of the internal structure of the wedge are obscured by multiples incompletely removed by stacking. Moreover, the 1977 survey was a reconnaissance level investigation, and the lines were widely spaced. Thus, despite the impact that the post-middle Miocene interval has had on the Gulf region, there is little publicly available seismic stratigraphic data for the region.

Koop and Stoneley (1982) prepared isopach and paleoenvironment maps for Iran and the Gulf from industry well data. These maps reveal that despite the thick sequence of debris eroded from the Zagros that accumulated proximal to the suture zone (as much as 5 km), little of the wedge reached the Arabian (southwest) side of the Gulf (see also Dunnington et al., 1959; James and Wynd, 1965; Powers, 1968). In Iran northeast of the Gulf (Fig. 2), the base of the wedge is a conformable transition from the Mishan Formation (mid-late Miocene marly shale with limestone interbeds) to the Agha Jari (late Miocene-Pliocene calcareous sandstone, marl, and siltstone). The Mishan contains fossils that are clearly shallow marine and represents the last major marine transgression in Iran. The paleoenvironment of the Agha Jari grades southeastward from lacustrine and estuarine deposits north of Karg Island (Fig. 1) to shallow marine shelf deposits north of the Straits of Hormuz. Sections of the Agha Jari are folded and eroded in Iran indicating that it pre-dates formation of the Zagros fold belt. In Iran, the age of Agha Jari formation decreases from northeast to southwest and from northwest to southeast. The Agha Jari formation is conformable with the underlying Mishan shale, and an angular unconformity separates the Agha Jari from the overlying Bakhtyari formation, a coarse conglomerate-sandstone deposited during folding of the Zagros in the latest Pliocene-Quaternary (James and Wynd, 1965). On the south side of the present basin, in the United Arab Emirates and Qatar, most of the post-Middle Miocene interval is a hiatus (Fig. 2). To the west in Saudi Arabia and to the northwest in Kuwait and southern Iraq, the thin sequences of sediments remaining are largely non-marine or evaporitic in origin throughout most of the Neogene and have a source to the west. Thus, clastic deposition from uplift of the Zagros towards the southwest evidently terminated against a stable-to-emergent block in the center of the present Gulf basin.

The nature of the Neogene wedge and its developmental history are the objectives of this study. There are two scenarios for the formation of these sediments. If the wedge correlates with the Agha Jari (late Miocene-Pliocene) in Iran, then the sediments beneath the Gulf seafloor were transported from the northeast, represent a coastal plain environment transitional between fluvial/lacustrine deposits near Karg Island southeastward to coastal marine, and pre-date the formation of coastal folding. Subsequent sedimentation was largely trapped in the valleys between the folds in land and less than ~0.1 km of late Pliocene-Pleistocene sediments are present. Alternatively, the upper 0.2-1.0 km beneath the Gulf was a late-stage distal deposit of the Plio-Pleistocene Bakhtyari and represents a southwestward shift of the depositional locus as more and more of Iran was affected by Zagros folding.

DATA

We investigated the Neogene wedge of sediments in the Persian Gulf with a grid of industry multi-channel seismic lines and wells. The seismic data comprise about 5,000 km of multi-fold cdp profiles shot in the central Gulf favoring the Iranian side by service companies (Fig. 3). Examples of the seismic data (Fig. 4) reveal signal at 50-60 Hz in the traces but very little energy above this frequency. Most of the profiles have a vertical scale of 2.5"/sec but some have a scale of ~3.9 "/sec. The horizontal scale varies from ~140 m/cdp to ~600 m/cdp. Line spacing ranges from 3-10 km and is dense enough for mapping regional structures larger than salt domes and swells, however, there are few cross lines. To reduce this problem, we also interpreted multi-channel profiles collected on *R/V Atlantis II* cruise 93 leg 18 in 1977 (Figure 3). Unconformities in the upper 0.5 sec two-way time (500 m @ 2 km/s) of the industry data are clear in profiles from the south-eastern portion of the data set (eg., Fig. 4a), but the quality of most of the profiles that cover wide-areas of the central Gulf is too poor to recognize Neogene unconformities (eg., Fig. 4d).

The industry data includes interval velocities computed from check-shot surveys for 26 wells and from calibrated sonic log results for 22 wells. Figure 6 shows the locations of the wells and Table 1 lists the data available. Figure 4 shows velocity logs for wells for which seismic profiles are available, and Figure 5 shows velocity logs for the remaining three wells. To determine if there were any differences from SW to NE across the Gulf, the wells were placed in three groups: southwest (Y1, R2, R3, R5, R6, R7a, R32, N1), central (A1, A2, Rak3, Rak6, Rak8, Rak10, B1, NE1, Rak2), and northeast (E1, D1, D2, O1, O3, O4b, OE1b, T2, V1). For each group, interval velocities from sonic logs were averaged in 120 m bins that overlapped by 30 m. Three wells (O1, O3, O4b) located on a broad, shallow salt dome in the northeast group were averaged separately. Figure 7 shows interval velocities from sonic logs plotted by group, and Figure 8 shows interval velocities from check-shot surveys. The well data also include logs of "average velocity" computed directly from check-shot travel times or integrated from calibrated sonic logs. The "average velocity" at a particular well depth integrates the effects of velocity layers above that depth and is used directly to convert vertical travel time to depth. Figures 9 and 10 show "average velocities" for sonic logs and check-shot surveys, respectively.

We obtained depths to the tops of formations or geologic time units for at least part of twelve wells (Tables 2 and 3) and are able to show how interval velocity varies with geologic unit (Figure 7). Formation depths also are available from Mina et al. (1967) for ten wells in the central Persian Gulf and for nine additional wells elsewhere in the Gulf (Table 4). Additional geological datums were obtained for 12 wells in Iraq and Kuwait from Al-Naqib (1967) (Table 5). Locations of all wells from which geologic data are available are shown in Figure 11.

METHODS

Unconformities were traced in the shallow portion of the seismic profiles, and travel times for each horizon were digitized every 10-20 shotpoints and converted to depth with a single velocity-depth function. The "average velocities" from the calibrated sonic log at well V-1 were used because they match the average for all wells reasonably well (Figure 12). To the northeast, average velocities are lower than average by 10-20% (300-500 m/sec) at 450-900 mbsf (Fig. 7), so the computed depths in the northeast are probably too deep by 5-15%. In the central to southwest side of the Gulf, average velocities are somewhat higher than the average by 5-10% at 800-1200 mbsf, so the computed depths in these regions are somewhat shallow. The computed depths were gridded into 5 minute latitude/longitude blocks and contoured using a tension of 0.2 (Smith and Wessel, 1990).

The well data can be used independently of seismics to determine the distribution of geologic horizons on a basin-wide scale. However, the wells are unevenly distributed and depths are susceptible to errors due to problems with determining lithology and paleontology datums from cuttings. Some wells are located on salt or tectonic anomalies (Table 1), so depths and thicknesses obtained should be considered minimum for the region. Additional uncertainty arises from significant lateral variations in lithology across the basin during the Cenozoic and the time transgressive nature of several formations (Figure 2; Kashfi, 1980; Koop and Stoneley, 1982). Compared to the errors in the seismic data, however, the well data provide a much more reliable picture of thickness and depth variations.

RESULTS

Stratigraphy

The stacks for much of the older (1960's-early 1970's) seismic data have poor resolution at shallow depths. As a result, several seismic unconformities could be correlated locally within portions of the seismic data set, but few of the Neogene unconformities could be carried throughout the data set. The deepest of these horizons, R3, is often marked by a relatively high-amplitude reflection (Fig. 4). It deepens northeastward reaching about 1.6 km below sealevel along the Iranian coast (Fig. 13). There is little variation in the NW-SE trend of R3 along the axis of the Gulf. A shallower unconformity, R4, could be traced over a somewhat smaller region (Fig. 14). In general, this horizon deepens to the northeast but there are several local variations in this trend. R4 shallows over Laven Island near 53°15'E and 26°48'N and above a large salt dome structure ("O" in the industry literature) near 53°20'E and 26°22'N. The horizon also deepens in a NW-SE trough near 51°E and 28°N.

Depth-to-formation data from wells provides a means to date the seismic unconformities. Unfortunately, there are no seismic profiles near two of the wells for which we have geologic data (D-1, E-1), and all but one of the other 10 wells with geologic data are clustered on a tectonic structure in the southeast or on the "O" salt dome. Near wells with geologic data, correlations between the depth to seismic horizons R3 and R4 in our structure maps (Figs. 13 and 14) and well data are often inconsistent. This disagreement is mostly due to smoothing inherent in the computer contouring and to tectonic and salt structures beneath wells that are too small to appear in the seismic structure maps. The correlations between seismic profiles and stratigraphy at individual wells provides a more reliable approach to determining the age of the horizons. Horizon R3 correlates with the unconformity at the top-of the Dammam/Jahrum formations (Eocene/Oligocene boundary) at wells O-1, R-3, R-5, and T-2 (Figs 4g, i, j, k). However, horizon R3 appears younger (Miocene) at wells D-2 and NE-1 (Figs. 4d), and older (Eocene) at wells R-2, R-7A, R-6 (Figs. 4i, k, l). We favor the correlation to the Eocene-Oligocene boundary unconformity because we observe reflector truncations along R3 in profiles close to Iran, and there are no other significant unconformities until the Pliocene-Pleistocene boundary. There is less certainty about the age of Horizon R4. At well D-2, horizon R4 occurs within the middle to upper Miocene and may correlate with the top of the evaporitic Gach Saren Formation or the top of the Asmari/Ghar formations dated to the lower Miocene (Figure 2). Clearly the horizon is Miocene in age, but the data do not allow more specific correlation. The interval between R3 and R4 thins towards the southwest, so R4 can not be reliably distinguished from R3 in wells NE-1, R-3, and R-6.

The well geology indicates a major change in sedimentation during the Miocene. In the Paleocene-Eocene, shallow marine carbonates and anhydrite were deposited relatively uniformly (roughly 300-800 m thickness, Fig. 15). The overlying lower-middle Miocene unit (Asmari-Ghar) is difficult to define due to time transgressive nature of the formation boundaries, strong lateral facies changes, and poor paleontological control in salt units. The thickness of this unit, however, also appears relatively uniform being somewhat greater in Kuwait where a southwest source fed the Ghar-Ahwaz delta (Fig. 16). The absence of the unit in some wells in the southeast at ~53°E is due to the poor quality of our well stratigraphic data. In contrast to the older formations with their uniform thickness, the post-middle Miocene unit (Fig. 17) clearly thickens from southwest to northeast. The high thickness variability displayed by this unit along the coast of Iran (3492 vs. 215 m) reflects sedimentation controlled by tectonics in the Zagros fold belt. The thick emplacement of the Neogene sediments to the northeast depressed the earlier formations causing all structure maps of the pre-late Miocene units to dip towards Iran (Fig. 18).

Velocity Structure

The compressional velocity structure of the sedimentary section in the central Gulf is controlled by lithology and age (Figure 7). The positive velocity gradient in the upper 1-1.5 km is ubiquitous and is likely due to dewatering, compaction, and carbonate alteration processes affecting all sediment types across the Gulf. Velocity increases from 1600-1900 m/sec at the seafloor to a peak in the Paleocene below which velocity decreases with depth in the Upper and middle Cretaceous. Velocity increases with depth again from an unconformity at the base of middle Cretaceous (top of the Shuaiba Formation, Fig. 2) through the Lower Cretaceous and Jurassic with local minimums in the middle of the Upper and Lower Jurassic. Velocities and velocity gradients in the Mesozoic section are very similar from region to region reflecting uniform sedimentation of predominantly shallow water platform carbonates with vertically varying proportions of evaporite and continental clastic facies.

Although the overall velocity structure is consistent across the Gulf, details of the shallow velocity structure reveal distinct regional differences controlled by the northeastward thickening of the post-middle Miocene sediment wedge. Figure 19 shows the average interval velocity profiles for three regions extending from southwest near Arabia to northeast near Iran. On average, the velocity peak that correlates with the Paleocene interval (see Figs. 7a and 7c) decreases in velocity from 5200 m/sec in the southwest to only 4400 m/sec in the northeast while the depth of the peak increases from 900 m to 1300 m. This velocity decrease is probably the result of the northeastward increase in the marl content of the Paleocene/early Eocene strata (see Fig. 10 in Koop and Stoneley, 1982). The Paleocene peak is missing in the salt dome section. In the northeast and central portion of the Gulf, a velocity peak above the regional gradient occurs in a 200-300 m thick layer that appears to correlate with the Asmari Limestone (wells A-1, A-2, B-1, D-1, D-2, and T-2 in Figs. 4a, 4b, 4c, 4d, 4s, 5a, 7b and 7c). The apparent absence of the peak at E-1 (Fig. 5b) may be due to the broad vertical spacing downhole of the velocity data in this well. The interval thins towards the southwest and disappears on the Arabian side of the Gulf. In the central region, velocity values cluster near 1900-2000 m/sec from the seafloor to ~350 m and near 2700 m/sec at 350-450 m depth, but these layers do not appear to the northeast and are less apparent in the profiles to the southwest (Fig. 7). The vertical uniformity of velocity in these units is likely due to rapid deposition of sediment of similar composition and grain size. The velocity gradient from the seafloor down to the Paleocene high increases from only 2.0 km/sec per km near Iran to 3.0 km/sec per km in the central Gulf and to 3.9 km/sec per km off Arabia (Fig. 19). The gradient change is due primarily to greater thicknesses of fine-grained clastics deposited proximal to the Zagros uplift in the Miocene-Pliocene and secondarily to the lateral facies change in the early Tertiary.

DISCUSSION

Geologic data in Iran indicate that the Tethys ocean closed in the Late Cretaceous (Falcon, 1974; Berberian and King, 1981; Koop and Stoneley, 1982; Ross et al., 1986). Uplift began in central Iran at that time, but a broad epicontinental sea above the Arabian plate remained connected with the deeper ocean to the southeast until early Pliocene. Molasse sediments were deposited near the collision zone and subsequently deformed by reverse faulting and folding. Initially these deposits were located close to the suture, but deformation propagated rapidly to the southwest after the Miocene (Falcon, 1974).

During deposition of the Asmari/Ghar formations in early to middle Miocene, the present Gulf region was a shallow marine shelf with a delta building northeastward from a continental source on the Arabian plate west of Kuwait. The basin narrowed during the middle to late Miocene, and the sediments became more diverse ranging from massive salt beds (Qesham) centered at 54°E, to a sandy-silty marl (Razak) near the suture in the northeast, to anhydrite (Gachsaren) over most the remaining basin (Kashfi, 1980). The wide-spread occurrence of salt and anhydrite suggest the shallow sea was only intermittently connected to the open ocean. Data for only one of our wells, D-1, indicates the presence of the Gachsaren unit (287 m thick, Table 2). This narrow basin was briefly connected to the open ocean, and shales interbedded with shallow-water limestones (Mishan) up to 700 m thick in southeast Iran were deposited (James and Wynd, 1965). Well and seismic data indicate that the effects of the Zagros Mountain uplift reached the Gulf region at the end of the Miocene. At well D-1 near Iran in the northern end of the study area, the sediments forming the thickest portion (100-590 mbsl) of the Neogene section are silty and sandy marls with sandstone interbeds that are late Miocene-Pliocene in age (Mishan-Agha Jari). These sediments were deposited at ~52 m/Ma (488 m in 9.4 myrs [late Miocene begins at ~11.25 Ma and the Pliocene ends at ~1.85 Ma, Cande and Kent, 1992, 1995]) in a shallow marine to lagoonal environment with thin evaporite layers indicating restricted circulation. Overlying this unit are ~80 m of Quaternary fine-grained clastics with well-preserved marine microfossils deposited at 43 m/Ma (80 m in 1.85 myrs) in a shallow, open-marine environment. This unit correlates with the Bakhtyari Formation in Iran where it is comprised mostly of conglomerates and other coarse-grained clastics. Although the paleoenvironment became more open marine at the end of the Agha Jari (end of the Pliocene), the gross accumulation rates remained about the same indicating that overall sediment supply rate did not change significantly as the Zagros deformation approached the present Gulf.

The geologic section at the D-1 well indicates that the present Gulf was a shallow restricted marine shelf during the early Neogene and received distal clastic sediments from the suture zone and region tectonic uplift in Iran. Falcon (1961) dates the first uplift to the latest Miocene. Most of the Neogene wedge of sediments defined by the seismic structure maps (Figs. 13-14) and well data was deposited during the early stages of uplift when rivers could transport sediment without restriction to the southwest. The relatively uniform velocity layers observed in some central Gulf wells (eg. Figs. 4a, b, c) indicates that emplacement was episodic. These events could be associated with sudden tectonic changes in the uplift region or to climatic or eustatic sealevel changes during this time. However, our well stratigraphy is not defined well-enough to confidently correlate these events to changes elsewhere in Iran or to global stratigraphy. Subsequent deformation in the Zagros Mountain fold belt did not reduce the rate of sediment supply to the Gulf region. Southwestward propagation of the deformation front substantially thickened the Phanerozoic sediment section on the plate causing subsidence in the present Gulf leading to more open marine conditions during the Quaternary. The present Gulf environment is not characteristic of sedimentation conditions during the deposition of the thickened Neogene sequence, although fine-grained clastics are the most common facies since the middle Miocene.

CONCLUSIONS

The uplift of the Zagros collision zone in the early Pliocene and the subsequent southwestward propagation of deformation and eroded sediments has profoundly affected the nature of the geology and seismic velocity structure of the Gulf. Geologic unconformities dip northeastward from a few hundred meters depth along the Arabia half of the Gulf to over 2 km along the Iranian coast. Similarly, average seismic velocities at 1 km depth decrease from near 5 km/sec near Arabia to 3.5 km/sec per km closer to Iran. The nearly linear velocity gradient above about 1 km decreases from about 4 km/sec per km near Arabia to 2 km/sec per km near Iran. The Neogene wedge is comprised of fine-grained clastic marls and was deposited in estuarine to restricted lagoonal environments during the latest Miocene-Pliocene correlative to the Agha Jari Formation. Subsequent southwestward propagation of the Zagros fold belt deepened water depths and opened circulation to the open ocean but did not reduce the rate at which sediment was supplied to the Gulf in the Quaternary.

ACKNOWLEDGEMENTS

This research was jointly supported by the Office of Naval Research, through grants N00014-96-1-0548 and 96PR04120-00, and by the Naval Oceanographic Office. We thank Joseph Kravitz, Richard Simmons, and Ashok Kalra for their encouragement and support. Tom Bolmer digitized industry tracklines and provided additional computer support.

REFERENCES

Al Naqib, K.M., 1967, Geology of the Arabian Peninsula, southwestern Iraq, U.S. Geol. Survey Prof. Paper 560-G, 54 pp.

Berberian, M., and G.C.P. King, 1981, Towards a paleogeography and tectonic evolution of Iran. Canadian J. Earth Sci., 18, 210-265.

Beydoun, Z.R., 1991, Arabian plate hydrocarbon geology and potential - a plate tectonic approach. Amer. Assoc. Petrol. Geol. Studies in Geology No. 33, 77 pp.

Cande, S.C., and D.V. Kent, 1992, A new geomagnetic polarity time scale for the Late Cretaceous and Cenozoic. J. Geophys. Res., 97, 13,917-13,951.

Cande, S.C., and D.V. Kent, 1995, Revised calibration of the geomagnetic polarity time scale for the Late Cretaceous and Cenozoic. J. Geophys. Res., 100, 6093-6095.

Dunnington, H.V., R.C. van Bellen, R. Wetzel, and D.M. Morton, 1959, Iraq. In: Lexique Stratigraphique International, Vol. III, Asie, L. Dubertret (ed.), Fascicule 10a, Centre National de la Recherche Scientifique, Paris, 333 pp.

Falcon, N.L., 1961, Major earth-flexuring in the Zagros mountains of south-west Iran., Quat. J. Geol. Soc., 117, 367-376.

Falcon, N.L., 1974, Southern Iran: Zagros Mountains, In: A.M. Spencer (ed.), Mesozoic-Cenozoic orogenic belts, London, The Geological Society, Spec. Publ. 4, 199-211.

Hartmann, M., Lange, H., Seibold, E. and Walger, E., 1971. Oberflächensedimente in Persichen Golf and Golf von Oman. I. Geologisch-hydrologischer Rahmen und erste sedimentologische Ergebnisse. "Meteor" Forschungsergebnisse, C, no. 4: 1-76.

James, G.A., and J.G. Wynd, 1965, Stratigraphic nomenclature of Iranian Oil Consortium agreement area. Bull. Amer. Assoc. Petrol. Geol., 49, 2182-2245.

Kashfi, M.S., 1980, Sedimentology and environmental sedimentology of Lower Fars Group (Miocene), south-southwest Iran, Bull. Am. Assoc. Petrol. Geol., 64, 2095-2107.

Koop, W.J., and R. Stoneley, 1982, Subsidence history of the Middle East Zagros basin. Permian to Recent. Phil. Trans. R. Soc. Lond. A, 305, 149-168.

Mina, P., M.T. Razaghnia, and Y. Paran, 1967, Geological and geophysical studies and exploratory drilling of the Iranian continental shelf-Persian Gulf. Proc. Seventh World Petroleum Congress (Mexico), v. 2, New York, Elsevier, 871-903.

Murris, R.J., 1980, Middle East: stratigraphic evolution and oil habitat. Bull. Amer. Assoc. Petrol. Geol., 64, 597-618.

Powers, R.W., 1968, Saudi Arabia (excluding Arabian Shield). In: Lexique Stratigraphique International, Vol. III, Asie, L. Dubertret (ed.), Fascicule 10b1, Centre National de la Recherche Scientifique, Paris, 173 pp.

Ross, D.A., Uchupi, E. and White, R.S., 1986. The geology of the Persian Gulf-Gulf of Oman Region. Reviews of Geophysics, 24: 537-556.

Uchupi, E. , S.A. Swift, D.A. Ross, 1996, Gas venting and late Quaternary sedimentation in the Persian (Arabian) Gulf. Marine Geology, 129, 237-269.

Smith, W.H.F., and P. Wessel, 1990, Griidding with continous curvature splines in tension. Geophysics, 55, 293-305.

Table 1. Industry well data in central Gulf.

Well	Longitude	Latitude	Water Depth (m)	KB Height (m)	Total Depth (mbsl)	(mbkb)	Depth to Formation Tops	Structure	Velocity data
A-1	53.070556	26.193611	74	11	2678	2689	No	Flat. Deep salt swell	Sonic log, ck-shot
A-2	53.064167	26.203889	74	11	2317	2328	No	Flat. Deep salt swell	Sonic log, ck-shot
B-1	52.918333	26.155833	70	11	2306	2317	No	Flat. Deep salt swell	Sonic log, ck-shot
D-1	51.524250	27.635139	23*	17	3927	3944	Yes	Salt dome	Sonic log, ck-shot
D-2	51.504444	27.646944	23*	11	4890	4901	No	Salt dome	Sonic log, ck-shot
E-1	51.789722	27.585833	16*	21	2918	2939	Yes	Not known/no seismic data	Sonic log, ck-shot
N-1	53.354444	25.564444	42	9	2531	2540^	No	Flat	Sonic log, ck-shot
O-1	53.315833	26.388056	77*	10	2388	2398	Yes	Crest of salt dome	Sonic log, ck-shot
O-3	53.335833	26.389167	77*	11	1607	1618	No	Salt dome	Sonic log, ck-shot
O-4B	53.324403	26.405050	77*	11	3291	3303	Notes	Salt dome	Sonic log, ck-shot
OE-1B	53.463889	26.446944	86	11	3073	3085	No	Low relief salt swell	Sonic log, ck-shot
R-2	52.897778	25.797222	35	18	2198	2216	Yes	Flank of deep salt swell	Ck-shot
R-3	52.892222	25.962222	55	19	1841	1860	Yes	Flank of deep salt swell	Sonic log, ck-shot
R-5	52.863806	25.911675	55	10	2240	2250^	Yes	Flank of a deep salt swell	Sonic log, ck-shot
R-6	52.803889	26.024444	56	10	2250	2260^	Yes	Crest of low relief swell	Ck-shot
R-7A	52.911667	25.907222	25	10	2200	2210^	Yes	Crest of low relief swell	Sonic log, ck-shot
R-32	52.930833	25.924722	48	11	3470	3481	Notes	Deep salt swell	Sonic log, ck-shot
NE-1	53.158333	25.983333	64	11	2414	2425	Notes	Monocline	Sonic log, ck-shot
Rak-2	53.128747	25.962917	63	11	2830	2841	No	Flat	Sonic log, ck-shot
Rak-3	53.201111	26.011111	65	11	2794	2805	Notes	Monocline/down to south	Sonic log, ck-shot
Rak-6	53.195000	25.999722	65	11	2359	2370	No	Monocline	Ck-shot
Rak-8	53.159722	26.020833	66	11	2412	2424	No	Monocline	Sonic log, ck-shot
Rak-10	53.178611	26.009444	65	11	2321	2334	No	Monocline	Ck-shot
T-2	53.477472	26.556750	65	11	2889	2900^	Yes	Salt dome	Sonic log, ck-shot
V-1	52.951111	26.576944	86	10	2718	2728^	No	Deep swell	Sonic log, ck-shot
Y-1	50.795222	27.506278	58	10	2956	2966^	No	Deep swell	Sonic log, ck-shot

* Water depths were obtained from industry documents. Otherwise, depths were interpolated from bathymetry map in Seibold and Vollbrecht (1969).

^ Total depth of well is estimated from logs. Otherwise depths are from industry documents.

Table 2. Depth to the top of formations in central Gulf wells from geology reports.

		E-1		*D-1*	
Age	Formation	Depth (mbsl)	Thickness (m)	Depth (mbsl)	Thickness (m)
Quaternary	Bakhtiari	16	100	23	80
Pliocene	Aghi Jari	116	893		
Miocene	Mishan sh			103	488
Miocene	Gach Saran			591	298
Oligocene-Mio	Asmari ls	1009	104	878	338
Paleo-Eocene	Radhuma/Rus/ Damman	1113	378	981	501
Maestrichtian	Simsima	1491	64	1483	257
U. Cretaceous	Shargi	1555	49		
U. Cretaceous	Laffan sh			1739	30
M. Cretaceous	Mishrif ls			1770	187
	Ahmadi sh	1604	32		
	Wara ss			1957	55
	Sarvak	1636	35		
	Mauddud ls	1671	36		
	Nahr Umr sh	1708	49		
Aptian	Shu Aiba ls	1756	73	2012	186
	Gadvan	1830	76		
Neocomian	Fhiliyan	1906	149		
	Yamama			2198	161
U. Jurassic	Hith	2054	56	2359	50
	Arab	2110	202	2409	90
	Jubaila			2498	236
	Manifa	2313	190	2734	36
	Tuwaiq			2770	91
M. Jurassic	Dhruma	2503	232	2861	233
L. Jurassic	Neyriz sh	2735	142	3094	145
Triassic	Khaneh Kat	2877	41	3239	235
Permian	Khail			3474	258
	Sudair sh			3732	195
Total depth (mbsl)		2918		3927	

Table 3a. Depth to time boundaries in central Gulf wells from stratigraphic columns on well velocity survey sheets.

		Wells: *D-1*		*E-1*		*O-1*		*T-2*	
Age	Probable Formation Tops	Depth (mbsl)	Thickness (m)	Depth (mbsl)	Thickness (m)	Depth (mbsl)	Thickness (m)	Depth (mbsl)	Thickness (m)
Quaternary	Bakhtyari					77	48	65	20
Pliocene	Aghi Jari	23?	439						
Mio-Plio				16(50)	989	125	395	85	753
Miocene	Mishan sh	462	403						
Oligocene-Mio	Asmari ls	865	95	1005	100	520	102	838	130
Eocene		960	275			622	511	968	612
Paleocene		1235	315					1580	28
Paleo-Eocene	Jahrum/Pabdeh			1105	375				
U. Cretaceous		1550	452	1480	145	1133	212	1608	252
m. Cretaceous				1625	120				
L. Cretaceous		2002	58	1745	298	1345	463	1860	515
U. Jurassic		2360	804	2043	687	1808	417	2375	45
	Arab							2420	380
m. Jurassic	Dhruma	2864	236			2225	153	2800	105
L. Jurassic (Lias)	Neyriz sh	3100	140	2730	135	2378	45		
Triassic	Khaneh Kat	3240	228	2865	45				
Permian	Khail	3468	219						
	Khuff	3687	237						
*Total depth**		3924		2910		2423		2905	

*Deepest depth (mbsl) shown in stratigraphic column on velocity survey sheet.

Table 3b. Depth to time boundaries in central Gulf wells from from stratigraphic columns on well velocity survey sheets.

		Wells: *R-2*		*R-3*		*R-5*		*R-6*		*R-7A*	
Age	Probable Formation Tops	Depth (mbsl)	Thickness (m)	Depth (mbsl)	Thickness (m)	Depth (mbsl)	Thickness (m)	Depth (mbsl)	Thickness (m)	Depth (mbsl)	Thickness (m)
Quaternary	Bakhtyari	35	55	55	65	55		56		25	
Mio-Plio		90	293	120	285	(55)	(320)	(56)	(356)	(25)	(407)
Eocene	Damman	383	230	405	199	375	603	412	198	432	153
	Rus	613	47	604	56			610	55	585	45
Paleocene	Radhuma	660	348	660	325			665	335	630	356
U. Cretaceous	Simsima	1008	46	985	50	978	35	1000	45	986	52
	Shargi	1054	96	1035	57	1013	65	1045	45	1038	55
	Halul	1150	102	1092	92	1078	102	1090	80	1093	92
	Laffan	1252	24	1184	33	1180	25	1170	36	1185	25
	Mishrif	1276	64	1217	93	1205	100	1206	119	1210	90
	Khatiyah	1340	117	1310	120	1305	130	1325	110	1300?	92
L. Cretaceous	Nahr Umr	1457	71	1430	55	1435	57	1435	68	1392	58
	Shu Aiba	1528	80	1485	85	1492	93	1503	82	1450	80
	Hawar	1608	19	1570	20	1585	25	1585	15	1530	20
	Kharib	1627	123	1590	126	1610	117	1600	135	1550	118
	Yamama	1750	300	1716	99	1727	195	1735	195	1668	187
	Sulay					1922	133	1930	132	1855	132
U. Jurassic		2050	58								
	Hith	2108	66			2055	75	2062	80	1987	61
	Arab	2174	46			2130	82	2142	78	2048	82
	Darb					2212	43	2220	20	2130	75
Total depth		2220		1815		2255		2240		2205	

*Deepest depth (mbsl) shown in stratigraphic column on velocity survey sheet.

Table 3c. Depth to time boundaries in central Gulf wells from notes well velocity survey sheets.

		Wells:	*O-4*		*NE-1*		*R-32*		*Rak-3*	
Age	Probable Formation Tops	Depth (mbsl)	Thickness (m)	Depth (mbsl)	Thickness (m)	Depth (mbsl)	Thickness (m)	Depth (mbsl)	Thickness (m)
Quaternary	Bakhtyari	77	418	64	(1032)	48		65	
Oligocene-Mio	Asmari ls	495	182						
Eocene				1096	94				
Paleo-Eocene	Jahrum/Pabdeh	677	393						
U. Cretaceous	Aruma	1070	122	1190	154				
	Ilam	1192	107						
m. Cretaceous	Mishrif	1299	103	1349	111	1235		1388	
	Kyatiyah			1460	116				
	Nahr Umr			1576	58				
L. Cretaceous	Dariyan/Shu Alba	1402	320	1634	550			1673	
	Kharaib					1579			
U. Jurassic	Hith	1722	260	2184	63	2006			
	Arab A			2247	28			2293	
	Arab B			2275					
	Diyab	1982	320						
	Upper Araej					2500			
Triassic	Gulailah	2302	228			2768			
	Kail/Sudair	2530	199			2945			
Permian	Khuff	2729	562			3186			
*Total depth**		3291		2414		3470		2794	

*Total depth drilled (mbsl)

Table 4a. Depth to time boundaries in Gulf wells from stratigraphy provided in Mina et al. (1967).

	Wells:	*A*	*B*	*C*	*D*	*E*	*F*
Longitude°E		50.094	50.362	51.226	51.508	51.792	51.044
Latitude °N		28.170	27.866	27.933	27.647	27.584	27.311
Water depth (mbsl)[1]		50	40	20	20	20	65
Total depth (m)[2]		2961	3140	2782	3924	2918	2317
Thickness (m) of section older than Eocene[3]		2455	2856	1984	3018	1790	1994
Thickness (m) of section younger than Eocene[4]		506	284	798	906	1128	323

Age	Formation Tops	Depth (mbsl)	Thick (m)	Depth (mbsl)	Thick (m)	Depth (mbsl)	Thick (m)	Depth (mbsl)	Thick (m)	Depth (mbsl)	Thick (m)	Depth (mbsl)	Thick (m)
mMio-Quat[6]	Gach Saran/ Mishan/Agha Jari/Bakhtyari	50	420	40	204	20	717	20	813	20	1014	65	168
Olig-Mio[5]	Asmari/Ghar	470	36	244	40	737	61	833	73	1034	94	233	90
Eoc-Paleoc	Jahrum/Pabdeh	506	744	284	255	798	342	906	534	1128	399	323	530
U. Cret	Gurpi/Ilam	1250	293	539	303	1140	121	1440	151	1527	168	853	195
m. Cret	Tayarat/Aruma Sarvak	1543	209	842	83	1261	42	1591	394	1695	98	1048	260
L. Cret	Mishrif/Magwa Shu'aiba	1752	408	925	447	1303	184	1985	342	1793	274	1308	381
U. Jurassic	Dariyan Hith/Gotnia	2160	447	1372	343	1487	410	2327	509	2067	452	1689	513
m. Jurassic	Uwainat	2607	354	1715	530	1897	267	2836	416	2519	350	2202	115
Triassic	Dhruma Gulailah			2245	895	2164	336	3252	390	2869	49		
Permian	Khuff					2500	282	3642	282				

[1]Negative values in parentheses are estimated heights of well datum above sealevel.
[2]Values are "TD sub-sea" given in Mina et al. appendices II and III and are assumed to be depth of the bottom below sealevel.
[3]Length of geologic section measured in Mina et al. figures 5-9 from the top of the Eocene to bottom of hole.
[4]Thickness of the post-Eocene section obtained by subtracting the length of the pre-Eocene section[3] shown in Figs. 5-9 from the depth to the bottom of the well[2].
[5]Thickness of the Asmari/Ghar formations was interpolated at well locations in Mina et al. Figure 25.
[6]Thickness of Neogene was obtained by subtracting thickness of Asmari/Ghar[5] from the thickness of the post-Eocene section[4].

Table 4b. Depth to time boundaries in Gulf wells from stratigraphy provided in Mina et al. (1967).

	Wells:	*G*	*O*	*R*	*Sassen (S)*	*U*	*Laven*
Longitude°E		51.350	53.319	52.880	53.1471	53.487	53.287
Latitude °N		27.320	26.368	25.880	25.4706	25.958	26.804
Water depth (mbsl)[1]		60	80	50	30	60	(-10)
Total depth (m)[2]		1957	2415	2780	2890	3577	2890[7]
Thickness (m) of section older than Eocene[3]		1602	1920	2474	2606	2952	2364
Thickness (m) of section younger than Eocene[4]		355	495	306	284	625	526

Age	Formation Tops	Depth (mbsl)	Thick (m)	Depth (mbsl)	Thick (m)	Depth (mbsl)	Thick (m)	Depth (mbsl)	Thick (m)	Depth (mbsl)	Thick (m)	Depth (mbsl)	Thick (m)
mMio-Quat[6]	Gach Saran/ Mishan/Agha Jari/Bakhtyari	60	204	80	327	50	195	30	239	60	492	0	430
Olig-Mio	Asmari/Ghar[5]	264	91	407	88	245	61	269	15	552	73	430	96
Eoc-Paleoc	Jahrum/Pabdeh	355	344	495	448	306	619	284	743	625	720	526	591
U. Cret	Gurpi/Ilam	699	186	943	352	925	109	1027	305	1345	252	1117	80
	Tayarat/Aruma												
m. Cret	Sarvak	885	228	1295	99	1034	453	1332	328	1597	295	1197	177
	Mishrif/Magwa												
L. Cret	Shu'aiba	1113	298	1394	419	1487	486	1660	581	1892	581	1374	442
	Dariyan												
U. Jurassic	Hith/Gotnia	1411	506	1813	464	1973	505	2241	501	2473	473	1816	396
m. Jurassic	Uwainat	1917	40	2277	127	2478	248	2742	148	2946	280	2212	300
	Dhruma												
Triassic	Gulailah			2404	11	2726	54			3226	351	2512	378
Permian	Khuff												

[7]Total thickness of stratigraphic section at the Laven and Binak wells was measured in Figs 8 and 9 in James and Wynd (1965).

Table 4c. Depth to time boundaries in Gulf wells from stratigraphy provided in Mina et al. (1967).

Wells:	*Bahragansar*	*Binak*	*Taub*	*Norouz*	*Cyrus*	*Burgan*
Longitude°E	49.70	50.38	49.933	49.42	49.50	48.00
Latitude °N	29.95	29.78	29.7435	29.50	29.08	28.90
Water depth (mbsl)[1]	10	(-20)	25	30	40	(-62)[9]
Total depth (m)[2]	3345	4990[7]	4081	4520	2251[8]	4218[11]
Thickness (m) of section older than Eocene[3]	1387	1218	2020	3330	2680	4163
Thickness (m) of section younger than Eocene[4]	1958	3772	2061	1190	854[8]	55

Age	Formation Tops	Depth (mbsl)	Thick (m)	Depth (m)	Thick (m)	Depth (mbsl)	Thick (m)	Depth (mbsl)	Thick (m)	Depth (mbsl)	Thick (m)	Depth (m)	Thick (m)
mMio-Quat[6]	Gach Saran/ Mishan/Agha Jari/Bakhtyari	10	1698	0	3492	25	1804	30	1006	40	703	0	0
Olig-Mio	Asmari/Ghar[5]	1708	250	3492	280	1829	232	1036	154	743	111	0	(55)[10]
Eoc-Paleoc	Jahrum/Pabdeh	1958	408	3772	599	2061	612	1190	576	854	751	55[11]	745
U. Cret	Gurpi/Ilam	2366	49	4371	348	2673	203	1766	223	1605	337	800[11]	216
m. Cret	Tayarat/Aruma Sarvak	2415	436	4719	271	2876	869	1989	487	1942	566	1016	511
L. Cret	Mishrif/Magwa Shu'aiba	2851	494			3745	336	2476	1094	2508	908	1527[11]	1122
U. Jurassic	Dariyan Hith/Gotnia							3570	362	3416		2649[11]	378
m. Jurassic	Uwainat							3932	588			3027	1000
Triassic	Dhruma Gulailah											4027[11]	191
Permian	Khuff												

[8]Mina et al give 2251 m as the depth to the Nahr-Umr Fm the mid-point of which is at 1397 m below the top of the Eocene in Mina et al Fig 7. From this we obtain the post-Eocene thickness of 854 m used to compute the rest of the depths.

[9]Height of section above sealevel was measured in Plate 3 of Naqib (1967).

[10]Post-Eocene section in Burgan well is refered to as the Kuwait Fm and is comprised of the Ghar Fm and Neogene sediments.

[11]Total depth and depths (feet below kelly bushing) to five time datums are given in Owen and Nasr (1958). Depths to the other two datums (mid-Cretaceous and mid-Jurassic) were obtained from Figure 7 in Mina et al.

Table 4d. Depth to time boundaries in Gulf wells from stratigraphy provided in Mina et al. (1967).

Wells:	*Darius*	*Kuh-i-mud*	*Dukhan*
Longitude°E	50.26	51.22	50.80
Latitude °N	29.22	28.46	25.45
Water depth (mbsl)[1]	40	(-10)	(-10)
Total depth (m)[2]	3571	4101	?
Thickness (m) of section older than Eocene[3]	2346	3795	2214
Thickness (m) of section younger than Eocene[4]	1225	306	?

Age	Formation Tops	Depth (mbsl)	Thick (m)	Depth (m)	Thick (m)	Depth (m)	Thick (m)
mMio-Quat[6]	Gach Saran/ Mishan/Agha Jari/Bakhtyari	0	1121	0	215	0	
Olig-Mio	Asmari/Ghar[5]	1121	104	215	91	?	0
Eoc-Paleoc	Jahrum/Pabdeh	1225	585	306	570	?	
U. Cret	Gurpi/Ilam Tayarat/Aruma	1810	257	876	246	314[12]	200
m. Cret	Sarvak Mishrif/Magwa	2067	328	1122	447	514[12]	420
L. Cret	Shu'aiba Dariyan	2395	664	1569	459	934[12]	581
U. Jurassic	Hith/Gotnia	3059	408	2028	475	1515[12]	589
m. Jurassic	Uwainat Dhruma	3467	104	2503	583	2104[12]	110
Triassic	Gulailah			3086	1015		
Permian	Khuff						

[12]The total depth at the Dukhan well is not known, so depths are measured downwards from the top-of-Eocene unconformity.

Table 5a. Depth to time boundaries in Kuwait and sothern Iraq wells from stratigraphy in Plate 3 Al Naqib (1967).

	Wells:	*Burgan 13*	*Magwa 1*	*Bahrah 2*	*Raudhatain 1*	*Zubair 19*	*Zubair 24*
Longitude°E		48.00	47.85	47.90	47.70	47.69	47.60
Latitude °N		28.85	29.09	29.565	29.87	30.44	30.20
Height above SL (m)		62	49	25	34	46	34
Total length (m)		4290	2310	2500	3210	3480	3660
Total depth (mbsl)		4228	2261	2475	3176	3434	3626

Age	Formation Tops	Depth (mbsl)	Thick (m)	Depth (mbsl)	Thick (m)	Depth (mbsl)	Thick (m)	Depth (mbsl)	Thick (m)	Depth (mbsl)	Thick (m)	Depth (mbsl)	Thick (m)
Plio-Quat	Dibdibba	--	--	--	--	--	--	-34	92	-46	231	-34	308
mid-Mio	L. Fars	--	--	--	--	--	--	58	120	185	194	274	190
mid-Mio	Ghar	-62	46	-49	92	-25	225	178	151	379	123	464	124
Eoc-Paleoc	Dammam/ Rus/Radhuma	-16	769	43	775	200	843	329	806	502	815	588	815
U. Cret/Maes	Tayarat	753	275	818	263	1043	712	1135	791	1317	987	1403	913
M. Cret/Ceno	Mishrif/ Kifl/Magwa	1028	480	1081	530	1755	720	1926	800	2304	880	2316	860
L. Cret/Aptian	Shu'aiba	1508		1611		--		2726		3184		3176	

Table 5b. Depth to time boundaries in Kuwait and sothern Iraq wells from stratigraphy in Plate 3 Al Naqib (1967).

	Wells:	*Rumaila 1*	*Ratawi 1*	*Shawiya 1*	*Samawa 1*	*Kifl 1*	*Ghalaisan 1*
Longitude °E		47.57	47.09	44.91	45.00	32.383	47.79
Latitude °N		30.23	30.56	30.59	31.15	44.426	31.01
Height above SL (m)		25	28	209	34	58	314
Total length (m)		3310	4000	1880	3540	3370	2070
Total depth (mbsl)		3285	3972	1671	3506	3312	1756

Age	Formation Tops	Depth (mbsl)	Thick (m)	Depth (mbsl)	Thick (m)	Depth (mbsl)	Thick (m)	Depth (mbsl)	Thick (m)	Depth (mbsl)	Thick (m)	Depth (mbsl)	Thick (m)
Plio-Quat	Dibdibba	-25	126	-28	172	--	--	--	--	-58	156	--	--
mid-Mio	L. Fars	101	114	144	160	--	--	--	--	98	50	--	--
mid-Mio	Ghar	215	160	304	99	--	--	--	--	148	40	--	--
Eoc-Paleoc	Dammam/ Rus/Radhuma	375	862	403	862	-209	566	-34	665	188	554	-314	415
U. Cret/Maes	Tayarat	1237	1018	1265	877	357	874	631	895	742	720	101	785
M. Cret/Ceno	Mishrif/ Kifl/Magwa	2255	720	2142	720	1231	380	1526	460	1462	510	886	350
L. Cret/Aptian	Shu'aiba	2975		2862		1611		1986		1972		1236	

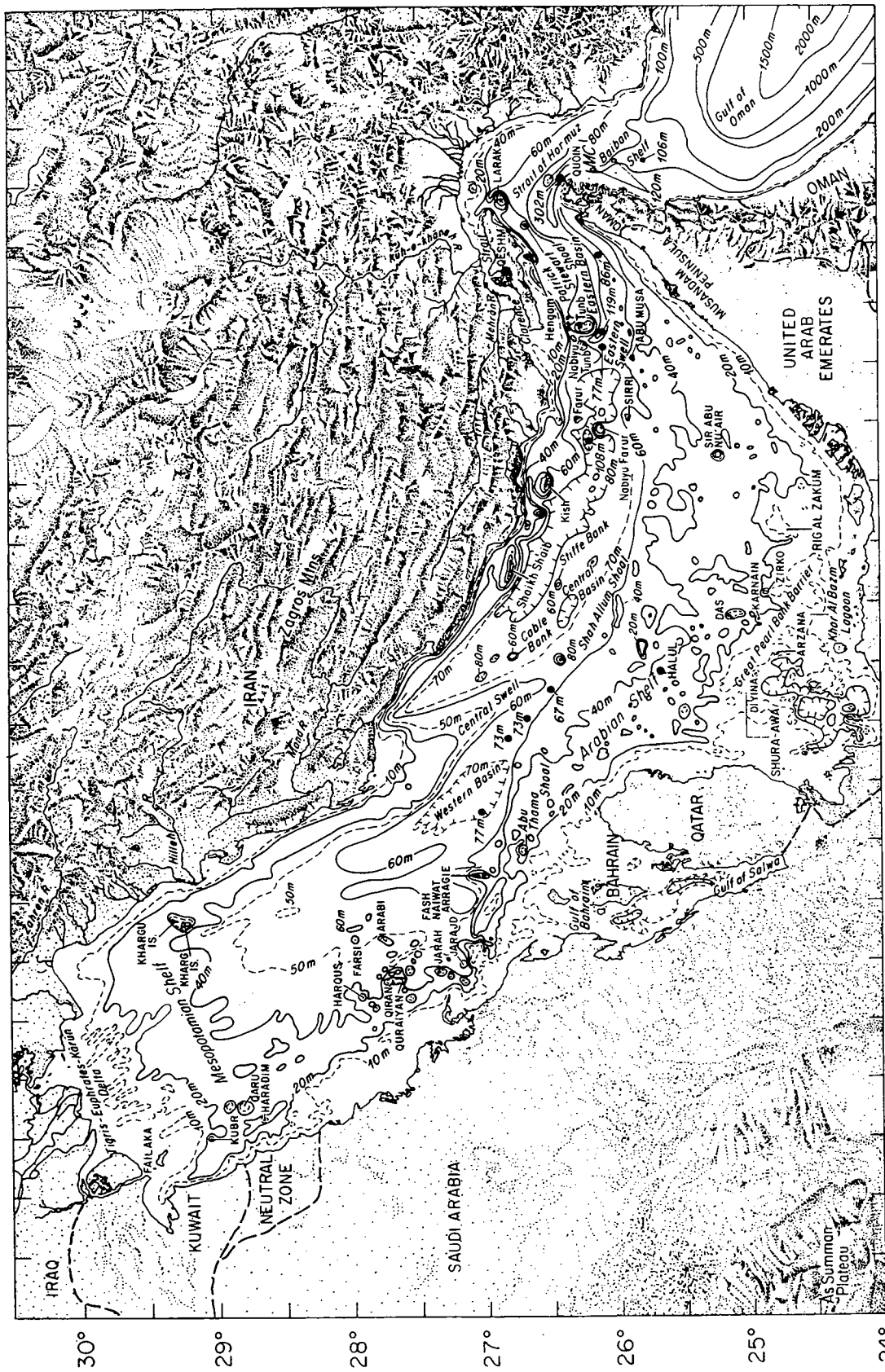

Figure 1. Bathymetry (meters) of the Persian (Arabian) Gulf and morphology of the adjacent land masses (from Uchupi et al., 1996). *MC* indicates the Musandam channel.

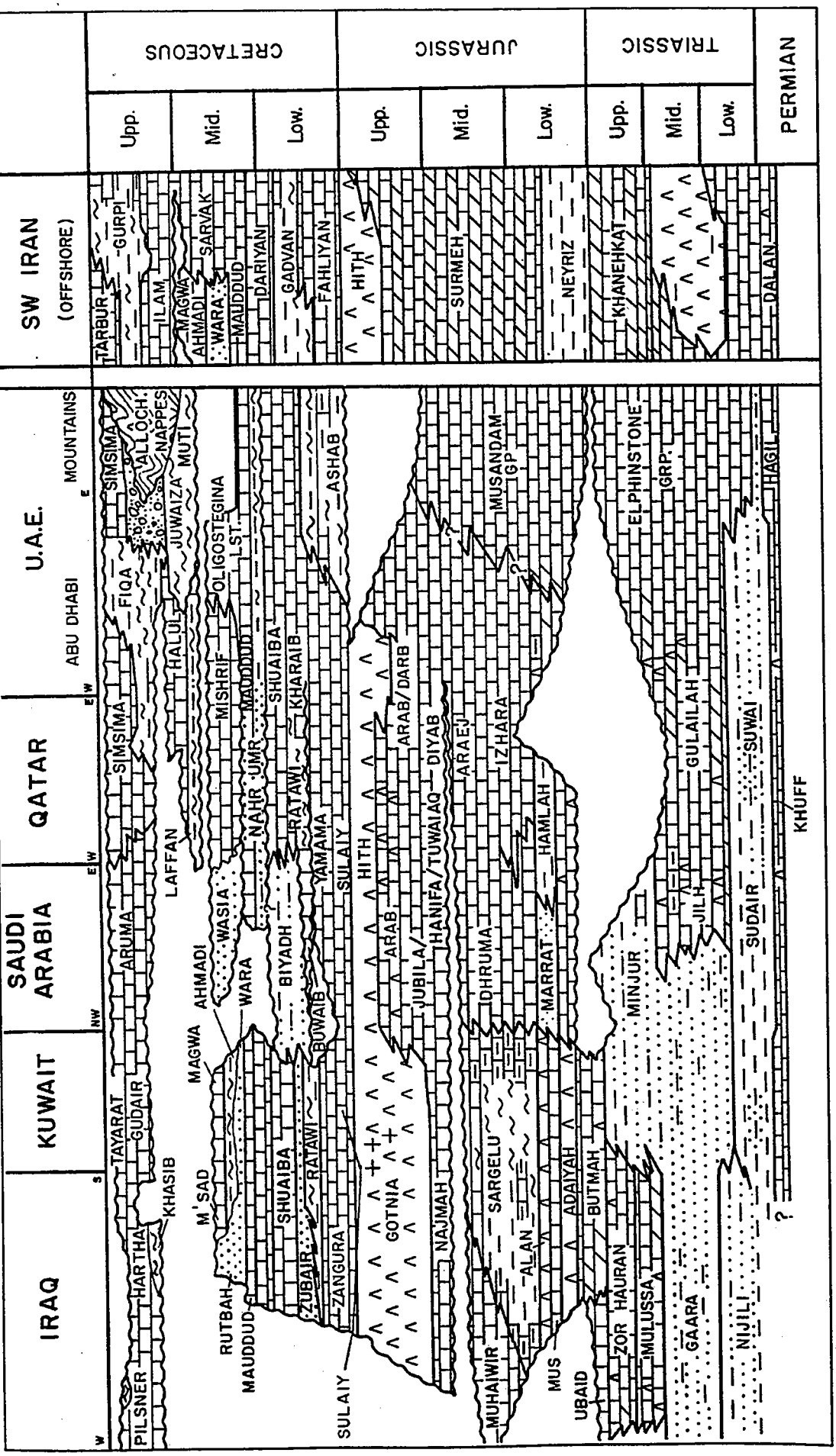

Figure 2a. Mesozoic stratigraphic correlation diagram for the Gulf region (from Beydoun, 1991).

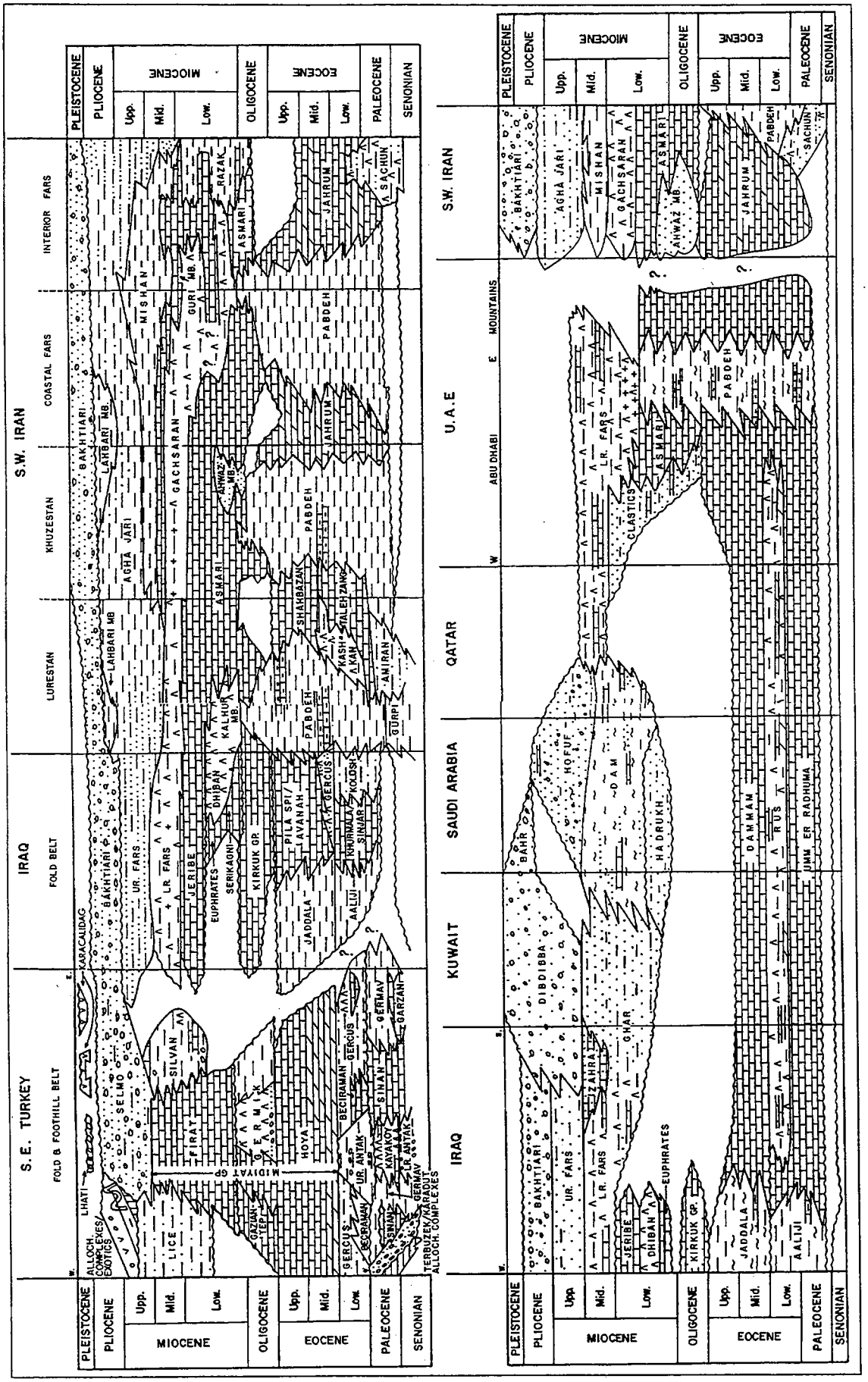

Figure 2b. Cenozoic stratigraphic correlation diagram for the Gulf region (from Beydoun, 1991).

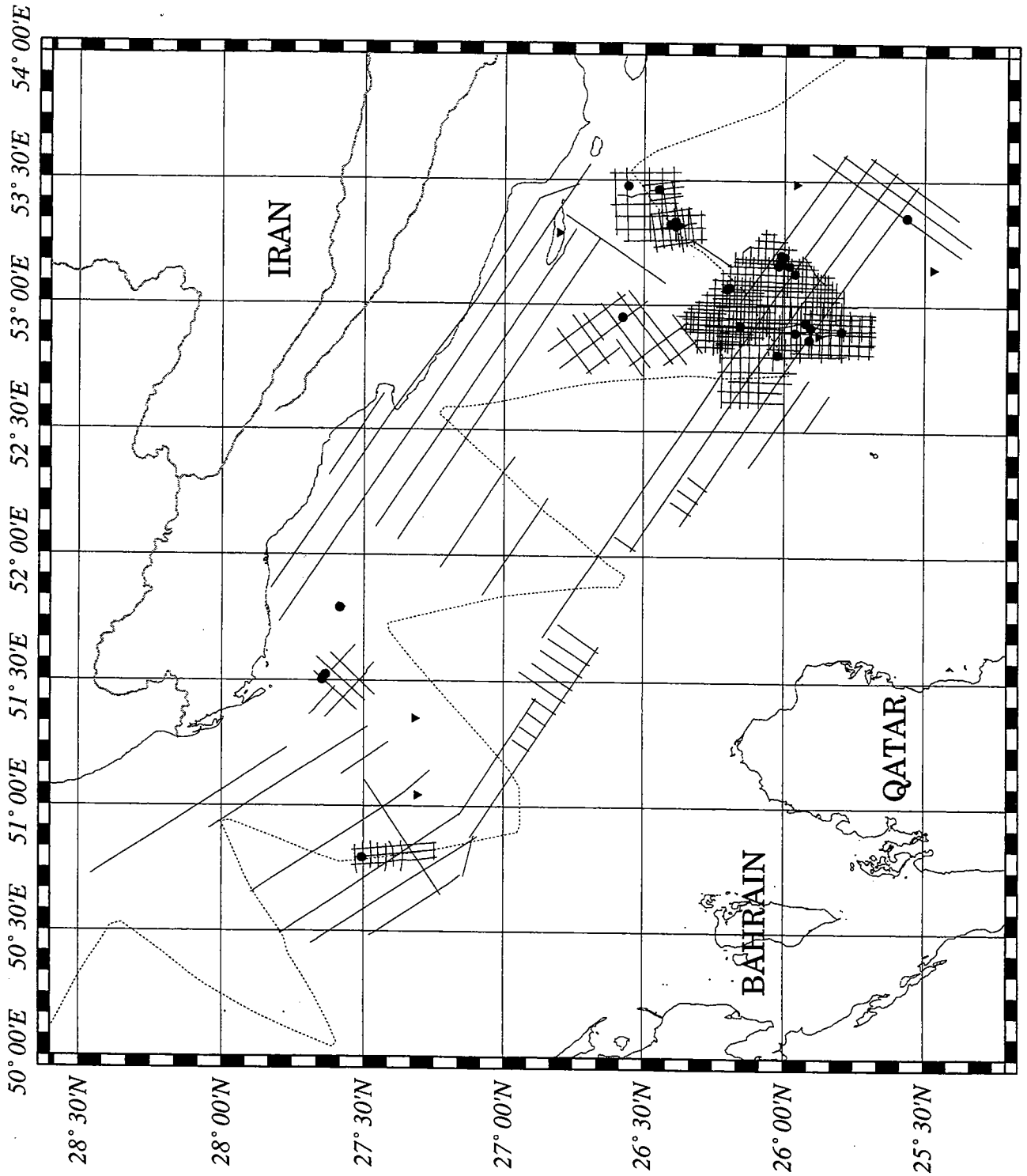

Figure 3. Industry seismic lines (solid) in the central Gulf are dense in a few local areas but provide only scattered coverage elsewhere. To improve correlations between strike lines, we used profiles from the *R/V Atlantis II*-93 cruise in 1977 (dotted, Ross et al., 1986). Triangles indicate locations of well data from Mina et al. (1968). Dots indicate other well data.

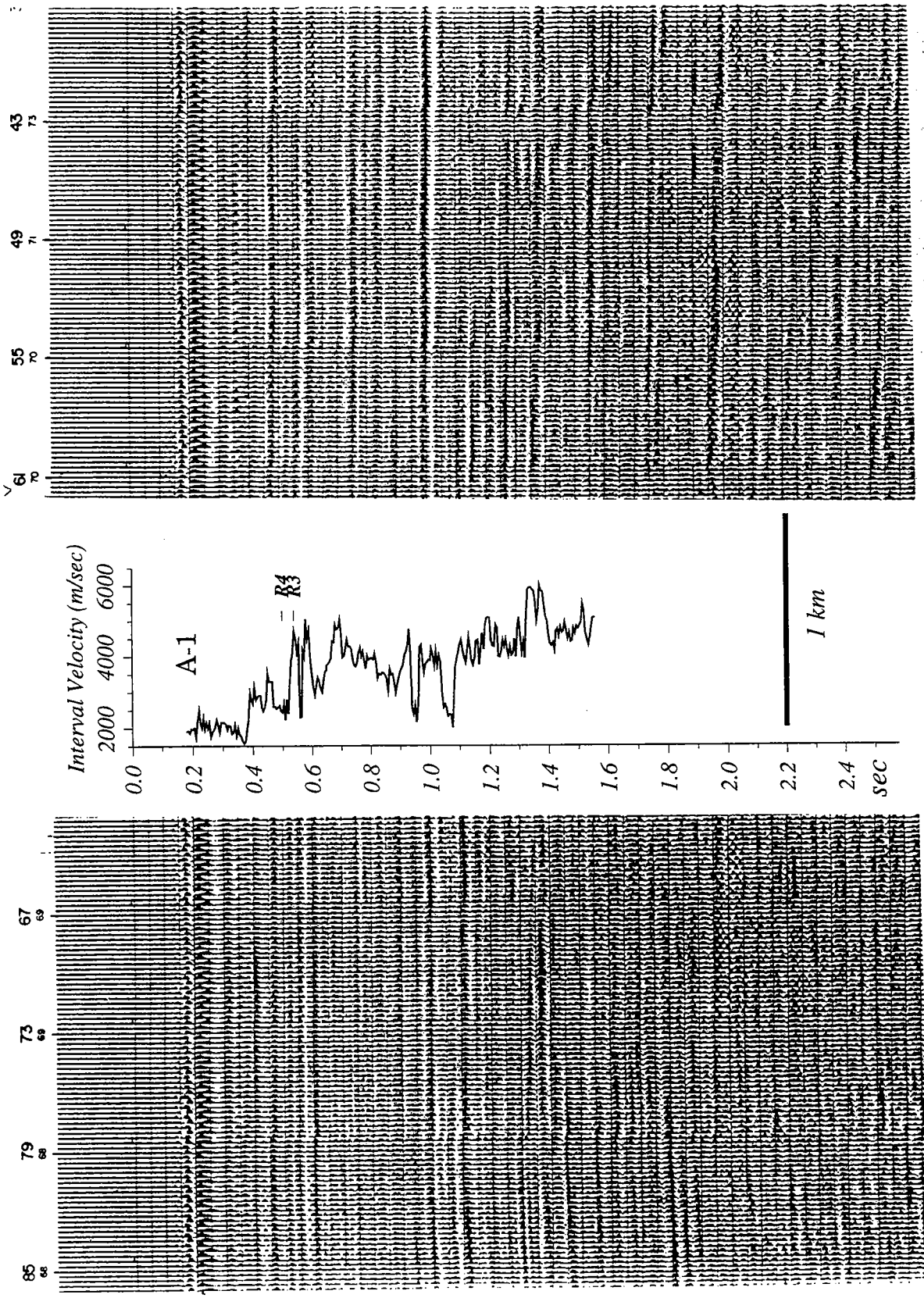

Figure 4a. North-south industry multi-channel seismic profile 420 (Area 5) across well A-1 (reflection point 61) showing interval velocities from the sonic log and the positions of horizons R3 and R4. Well A-2 projects to reflection point 55. Larger numbers along the top of the profile are reflection points, and smaller numbers are water depths (m).

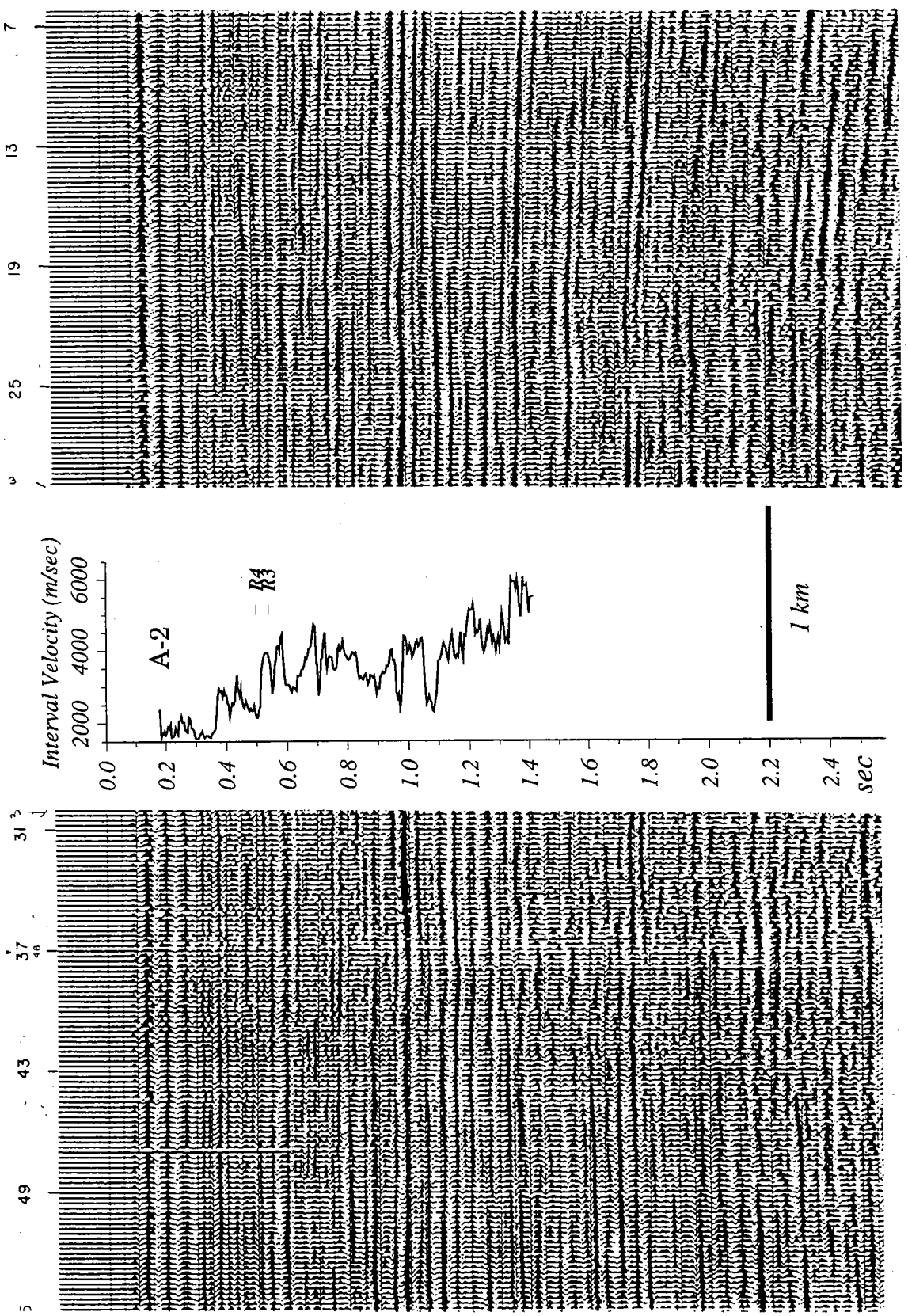

Figure 4b. East-west industry multi-channel seismic profile 511 (Area 6) across well A-2 (reflection point 30) showing interval velocities from the sonic log and the positions of horizons R3 and R4. Well A-1 projects to reflection point 25. Numbers along the top of the profile are reflection points.

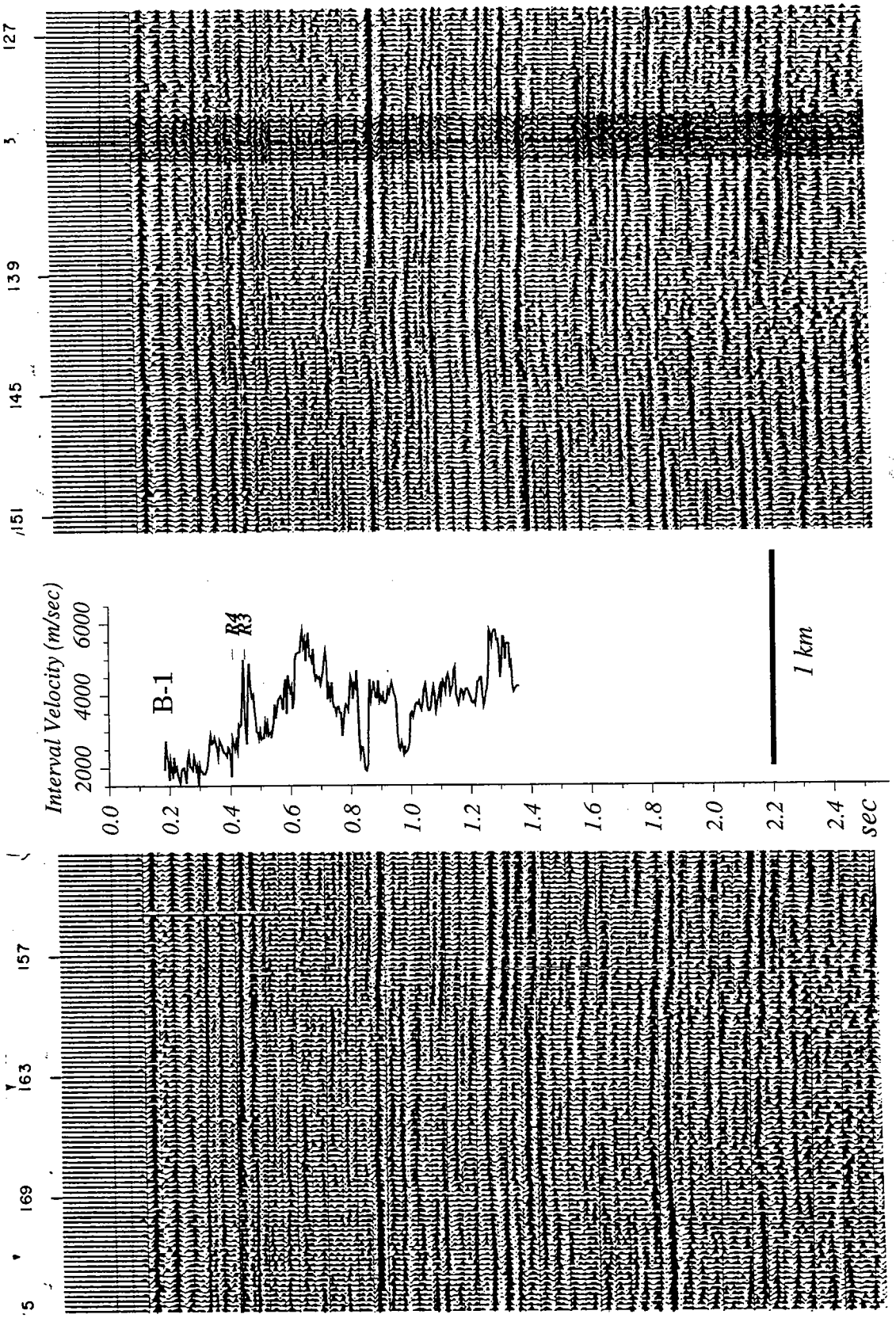

Figure 4c. East-west industry multi-channel seismic profile 517 (Area 6) across well B-1 (reflection point 152) showing interval velocities from the sonic log and the positions of horizons R3 and R4. Numbers along the top of the profile are reflection points.

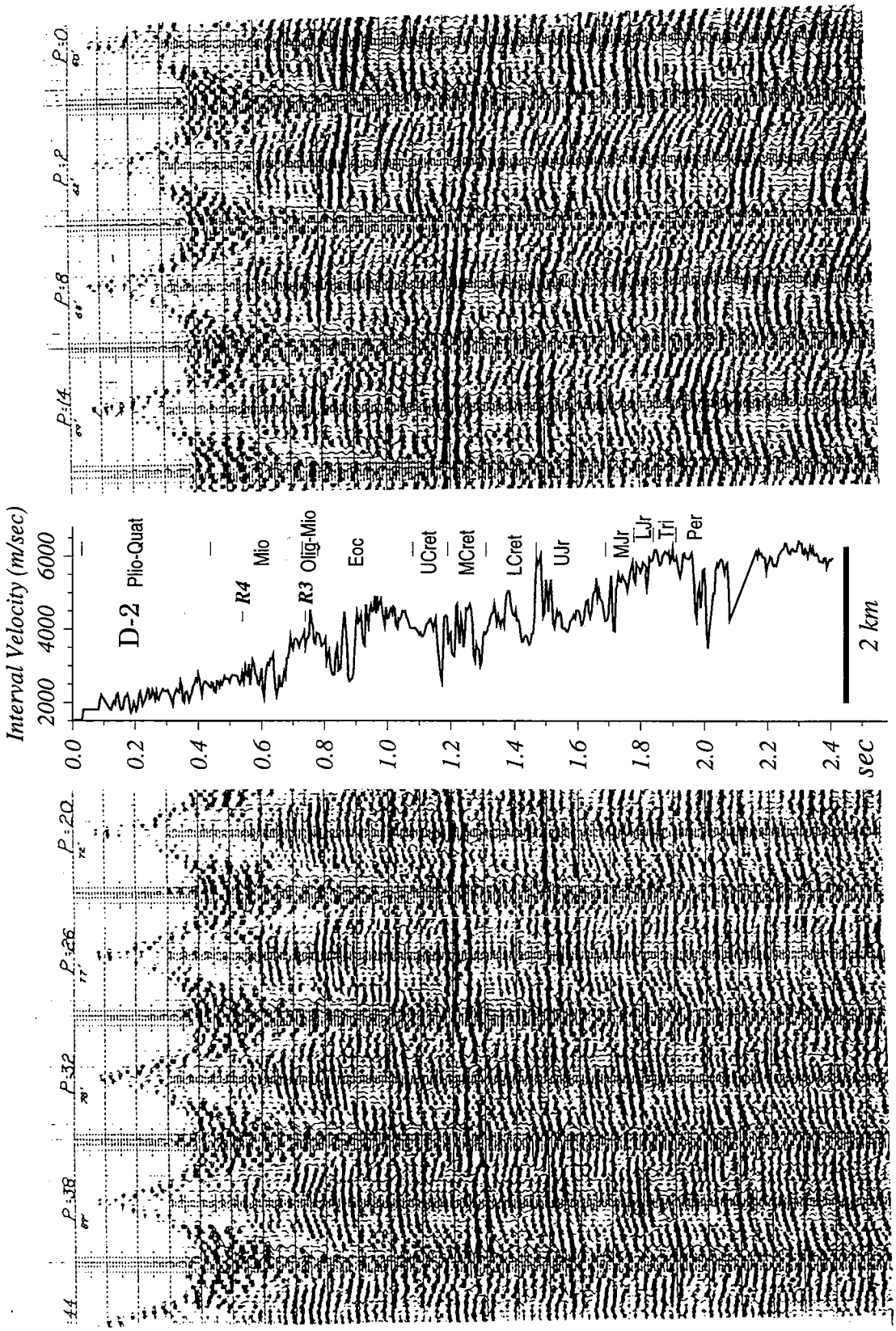

Figure 4d. SW-NE industry multi-channel seismic profile P (Area 2) across well D-2 (reflection point 18) showing interval velocities from the sonic log and the positions of horizons R3 and R4. Geologic units are from nearby well D-1. Numbers along the top of the profile are reflection points, and smaller numbers are water depths (ft).

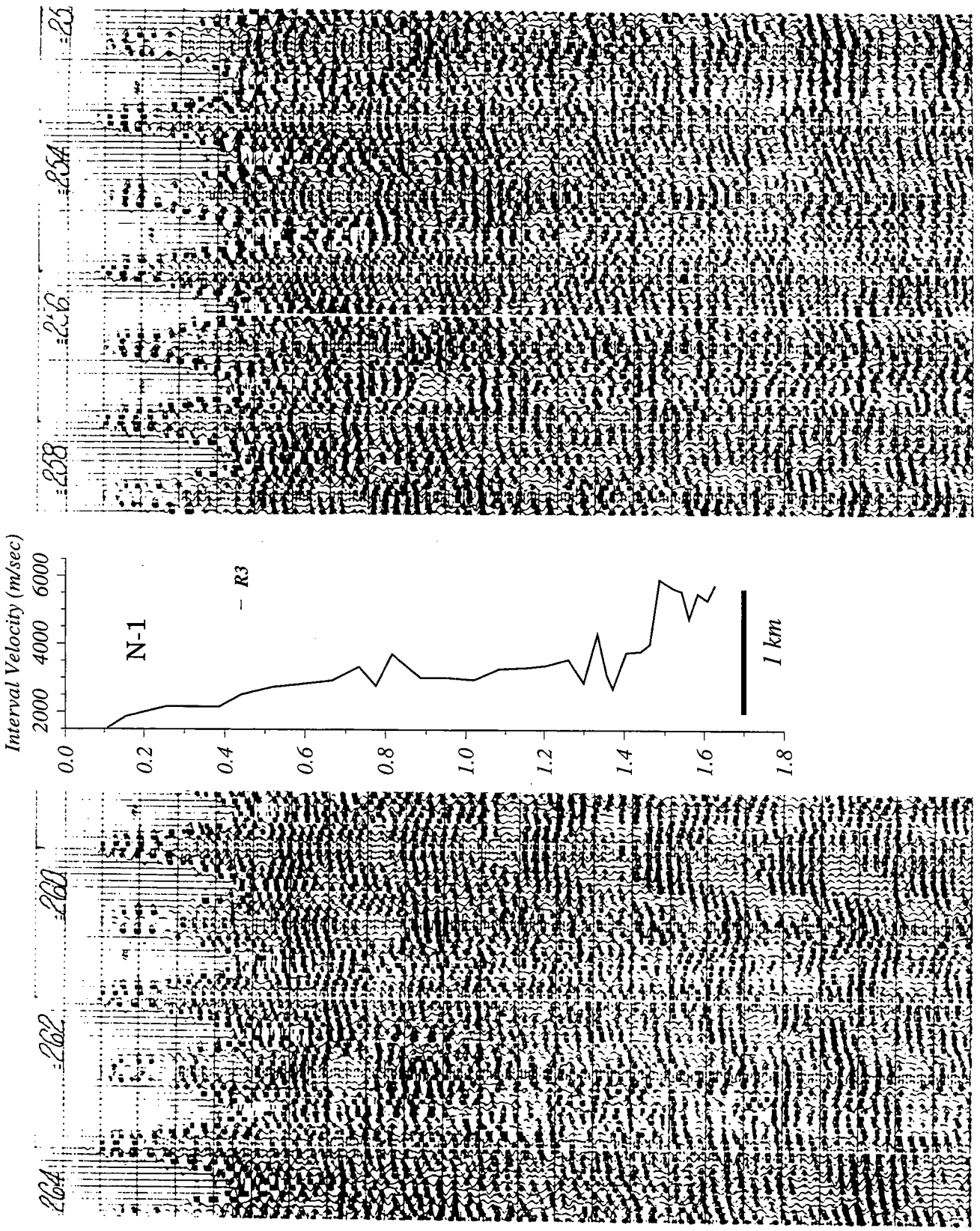

Figure 4e. SW-NE industry multi-channel seismic profile 153 (Area 8) across well N-1 (reflection point 259) showing interval velocities from the sonic log and the positions of horizons R3 and R4. Numbers along the top of the profile are reflection points.

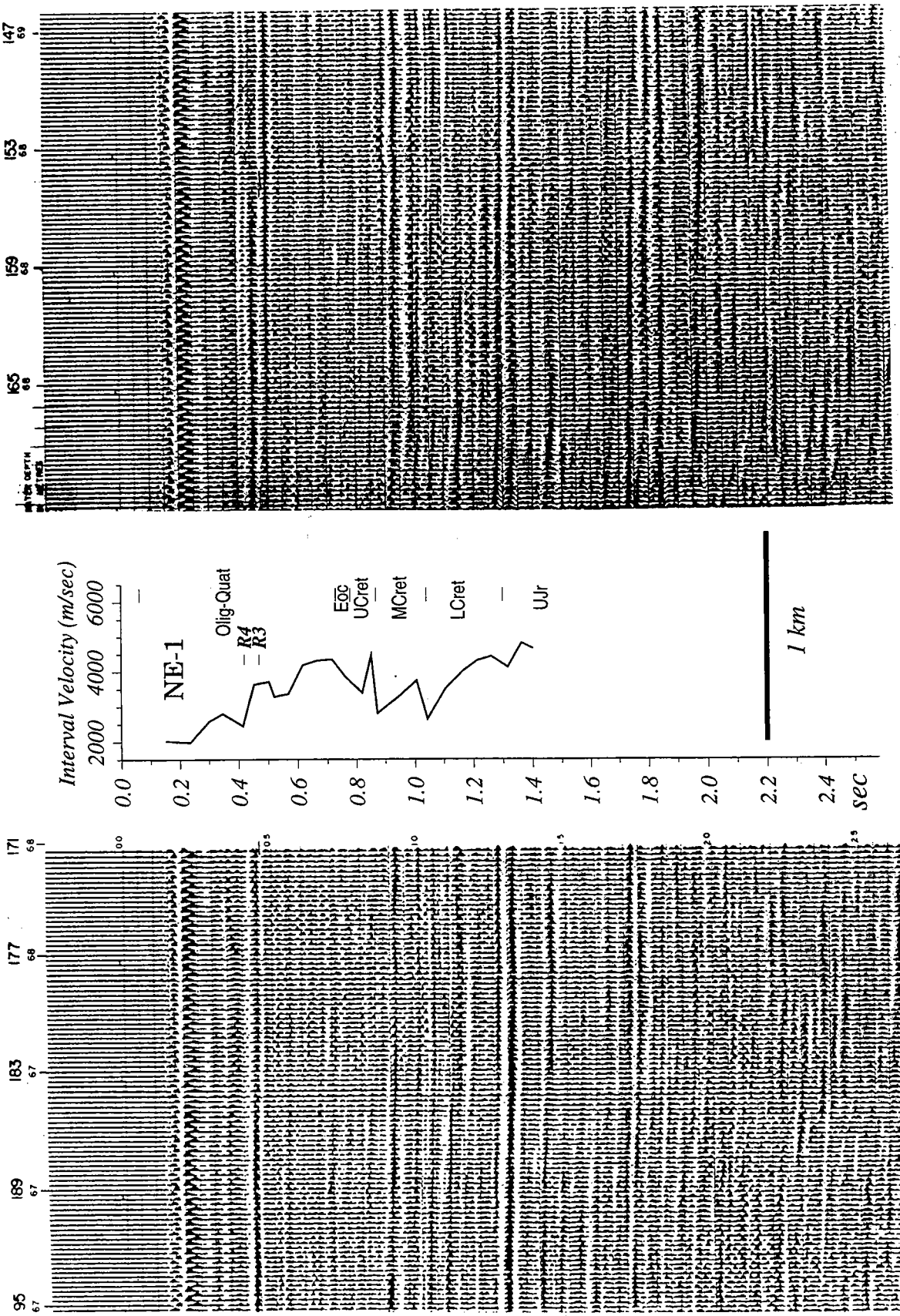

Figure 4f. North-south industry multi-channel seismic profile 411 (Area 5) across well NE-1 (reflection point 173) showing interval velocities from the sonic log and the positions of horizons R3 and R4. Geologic units are from well NE-1. Larger numbers along the top of the profile are reflection points, and smaller numbers are water depths (m).

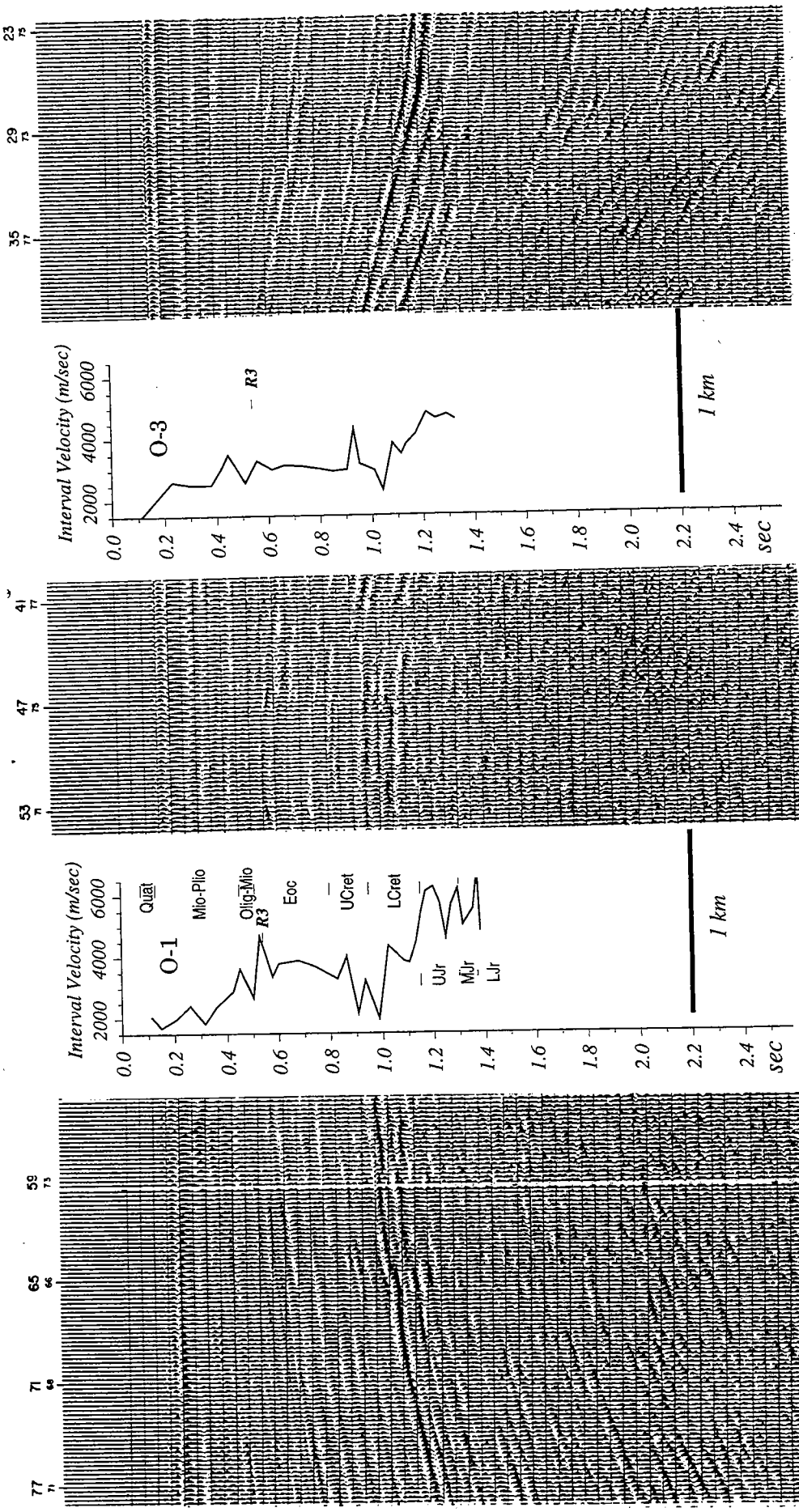

Figure 4g. East-west industry multi-channel seismic profile 451 (Area 5) across well O-1 (reflection point 54) and across well O-3 (reflection point 40) showing interval velocities from the sonic logs and the position of horizon R3. Geologic units are from well O-1. Larger numbers along the top of the profile are reflection points, and smaller numbers are water depths (m).

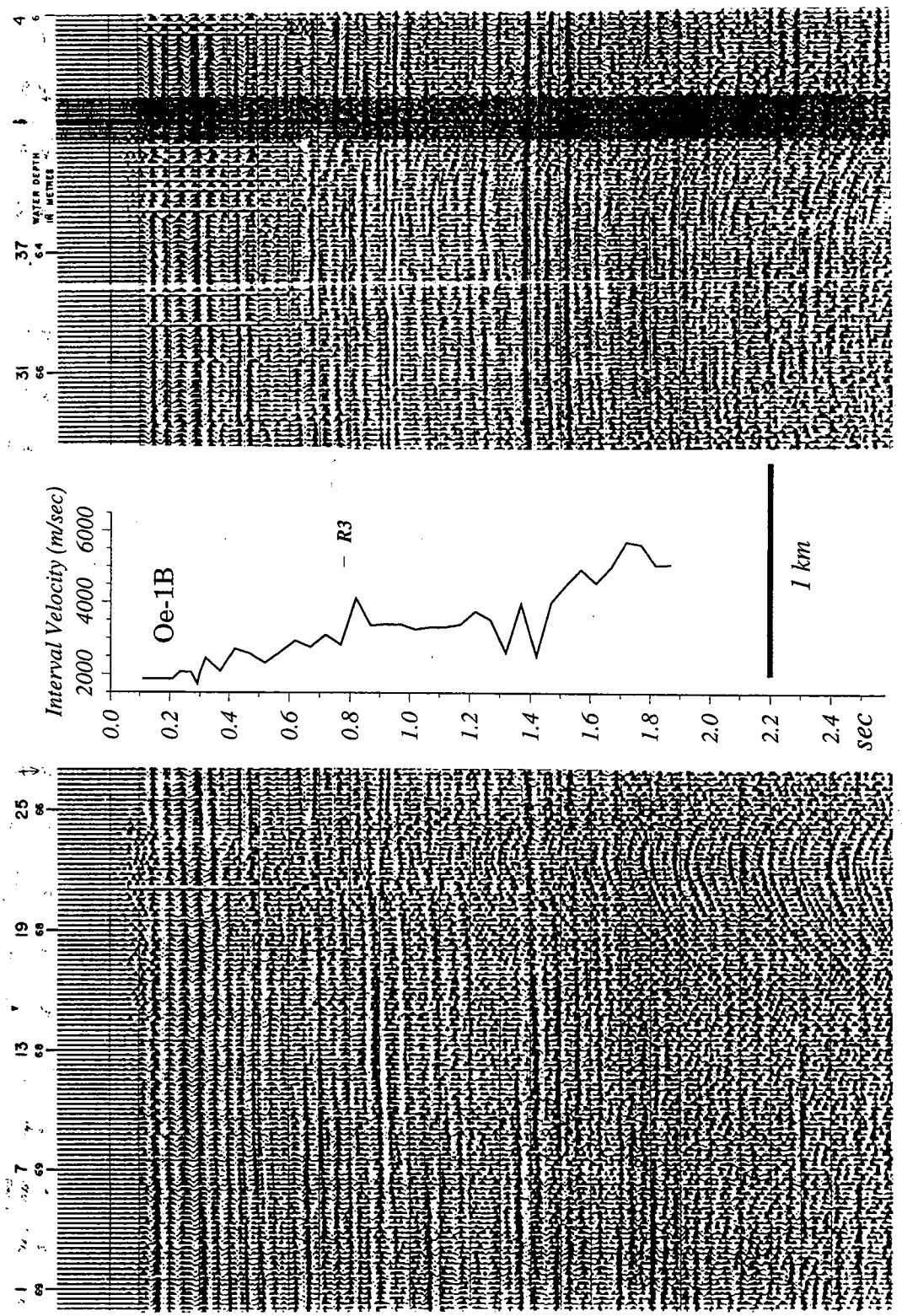

Figure 4h. North-south industry multi-channel seismic profile 550 (Area 7) across well Oe-1B (reflection point 27) showing interval velocities from the sonic log and the position of horizon R3. Larger numbers along the top of the profile are reflection points, and smaller numbers are water depths (m).

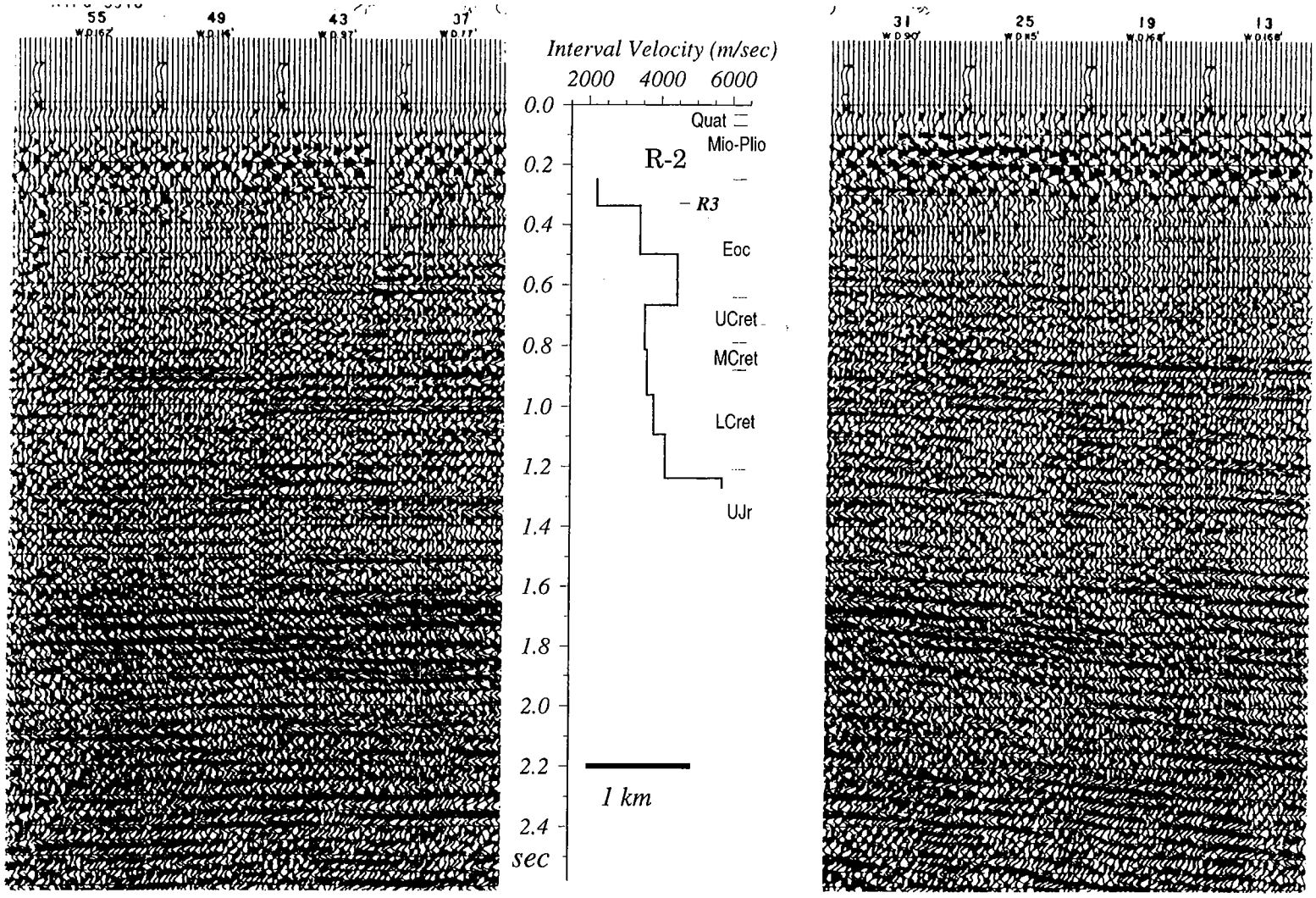

Figure 4i. East-west industry multi-channel seismic profile 243 (Area 3) across well R-2 (reflection point 37) showing interval velocities from the check-shot survey and the position of horizon R3. Geologic units are from well R-2. Larger numbers along the top of the profile are reflection points, and smaller numbers are water depths (ft).

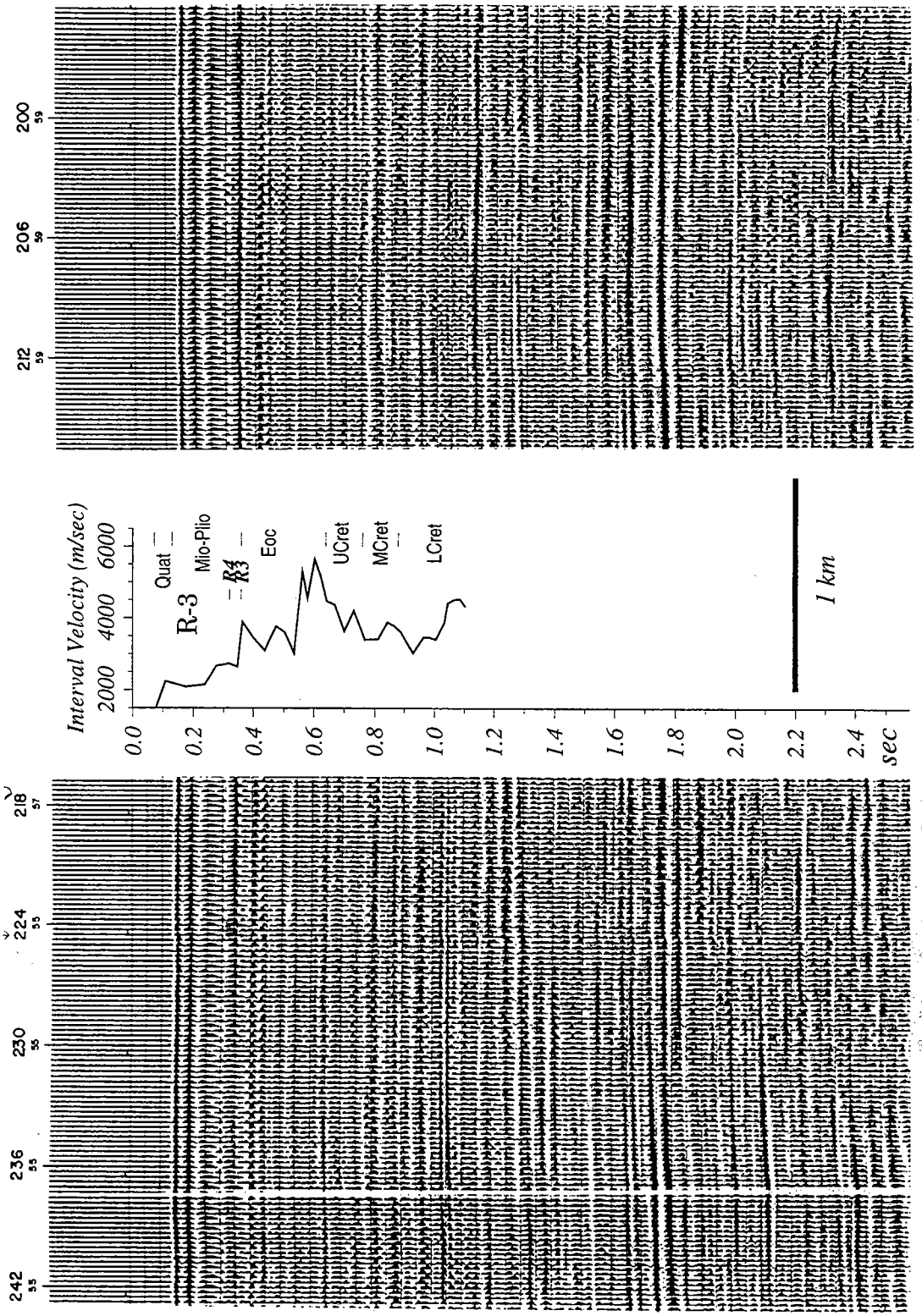

Figure 4j. East-west industry multi-channel seismic profile 431 (Area 5) across well R-3 (reflection point 217) showing interval velocities from the sonic log and the positions of horizons R3 and R4. Geologic units are from well R-3. Larger numbers along the top of the profile are reflection points, and smaller numbers are water depths (m).

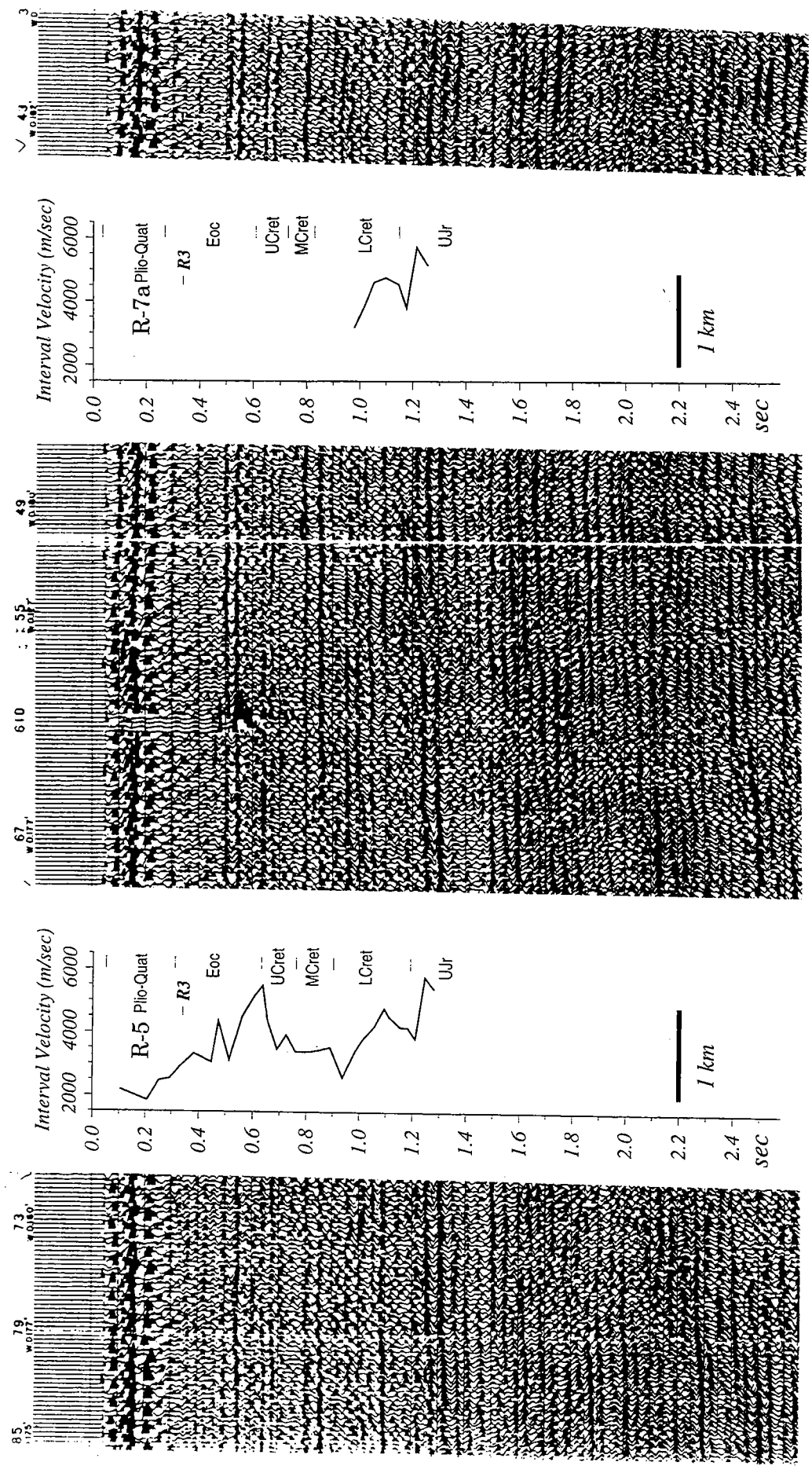

Figure 4k. East-west industry multi-channel seismic profile 237 (Area 3) across well R-5 (reflection point 70) and well R-7A (reflection point 45) showing interval velocities from the sonic logs and the position of horizon R3. Geologic units are from both wells. Larger numbers along the top of the profile are reflection points, and smaller numbers are water depths (ft).

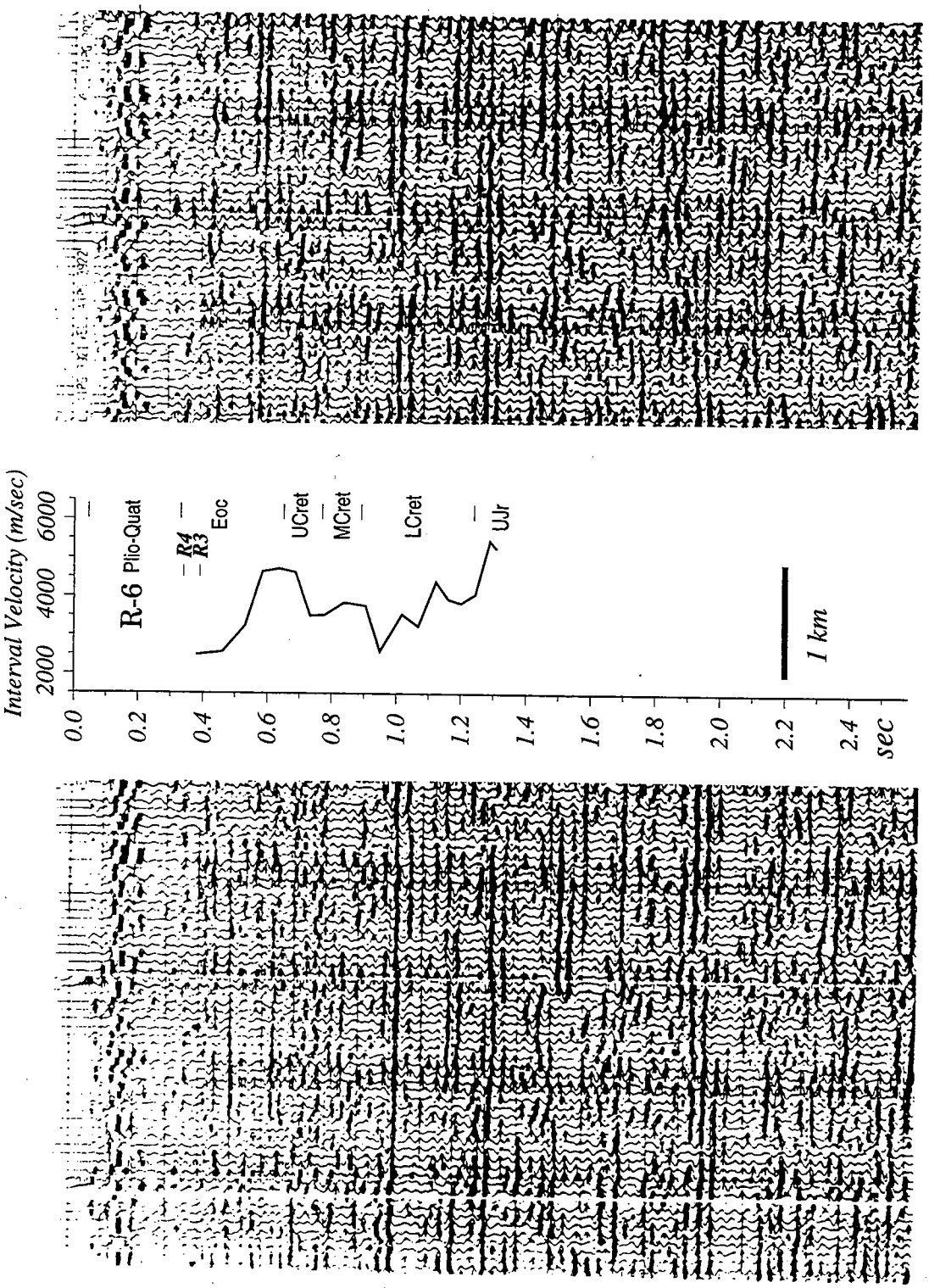

Figure 41. East-west industry multi-channel seismic profile 231 (Area 3) across well R-6 (reflection point 88) showing interval velocities from the check-shot survey and the positions of horizons R3 and R4. Geologic units are from well R-6.

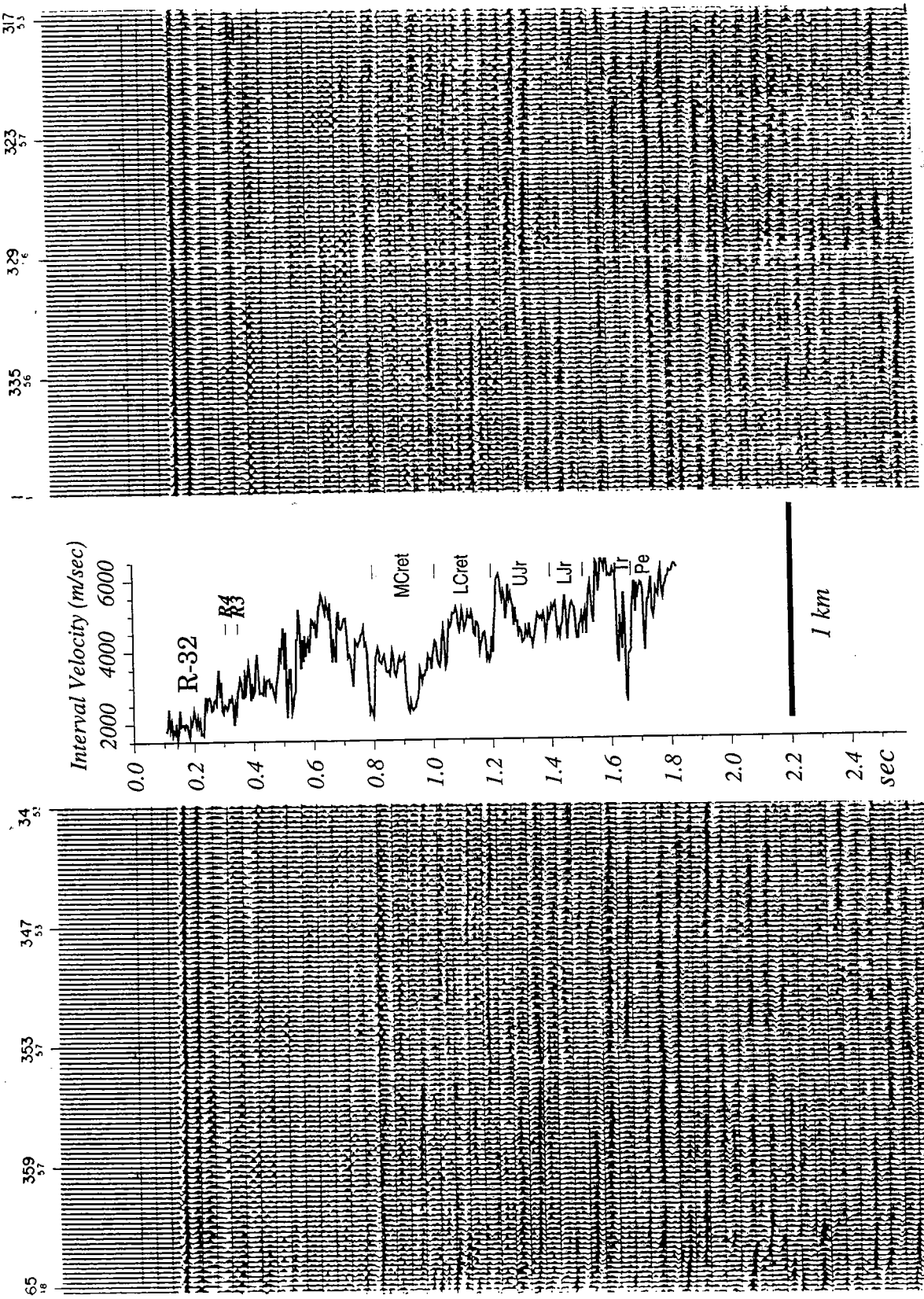

Figure 4m. North-south industry multi-channel seismic profile 410 (Area 5) across well R-32 (reflection point 341) showing interval velocities from the sonic log and the positions of horizons R3 and R4. Geologic units are from well R-32. Larger numbers along the top of the profile are reflection points, and smaller numbers are water depths (m).

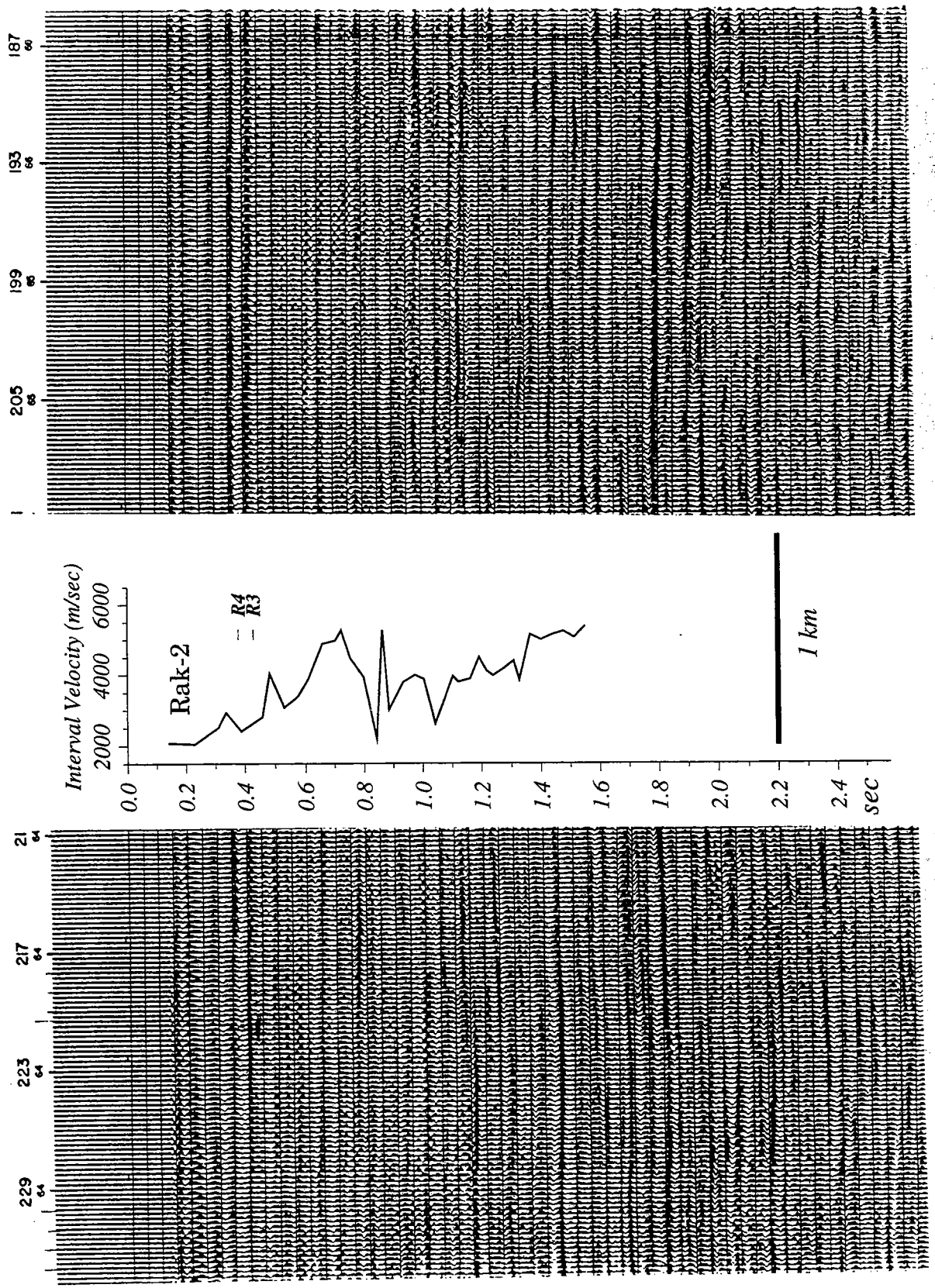

Figure 4n. North-south industry multi-channel seismic profile 424 (Area 5) across well Rak-2 (reflection point 211) showing interval velocities from the sonic log and the positions of horizons R3 and R4. Larger numbers along the top of the profile are reflection points, and smaller numbers are water depths (m).

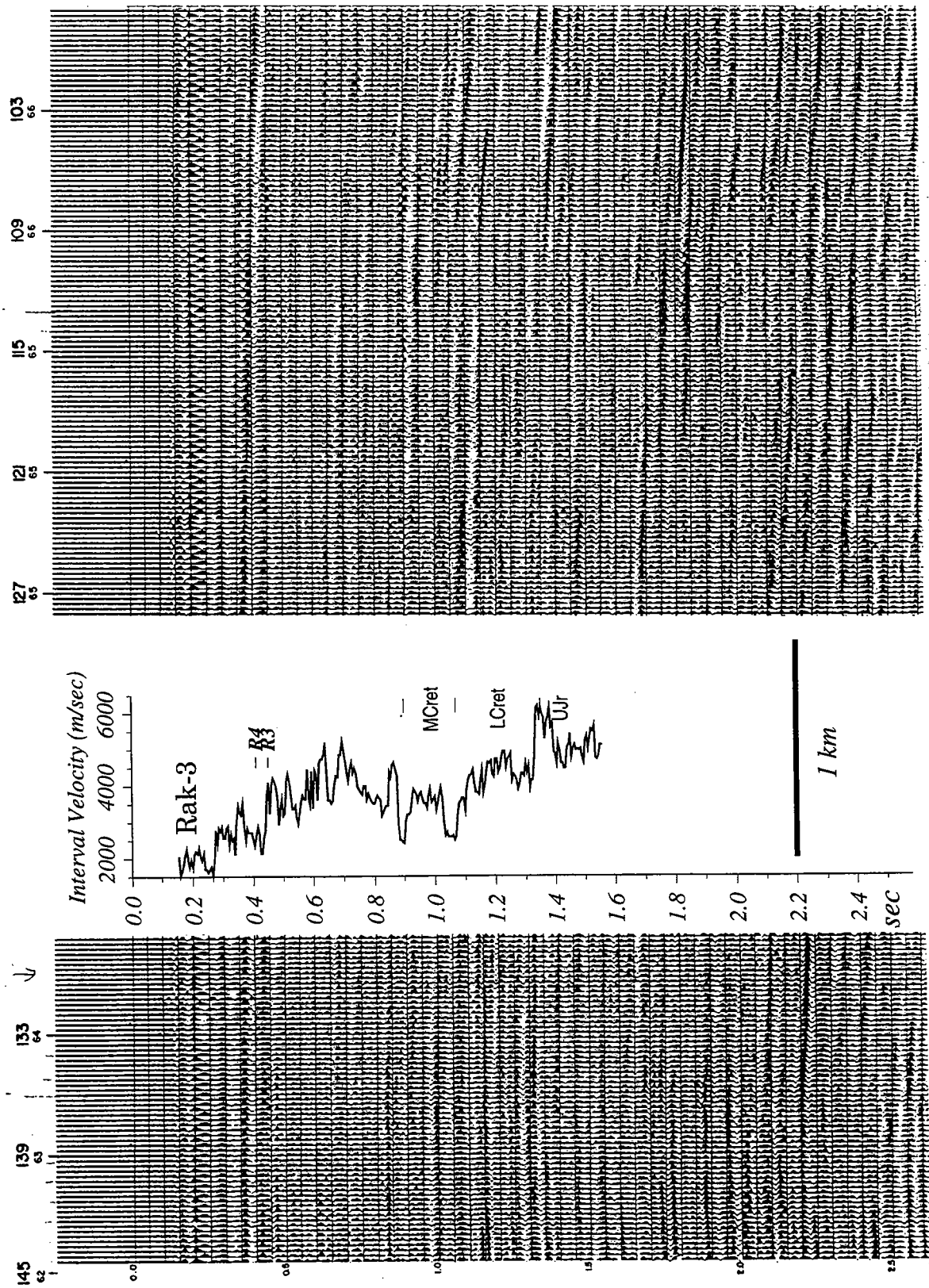

Figure 46. North-south industry multi-channel seismic profile 428 (Area 5) across well Rak-3 (reflection point 128) showing interval velocities from the sonic log and the positions of horizons R3 and R4. Geologic units are from well Rak-3. Larger numbers along the top of the profile are reflection points, and smaller numbers are water depths (m).

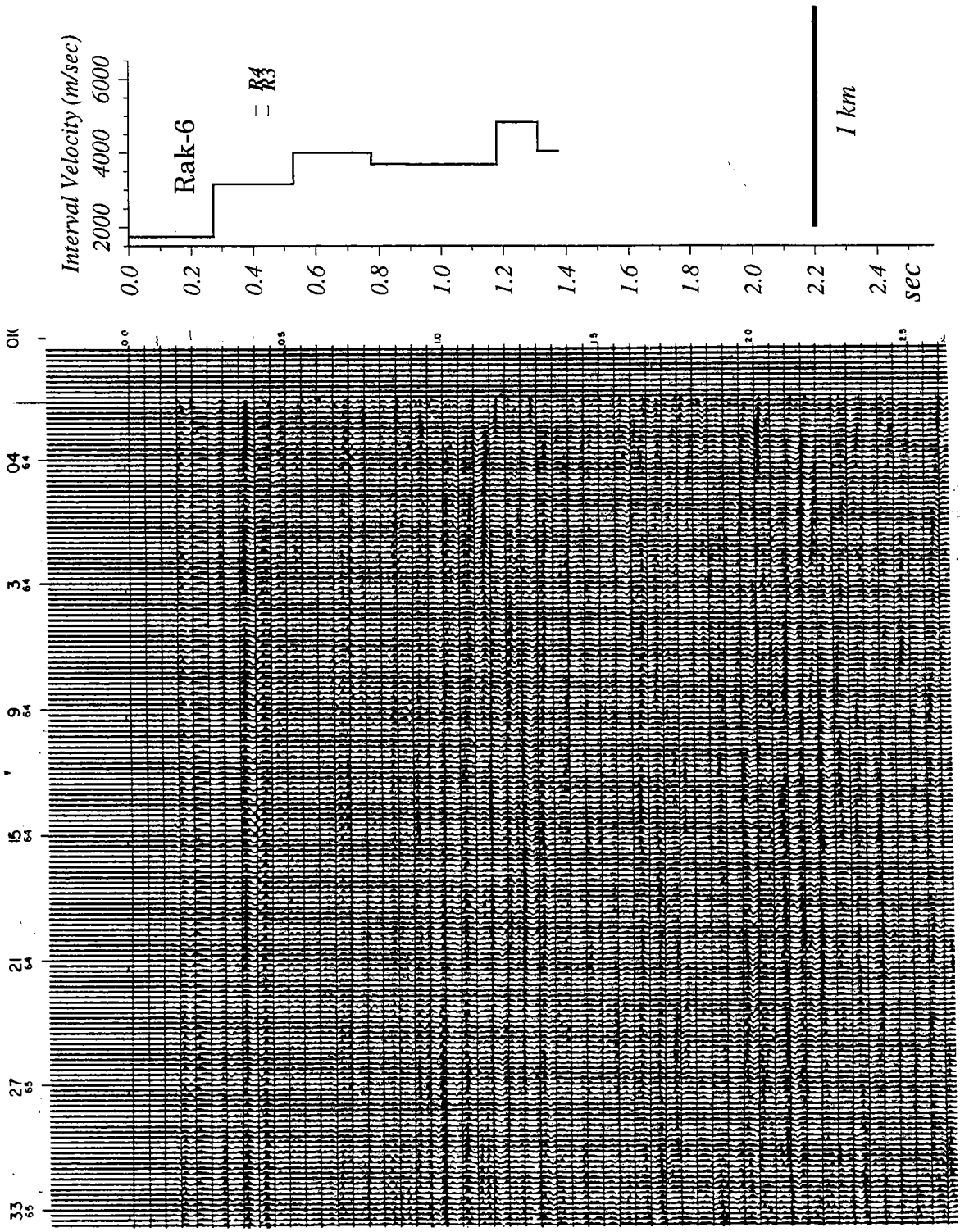

Figure 4p North-south industry multi-channel seismic profile 427 (Area 5) that begins near well Rak-6 (reflection point 0) showing interval velocities from the check-shot survey and the positions of horizons R3 and R4. Larger numbers along the top of the profile are reflection points, and smaller numbers are water depths (m).

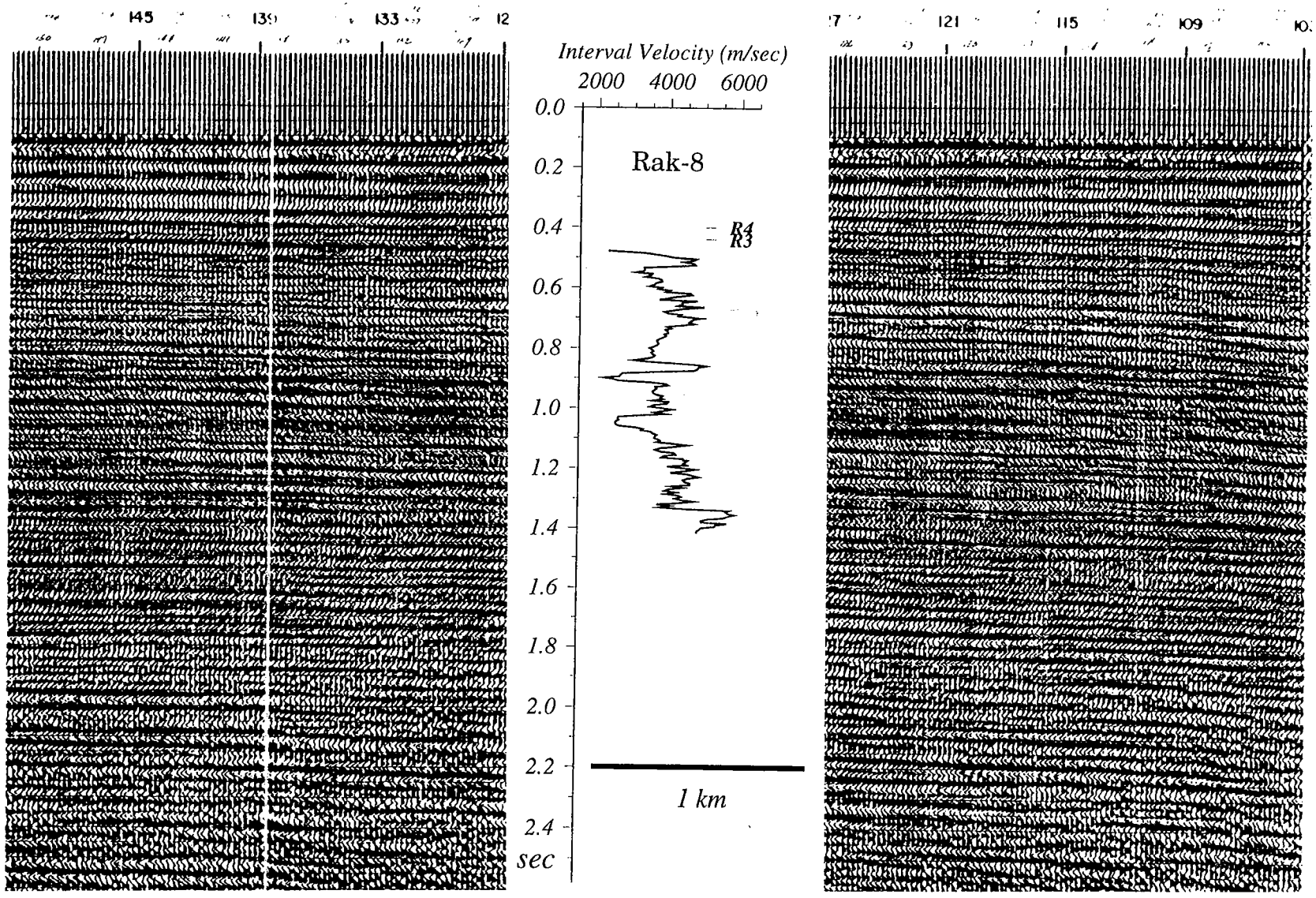

Figure 4q North-south industry multi-channel seismic profile 530 (Area 6) across well Rak-8 (reflection point 127) showing interval velocities from the sonic log and the positions of horizons R3 and R4. Numbers along the top of the profile are reflection points.

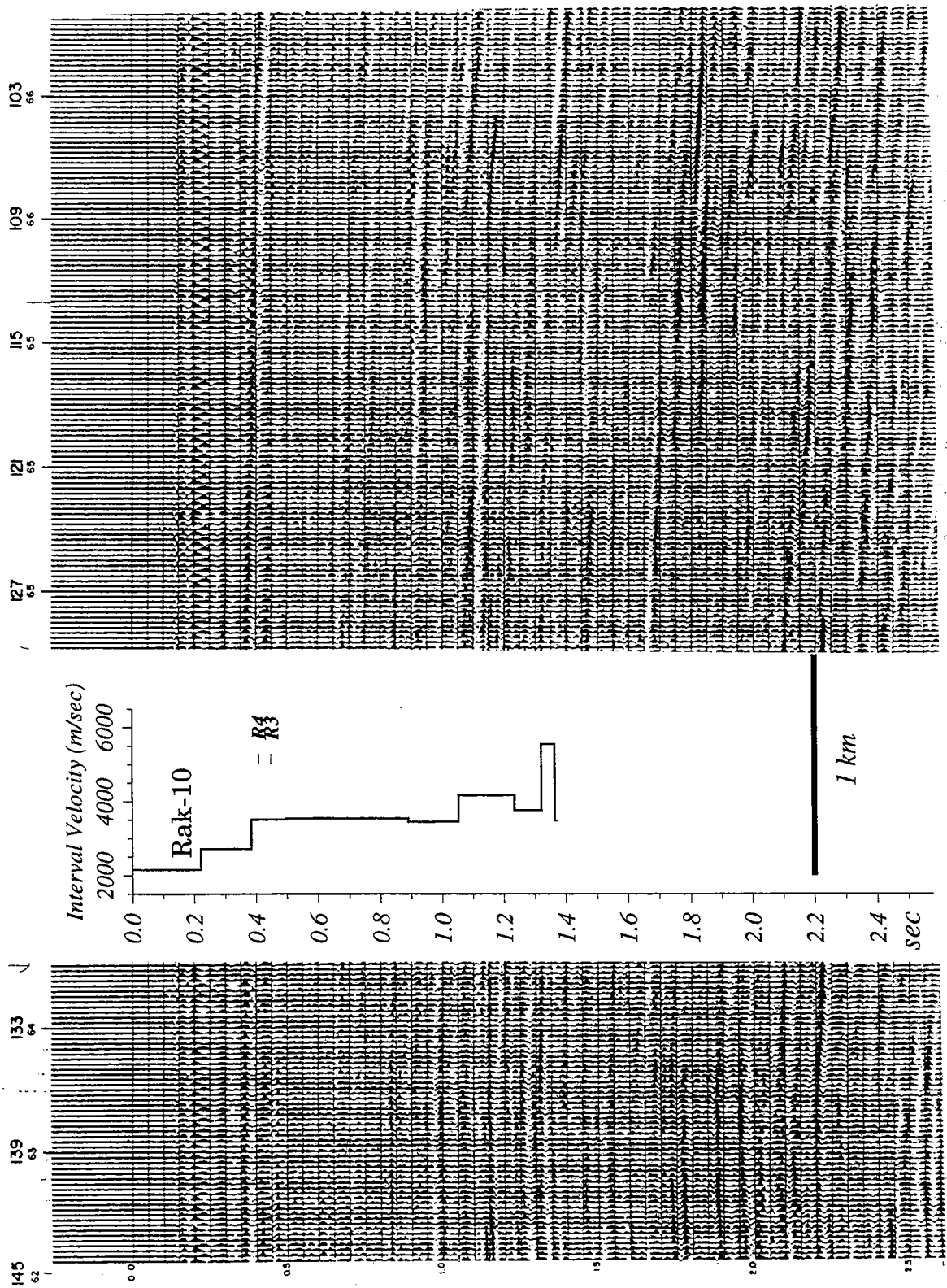

Figure 4r North-south industry multi-channel seismic profile 428 (Area 5) across well Rak-10 (reflection point 130) showing interval velocities from the check-shot survey and the positions of horizons R3 and R4. Larger numbers along the top of the profile are reflection points, and smaller numbers are water depths (m).

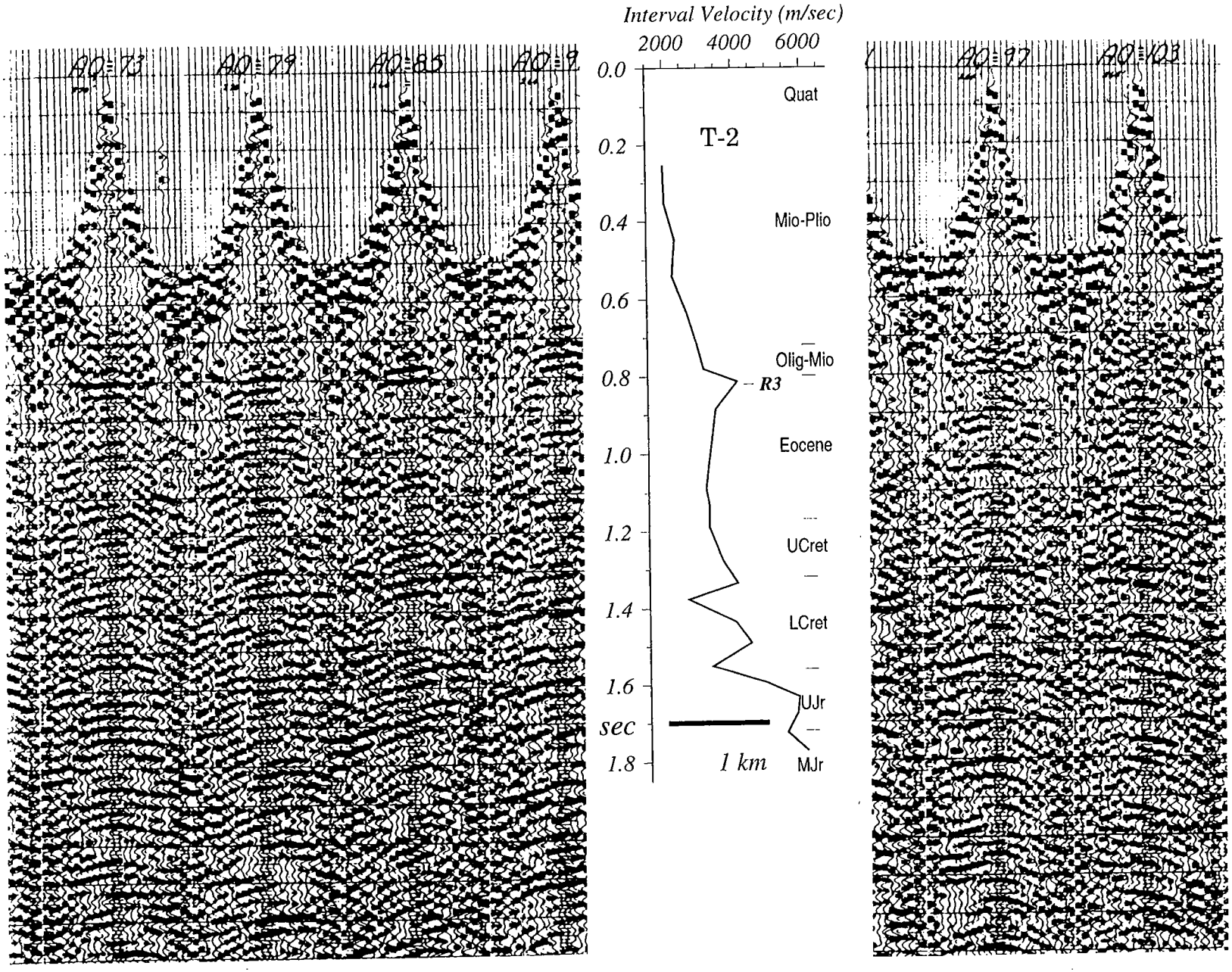

Figure 4s East-west industry multi-channel seismic profile "aq" (Area 7) across well T-2 (reflection point 92) showing interval velocities from the sonic log. The positions of horizons R3 and R4 were extrapolated from nearby line 556. Numbers along the top of the profile are reflection points.

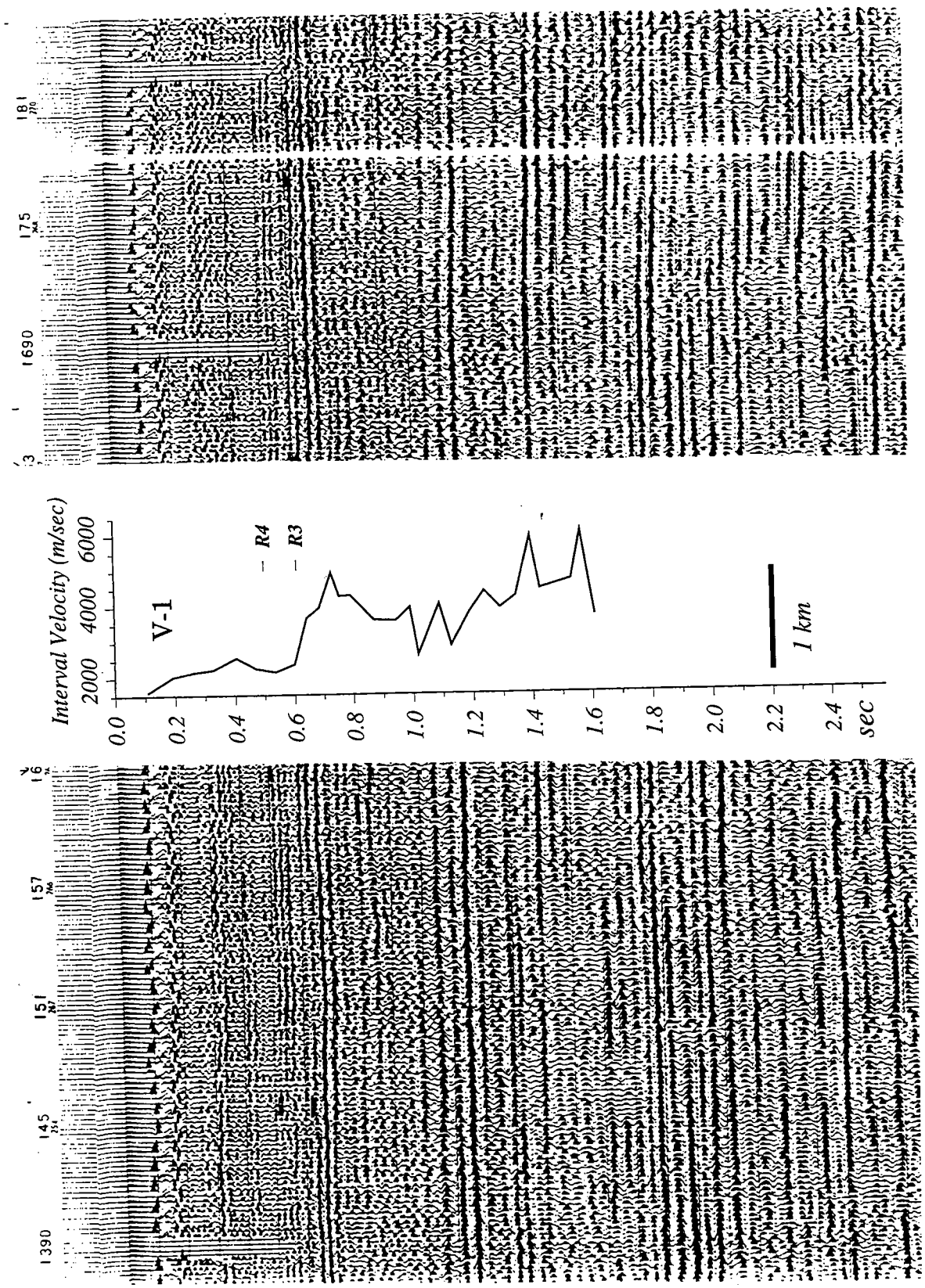

Figure 4t NW-SE industry multi-channel seismic profile 206 (Area 3) across well V-1 (reflection point 163) showing interval velocities from the sonic log and the positions of horizons R3 and R4. Numbers along the top of the profile are reflection points, and smaller numbers are water depths (ft).

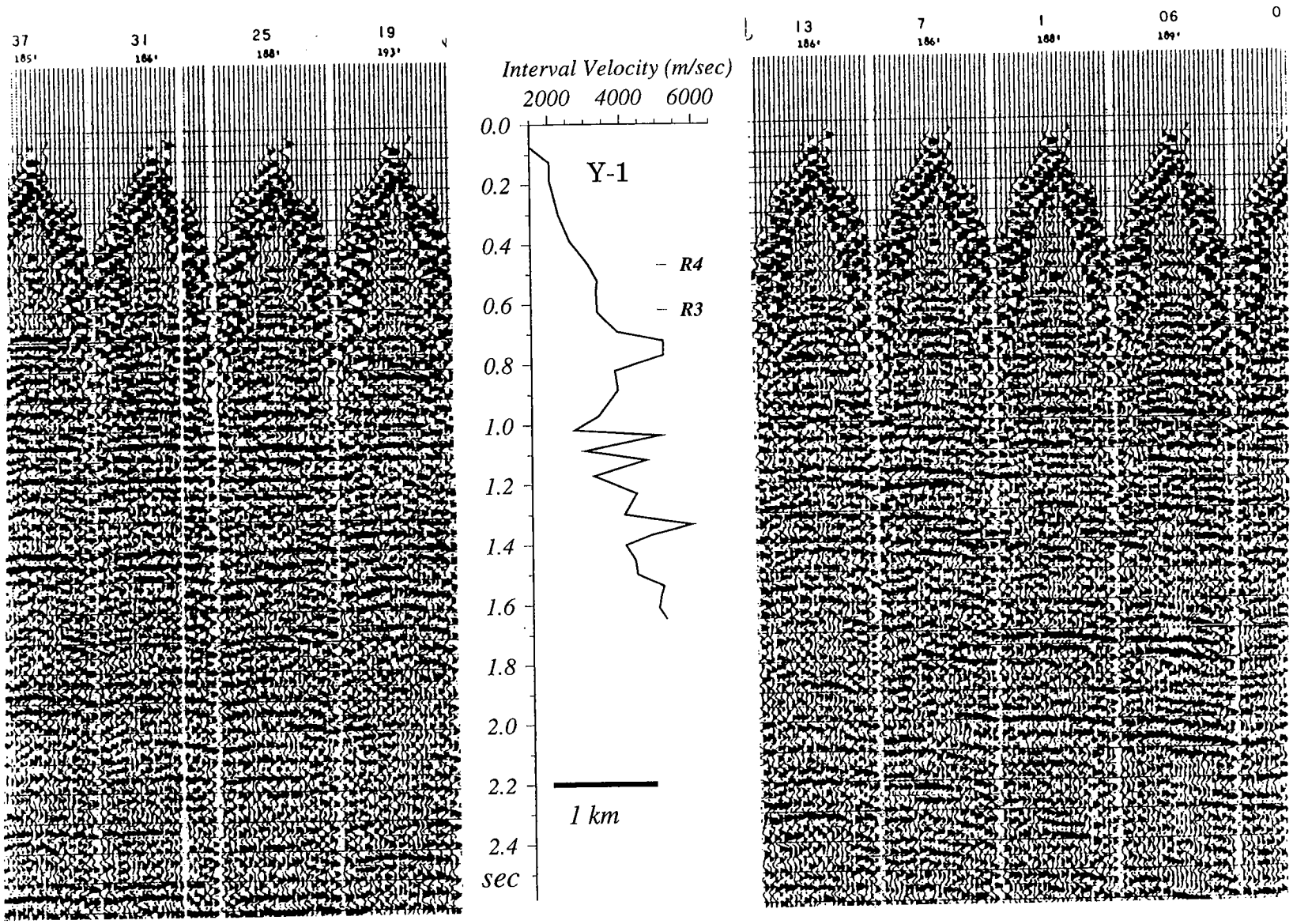

Figure 4u East-west industry multi-channel seismic profile 303 (Area 1) across well Y-1 (reflection point 16) showing interval velocities from the sonic log. The positions of horizons R3 and R4 were extrapolated from nearby lines 22 and 26 (area 8). Numbers along the top of the profile are reflection points, and smaller numbers are water depths (ft).

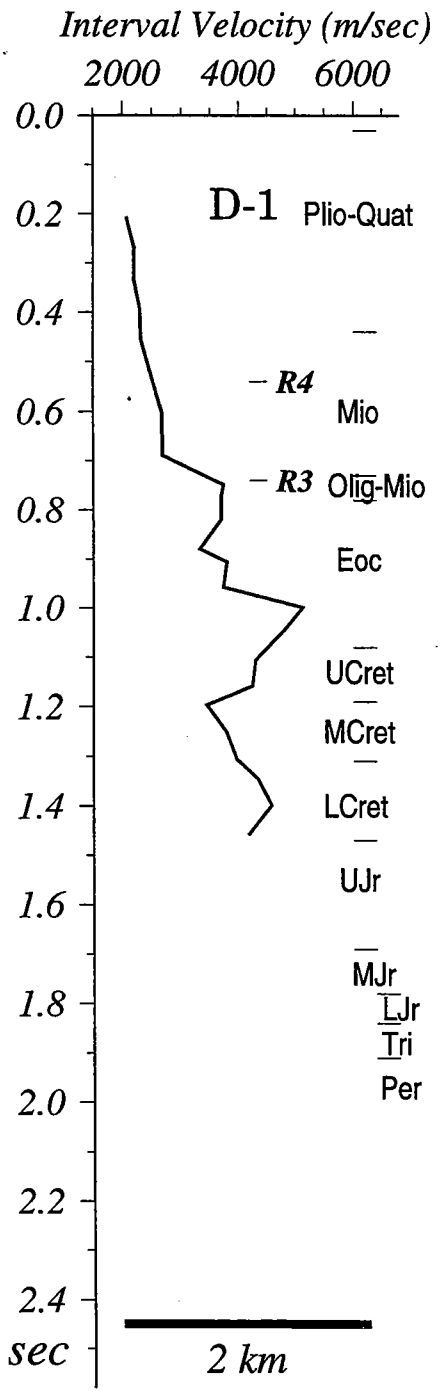

Figure 5a. Sonic log interval velocities at well D-1. The positions of horizons R3 and R4 were extrapolated from nearby line P (area 2).

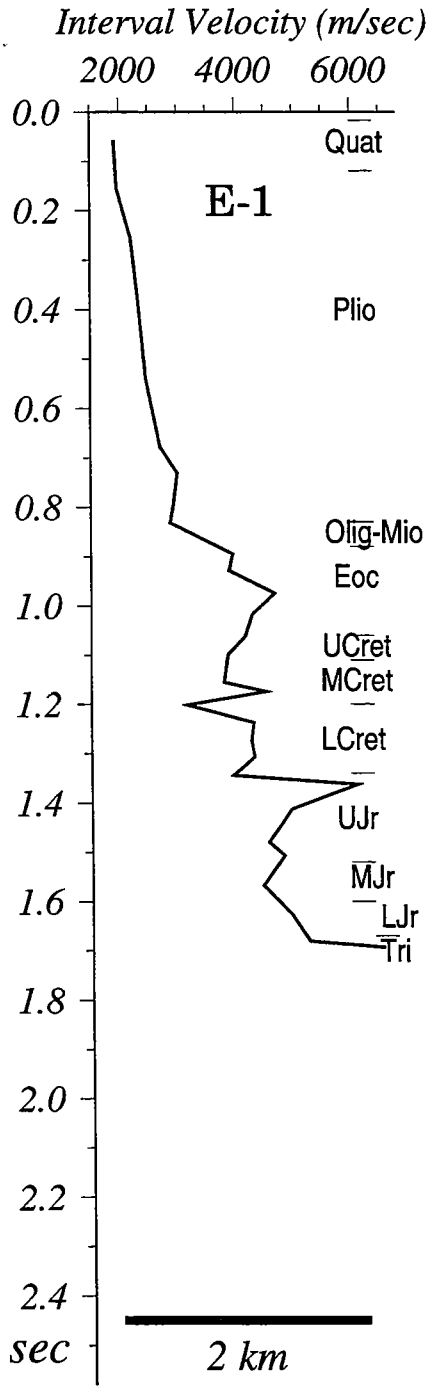

Figure 5b. Sonic log interval velocities and stratigraphy at well E-1.

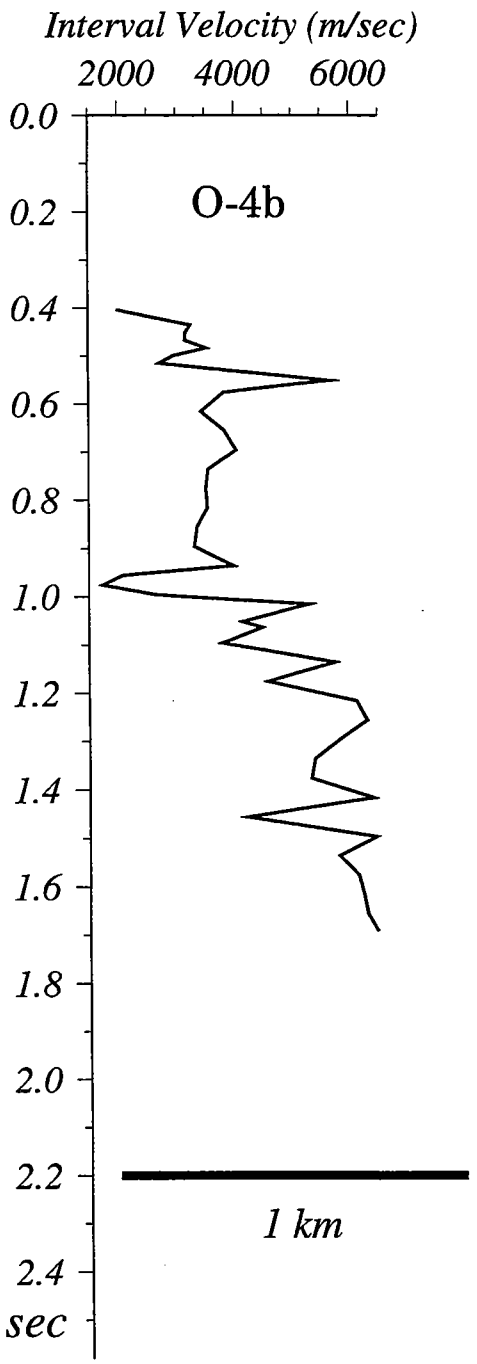

Figure 5c. Sonic log interval velocities at well O-4b.

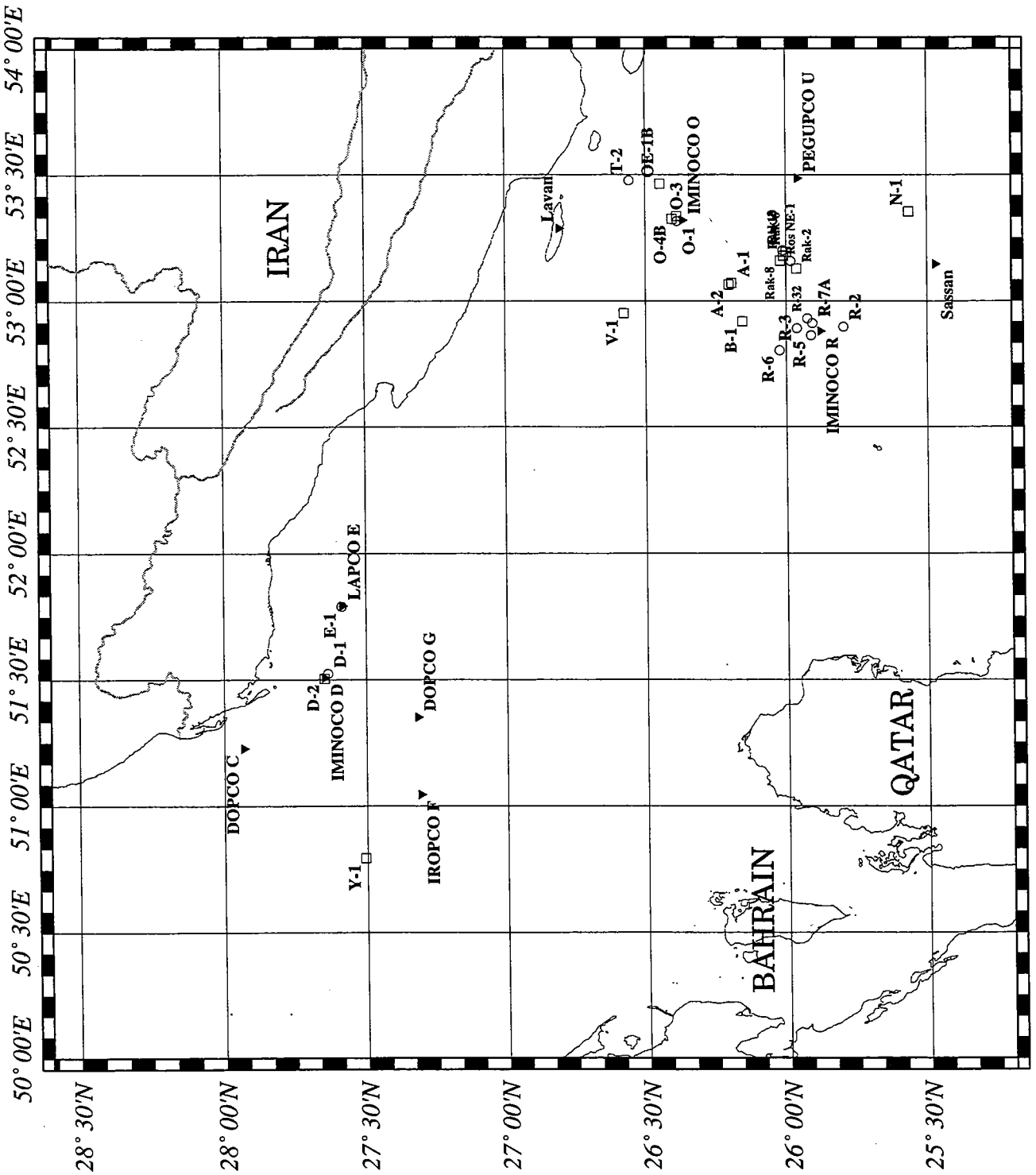

Figure 6a. Locations of central Gulf wells used in this study. Solid triangles indicate locations of well data from Mina et al. (1968). Circles indicate other wells for which we have geology information and velocity logs, whereas squares indicate wells for which only velocity data are available.

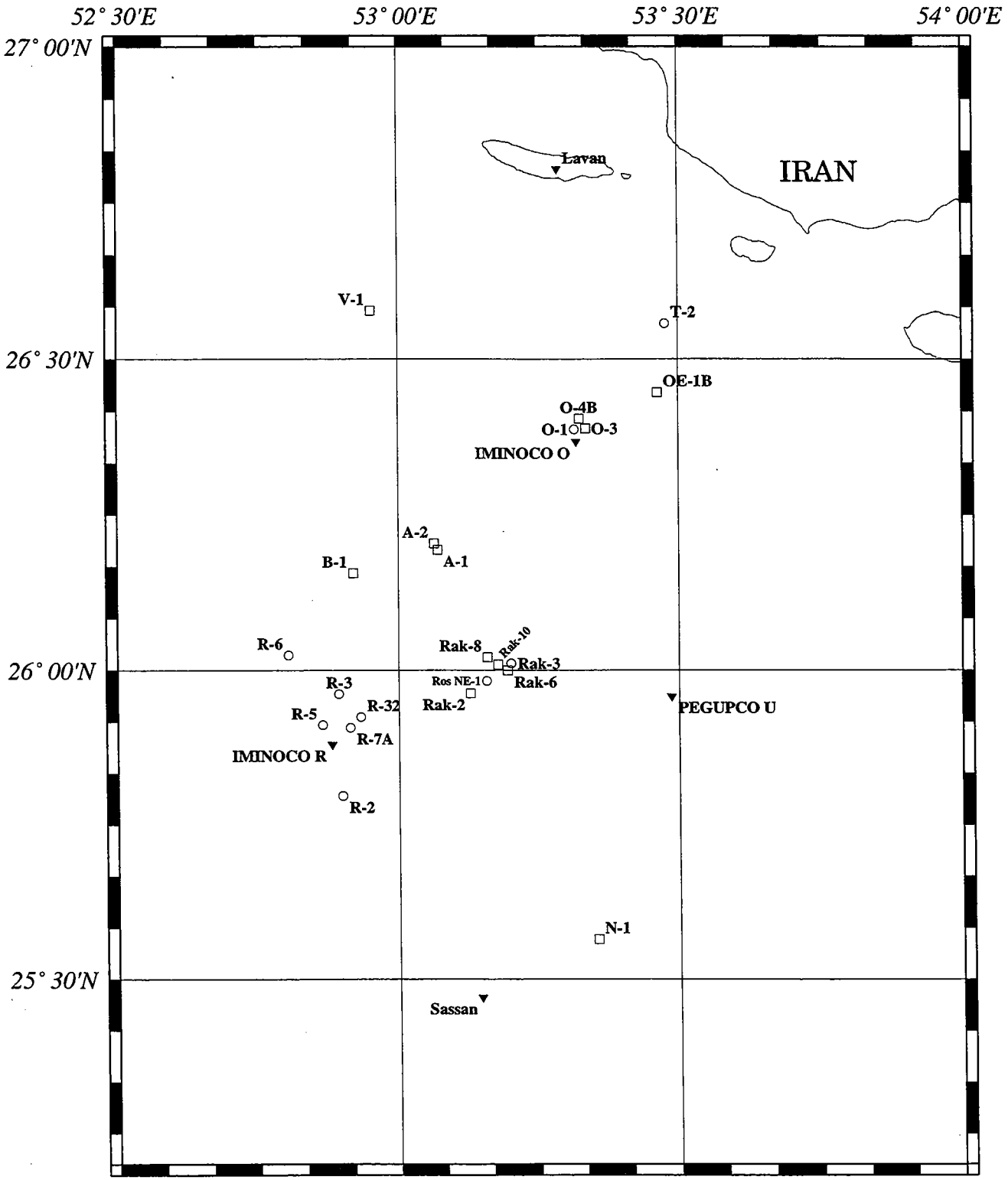

Figure 6b. Enlargement of the central Gulf in the southeast corner of Figure 6a showing locations of central Gulf wells near 53°E and 26°N that were used in this study. Symbols as in Figure 6a.

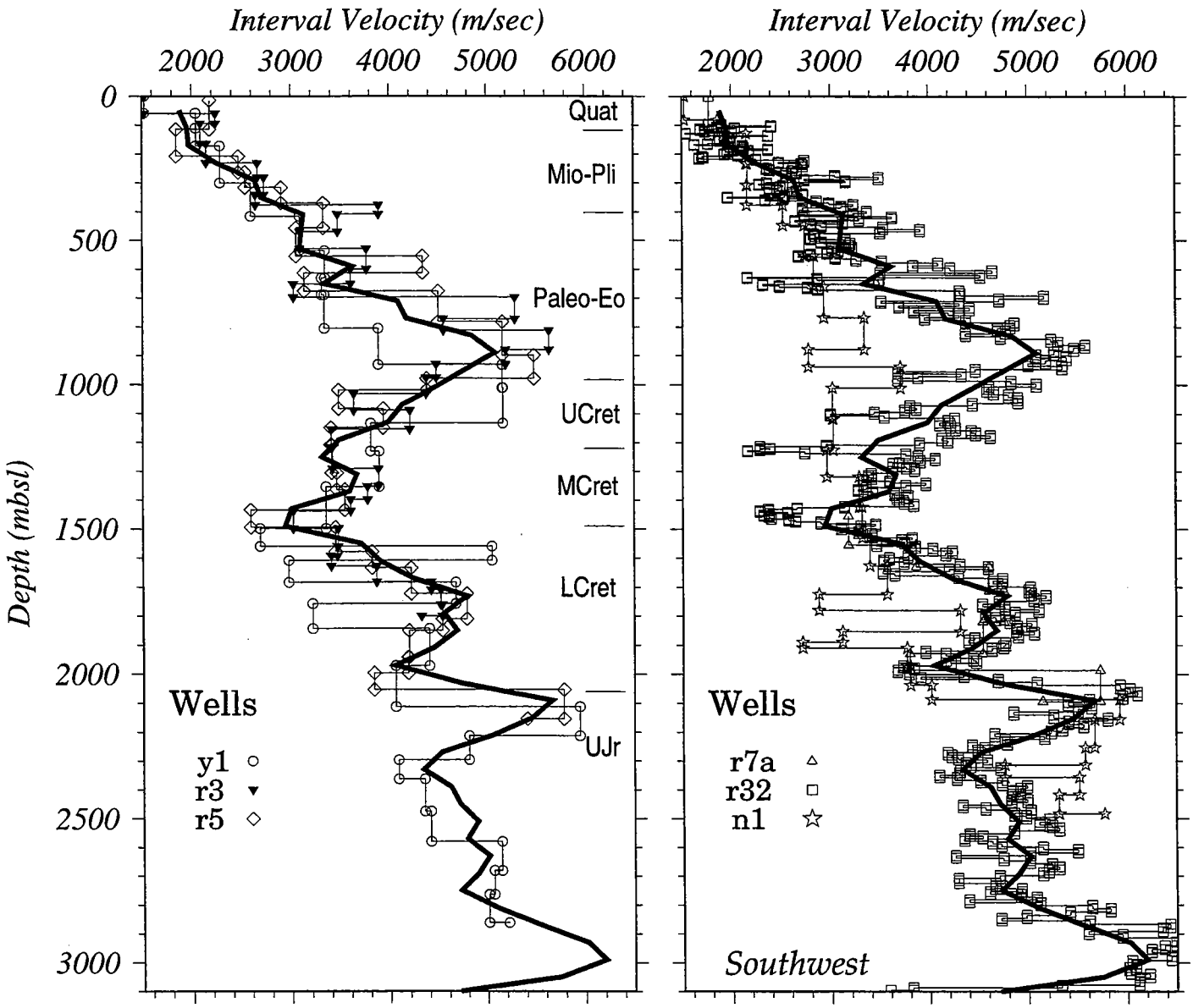

Figure 7a. Velocities (m/sec) are from sonic logs run in the southwest group of wells (1960's) and calibrated with results from check-shot surveys. Heavy line is the average of the wells in this group. Depths to geologic age datums are taken from well R-3 (filled inverted triangle).

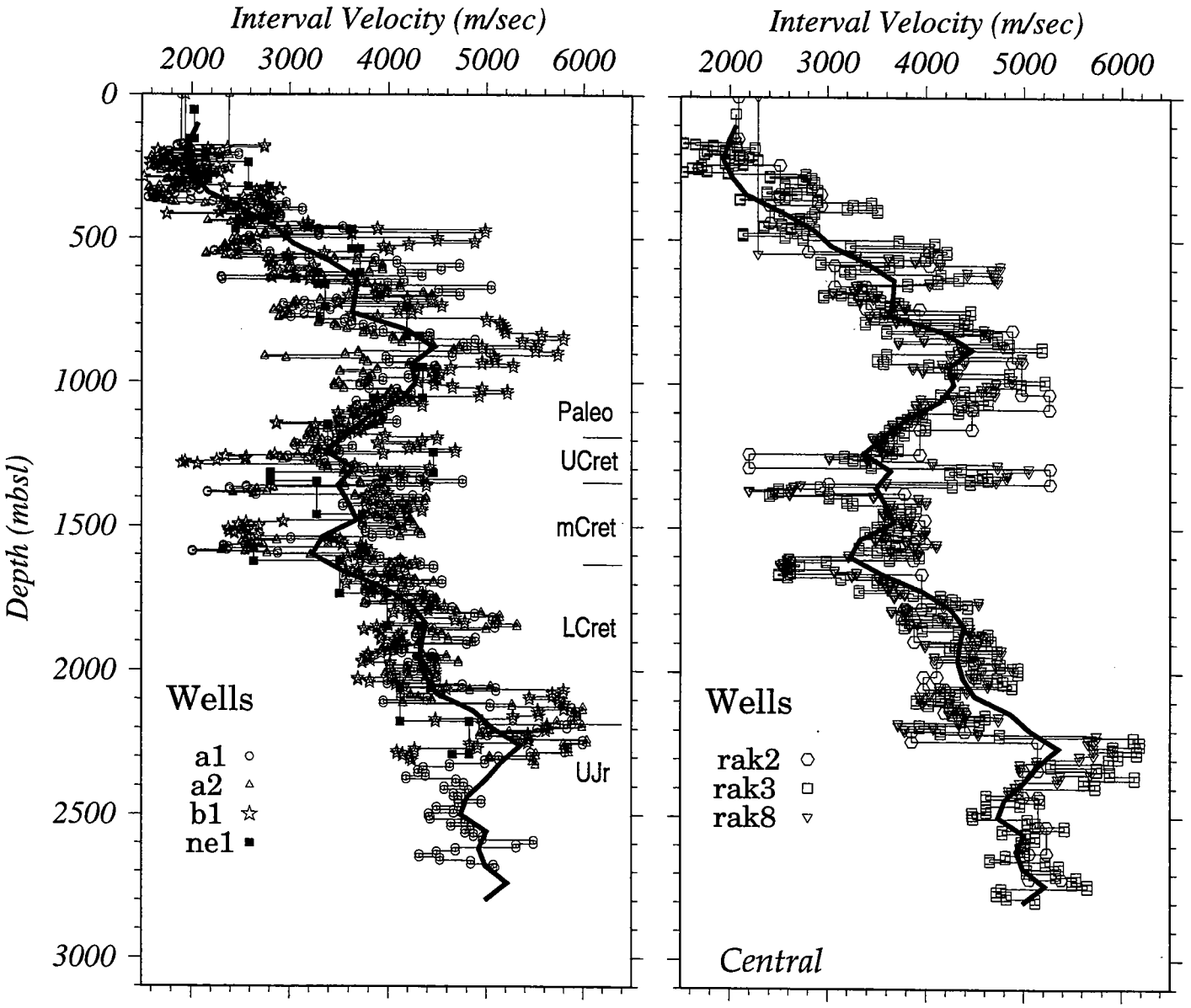

Figure 7b Velocities (m/sec) are from sonic logs run in the central group of wells (1960's) and calibrated with results from check-shot surveys. Heavy line is the average of the wells in this group. Depths to geologic age datums are taken from well NE-1 (filled square).

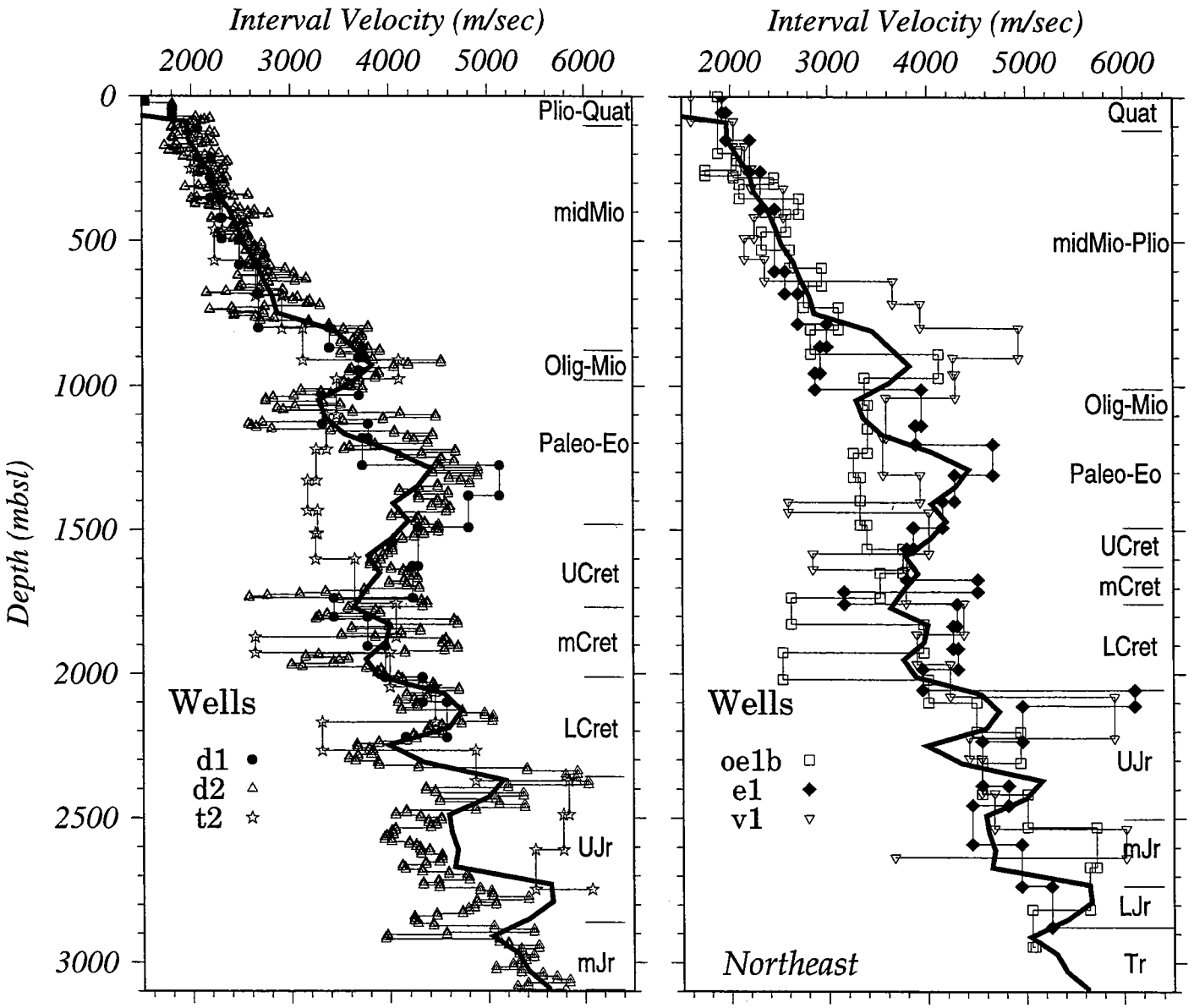

Figure 7c Velocities (m/sec) are from sonic logs run in the northeast group of industry wells (1960's) and calibrated with results from check-shot surveys. Heavy line is the average of the wells in this group. Depths to geologic age datums are taken from wells D-1 (filled circle) and E-1 (filled diamond).

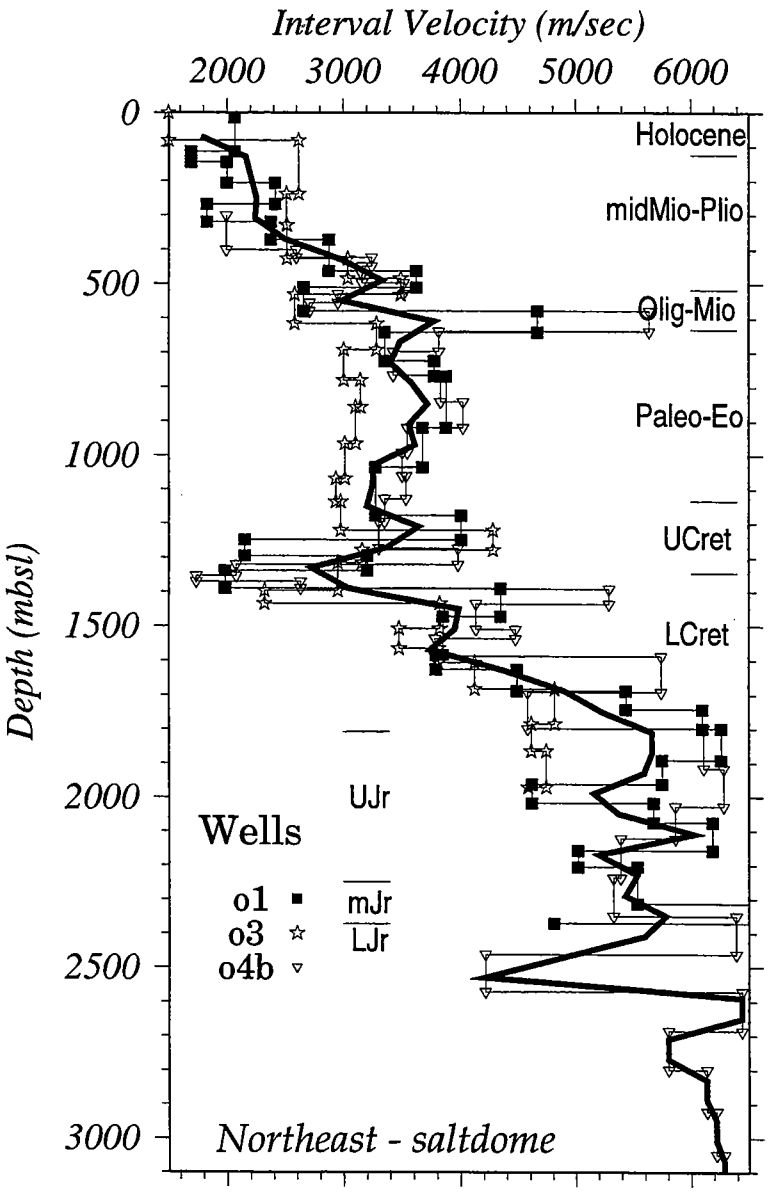

Figure 7d Velocities (m/sec) are from sonic logs run in the northeast group of wells located on the "O" salt dome and calibrated with results from check-shot surveys. Heavy line is the average of the wells in this group. Depths to geologic age datums are taken from well O-1 (filled square).

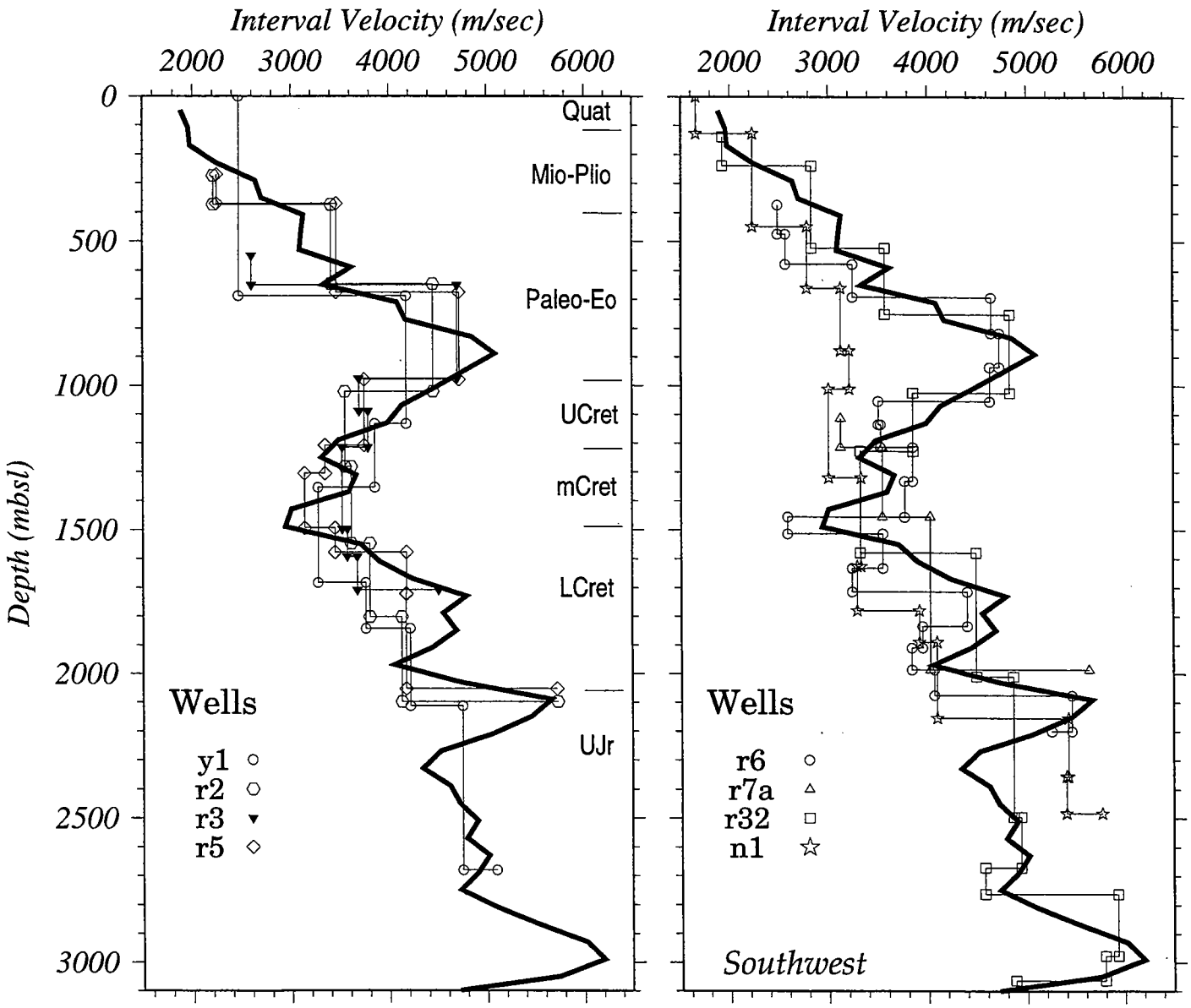

Figure 8a. Interval velocities (m/sec) are from check-shot surveys in the southwest group of wells. Heavy lines indicate the average velocity profile from the sonic logs (Figure 7a). Depths to geologic age datums are taken from the well R-3 (filled inverted triangle).

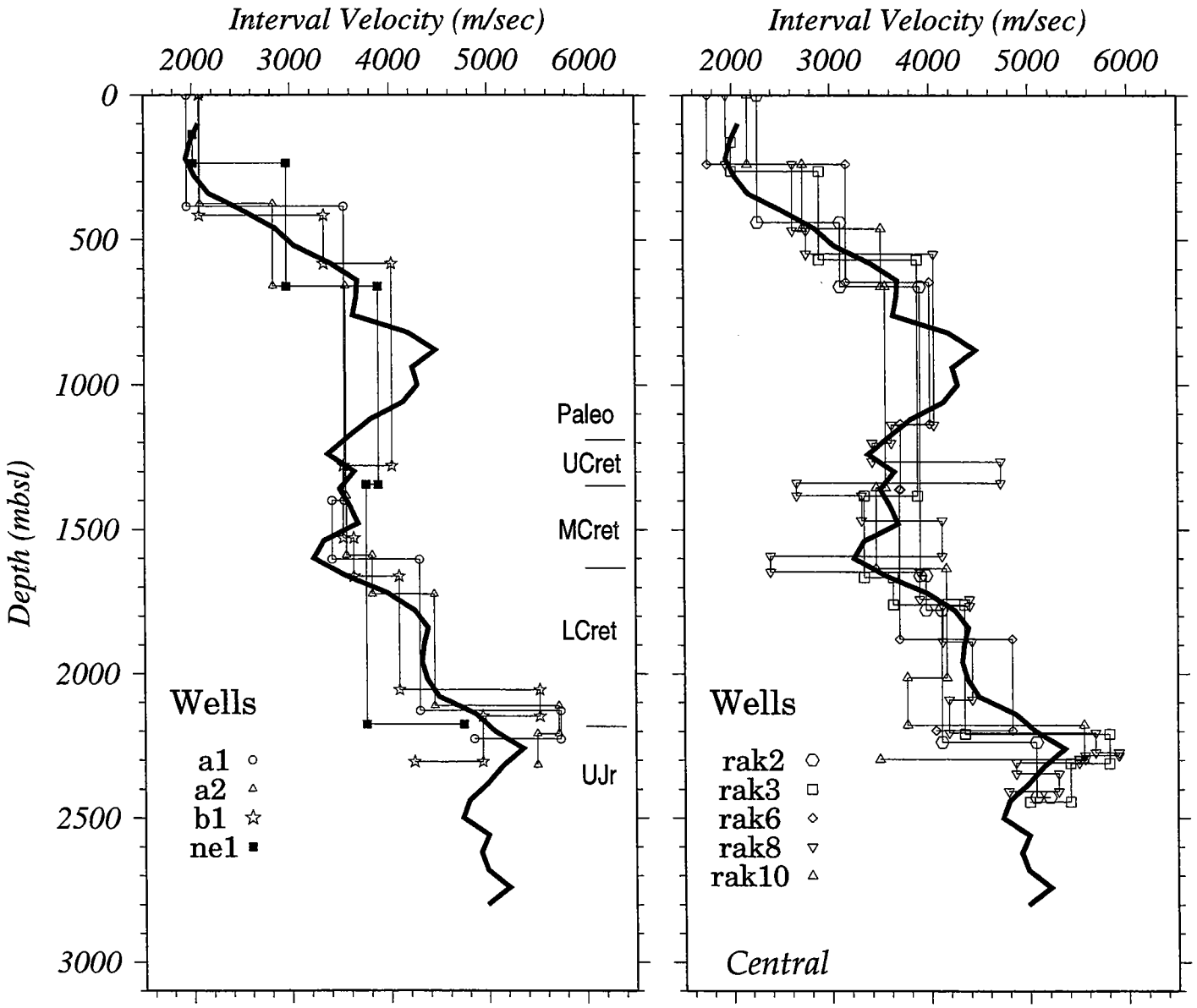

Figure 8b Interval velocities (m/sec) are from check-shot surveys in the central group of wells. Heavy lines indicate the average velocity profile from the sonic logs (Figure 7b). Depths to geologic age datums are taken from the well NE-1 (filled square).

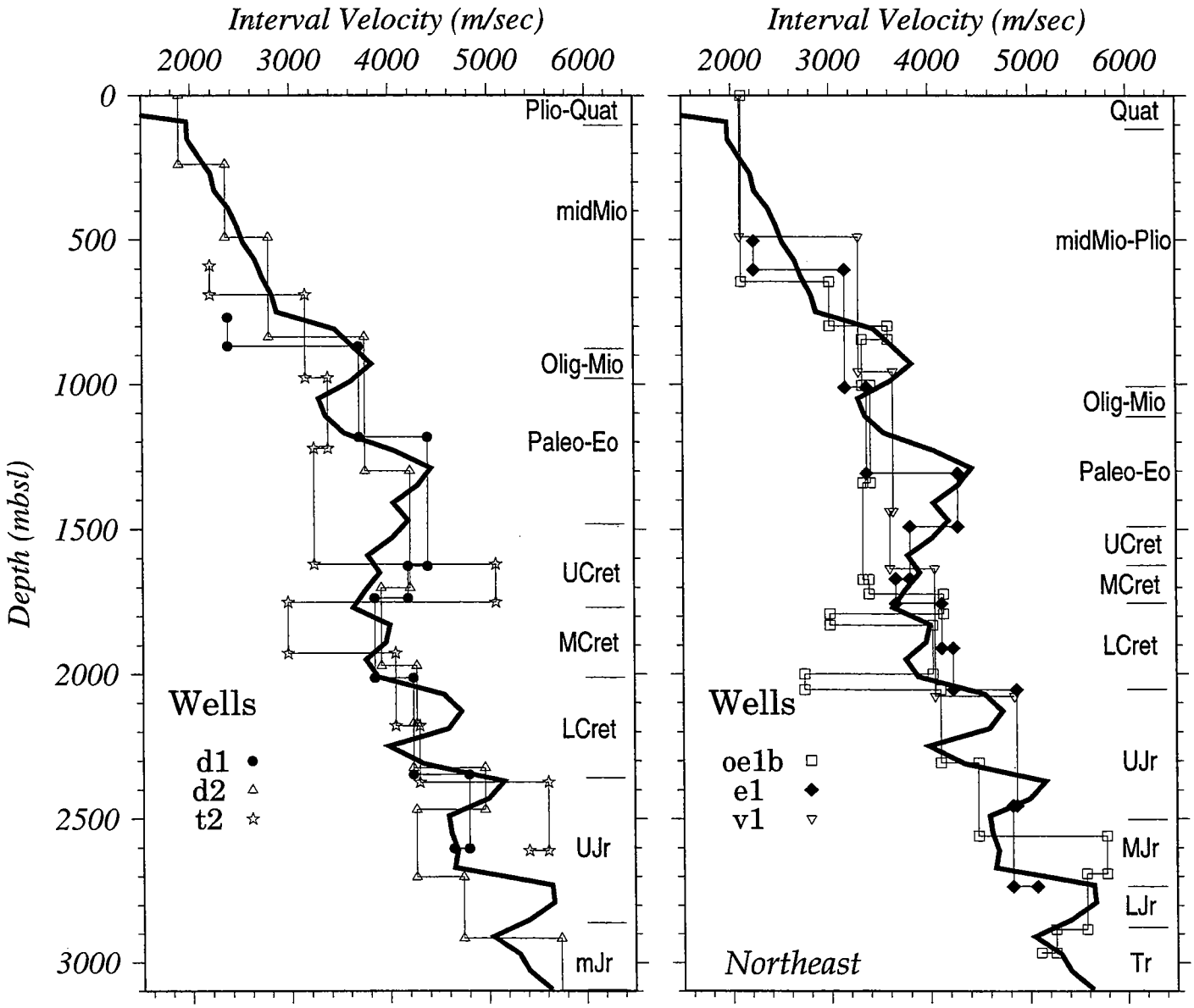

Figure 8c Interval velocities (m/sec) are from check-shot surveys in the northeast group of wells. Heavy lines indicate the average velocity profile from the sonic logs (Figure 7c). Depths to geologic age datums are taken from wells D-1 (filled circle) and E-1 (filled diamond).

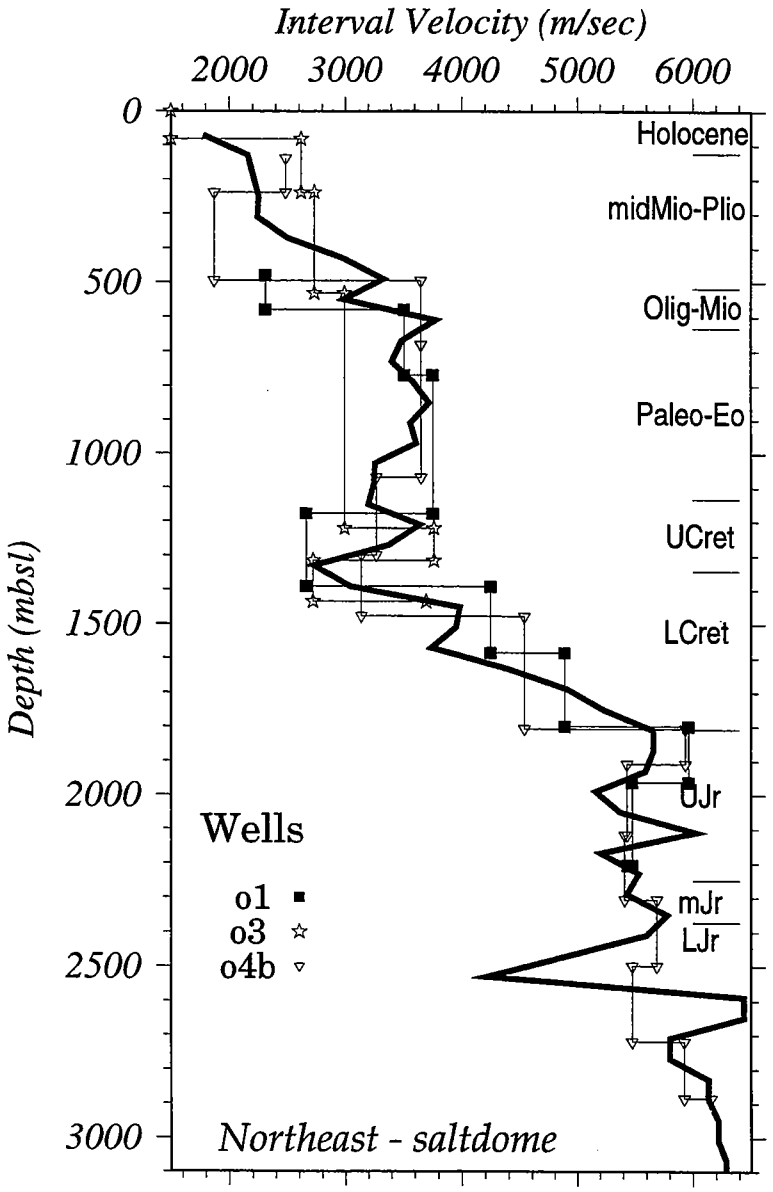

Figure 8d Interval velocities (m/sec) are from check-shot surveys in the northeast group of wells located on the "O" salt dome. Heavy line indicates the average velocity profile from the sonic logs (Figure 7c). Depths to geologic age datums are taken from the well O-1 (filled square).

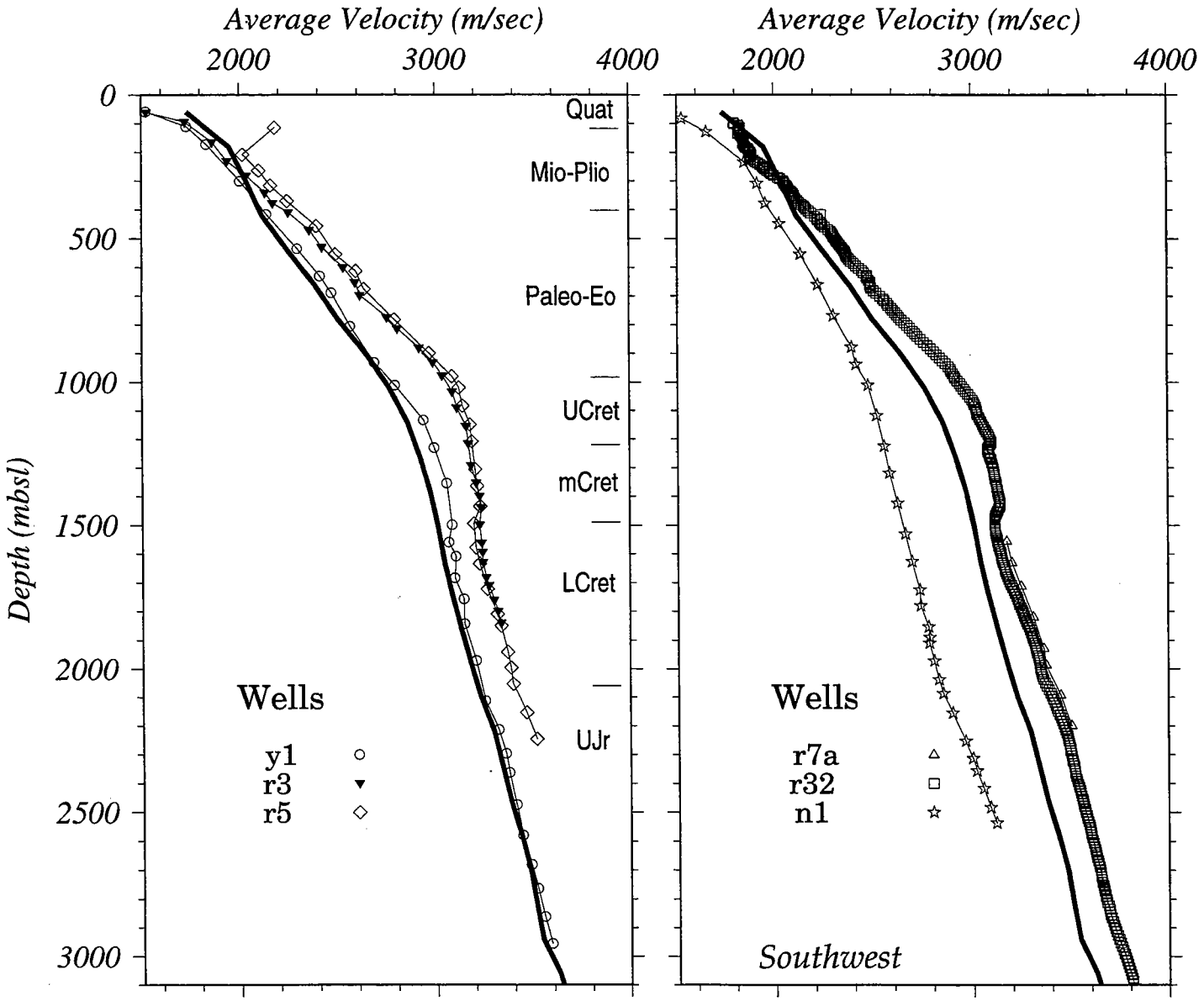

Figure 9a. "Average" velocities (m/sec) are from sonic logs run in the southwest group of wells and calibrated with results from check-shot surveys. Heavy lines are the average of *all* wells for which data were available. Depths to geologic age datums are taken from the well R-3 (filled inverted triangle).

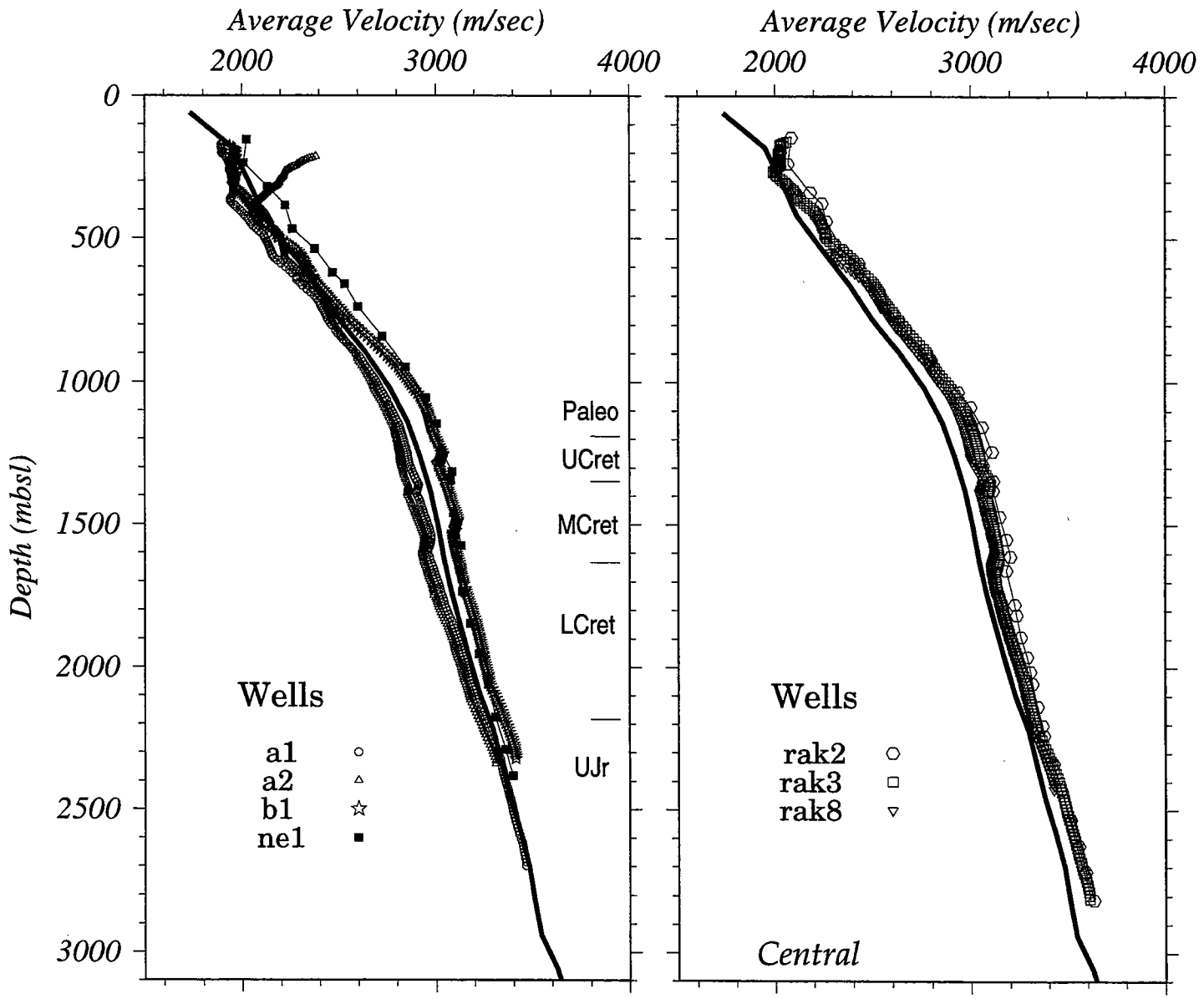

Figure 9b "Average" velocities (m/sec) are from sonic logs run in the central group of wells and calibrated with results from check-shot surveys. Heavy lines are the average of *all* wells for which data were available. Depths to geologic age datums are taken from the well NE-1 (filled square).

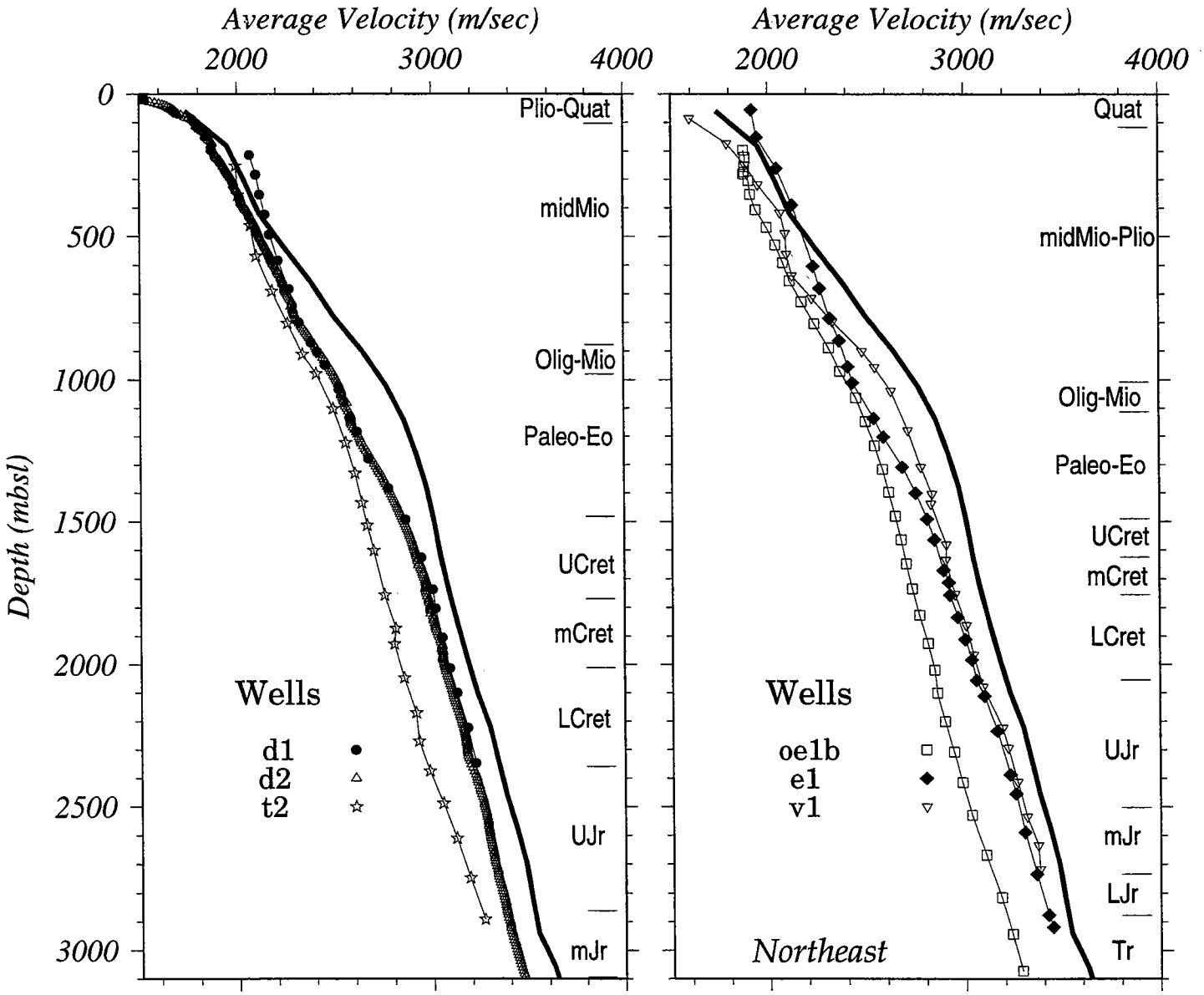

Figure 9c "Average" velocities (m/sec) are from sonic logs run in the northeast group of wells and calibrated with results from check-shot surveys. Heavy lines are the average of *all* wells for which data were available. Depths to geologic age datums are taken from wells D-1 (filled circle) and E-1 (filled diamond).

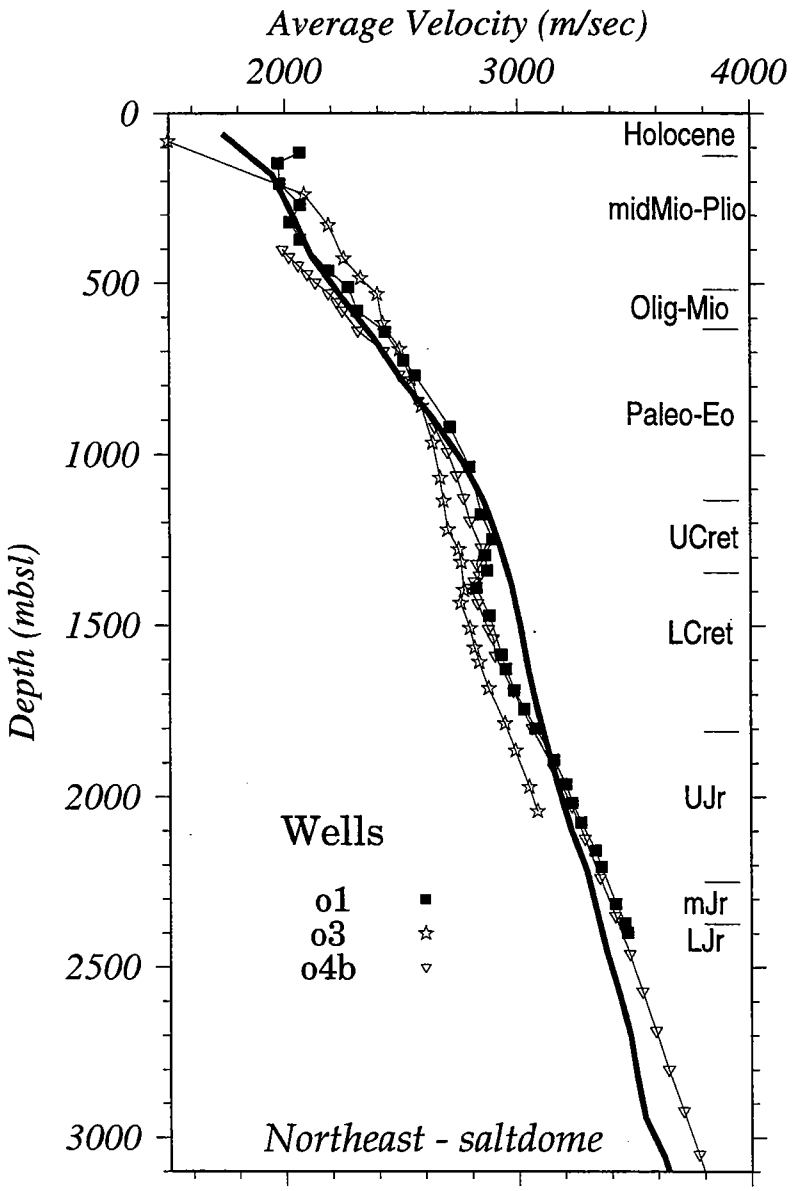

Figure 9d "Average" velocities (m/sec) are from sonic logs run in the northeast group of wells located on the "O" salt dome and calibrated with results from check-shot surveys. Heavy line is the average of *all* wells for which data were available. Depths to geologic age datums are taken from the well O-1 (filled square).

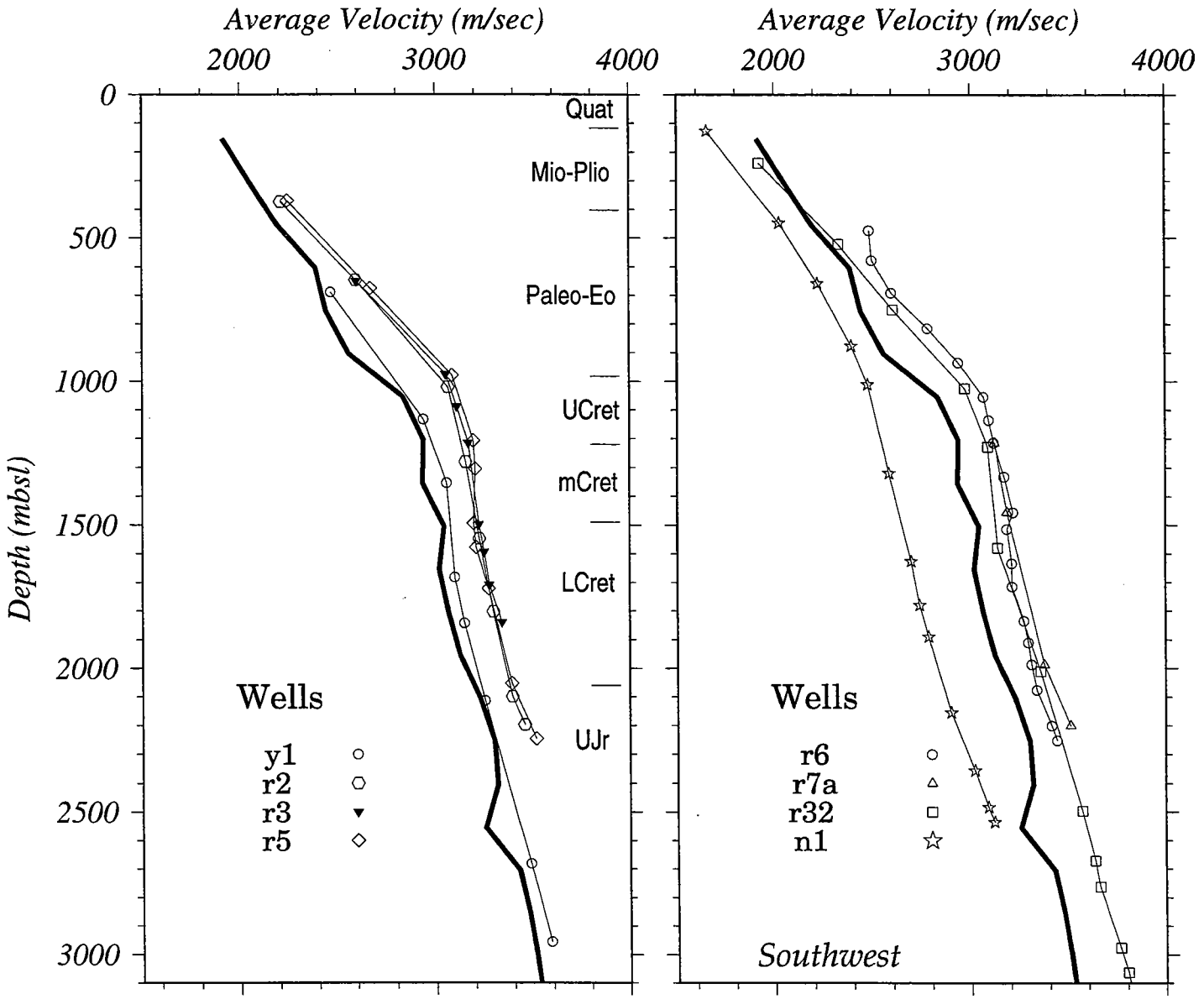

Figure 10a. "Average" velocities (m/sec) are from check-shot surveys run in the southwest group of wells. Heavy lines are the average of sonic logs from *all* wells for which data were available. Depths to geologic age datums are taken from the well R-3 (filled inverted triangle).

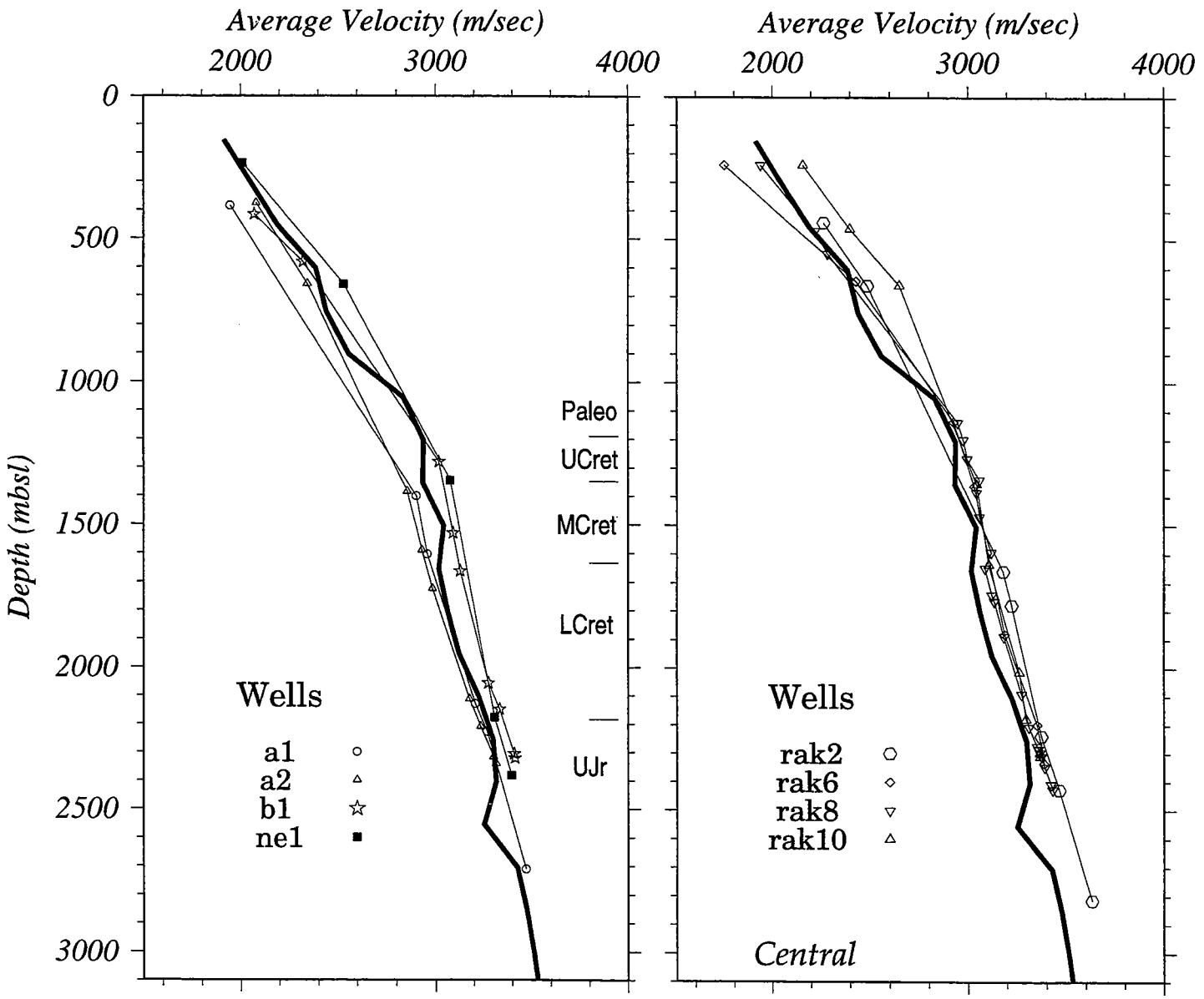

Figure 10b "Average" velocities (m/sec) are from check-shot surveys run in the central group of wells. Heavy lines are the average of sonic logs from *all* wells for which data were available. Depths to geologic age datums are taken from the well NE-1 (filled square).

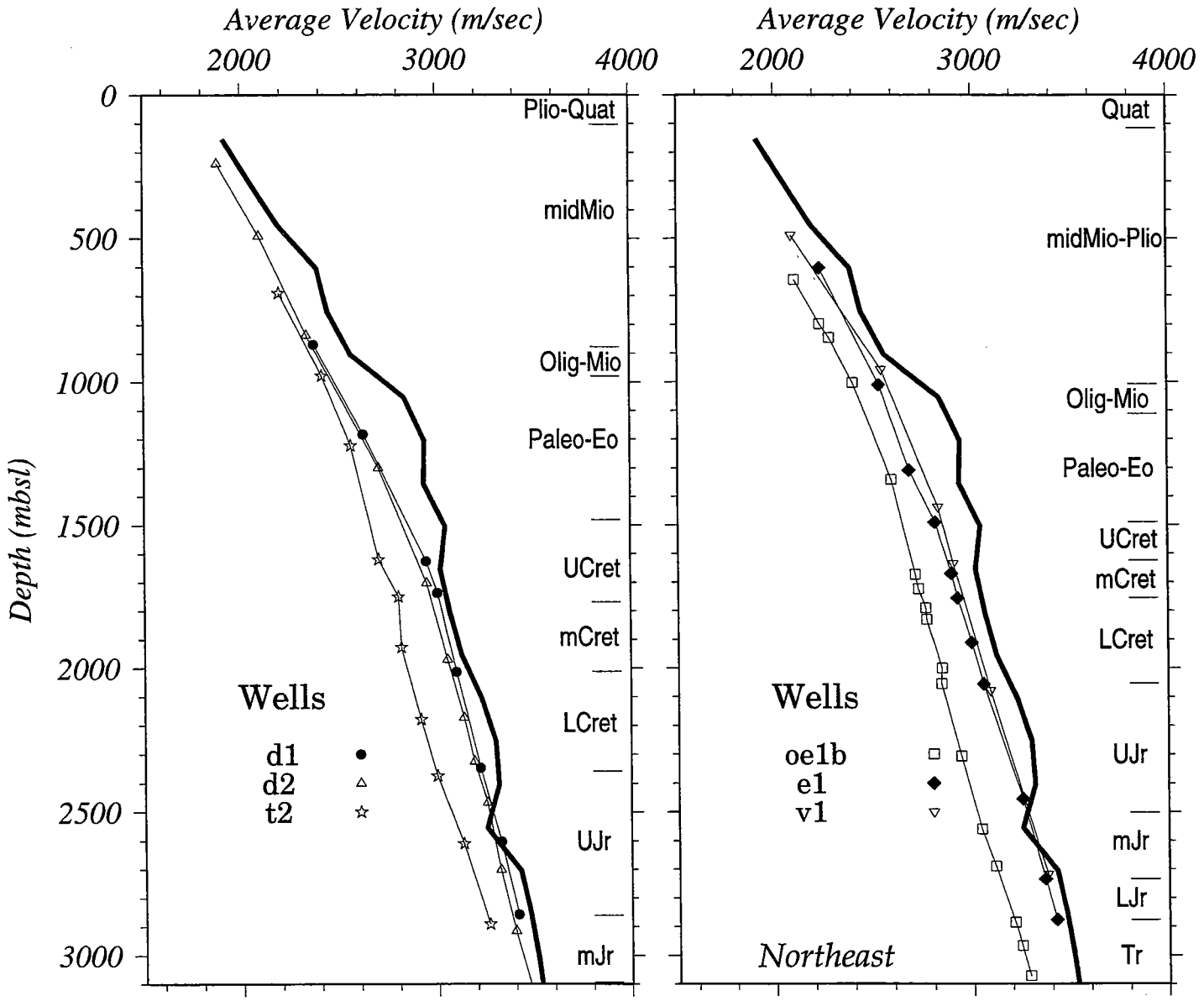

Figure 10c "Average" velocities (m/sec) are from check-shot surveys run in the northeast group of wells. Heavy lines are the average of sonic logs from *all* wells for which data were available. Depths to geologic age datums are taken from wells D-1 (filled circle) and E-1 (filled diamond).

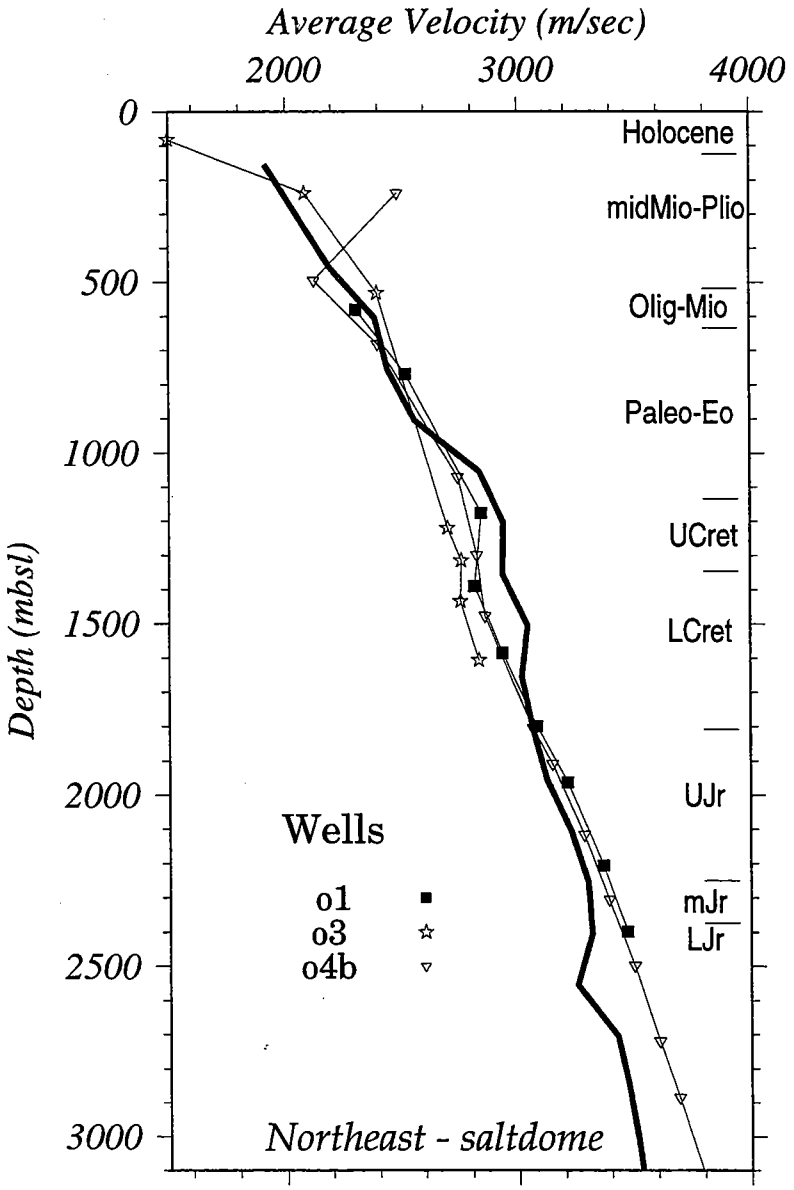

Figure 10d. "Average" velocities (m/sec) are from check-shot surveys run in the northeast group of wells located on the "O" salt dome. Heavy line is the average of sonic logs from *all* wells for which data were available. Depths to geologic age datums are taken from the well O-1 (filled square).

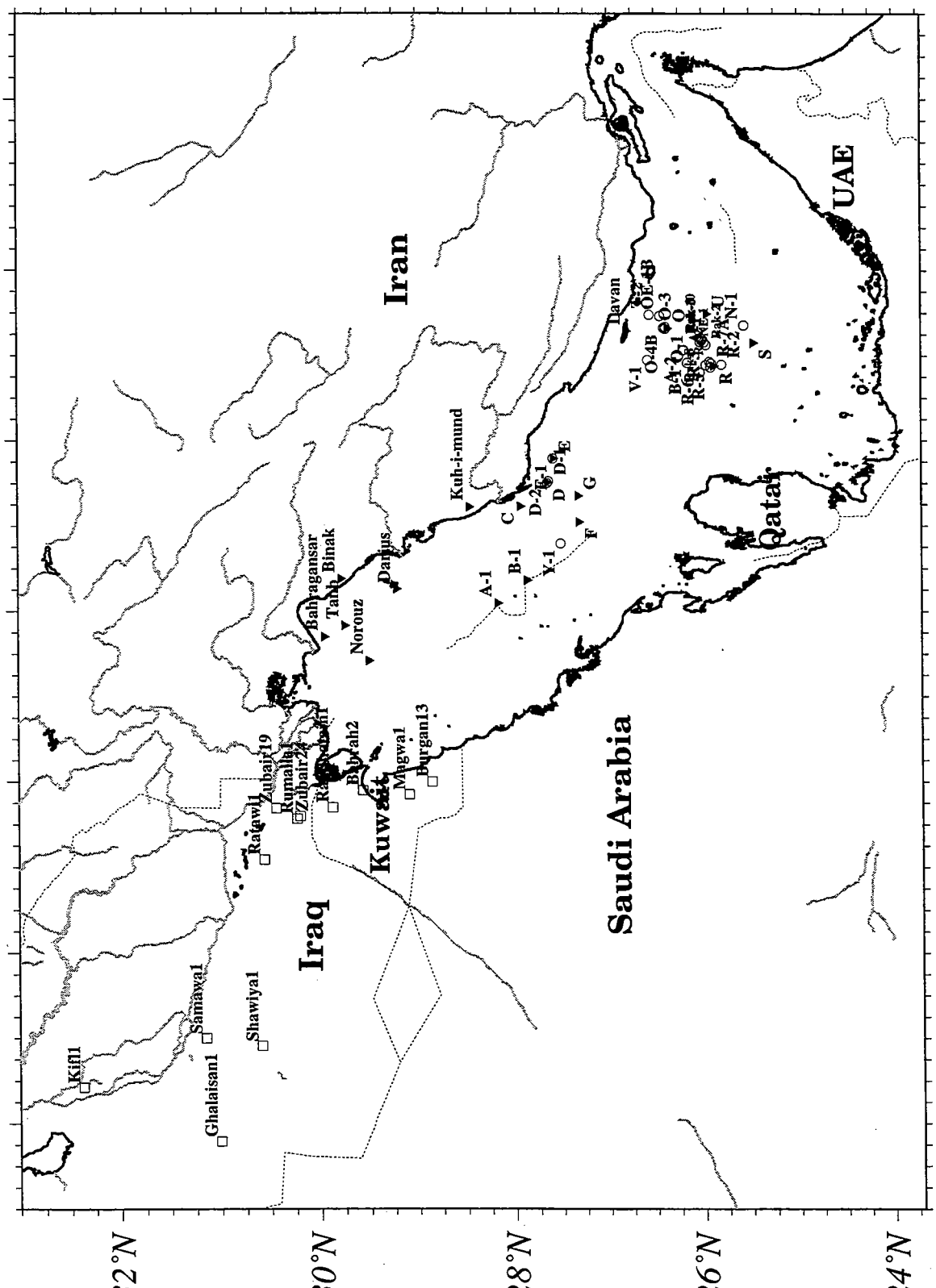

Figure 11. Locations of all wells for which data were obtained for this study. Squares indicate the locations of wells from Al-Naqib (1967). Inverted-triangles are wells from Mina et al. (1967). Circles are additional wells listed in Table 1. Solid lines on land are locations of rivers, both permanent and ephemeral, and dotted lines are political boundaries.

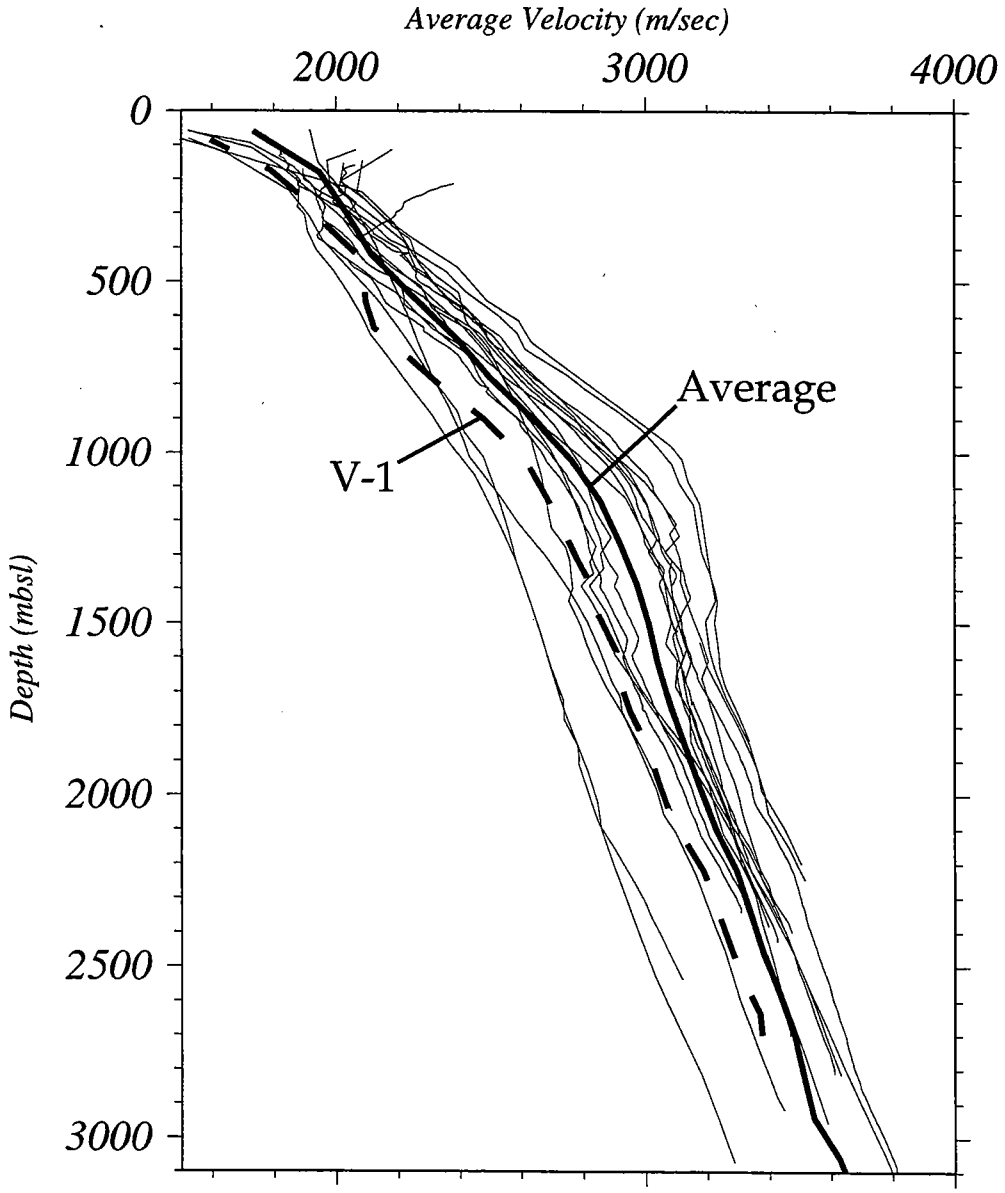

Figure 12. "Average" velocities (m/sec) profiles for all wells for which data are available. Heavy solid line in the avaerage of all data. The heavy dashed line indicates the profile from the V-1 well. The V-1 profile was used to convert depth in two-way travel time obtained from the seismic profiles to depth in meters.

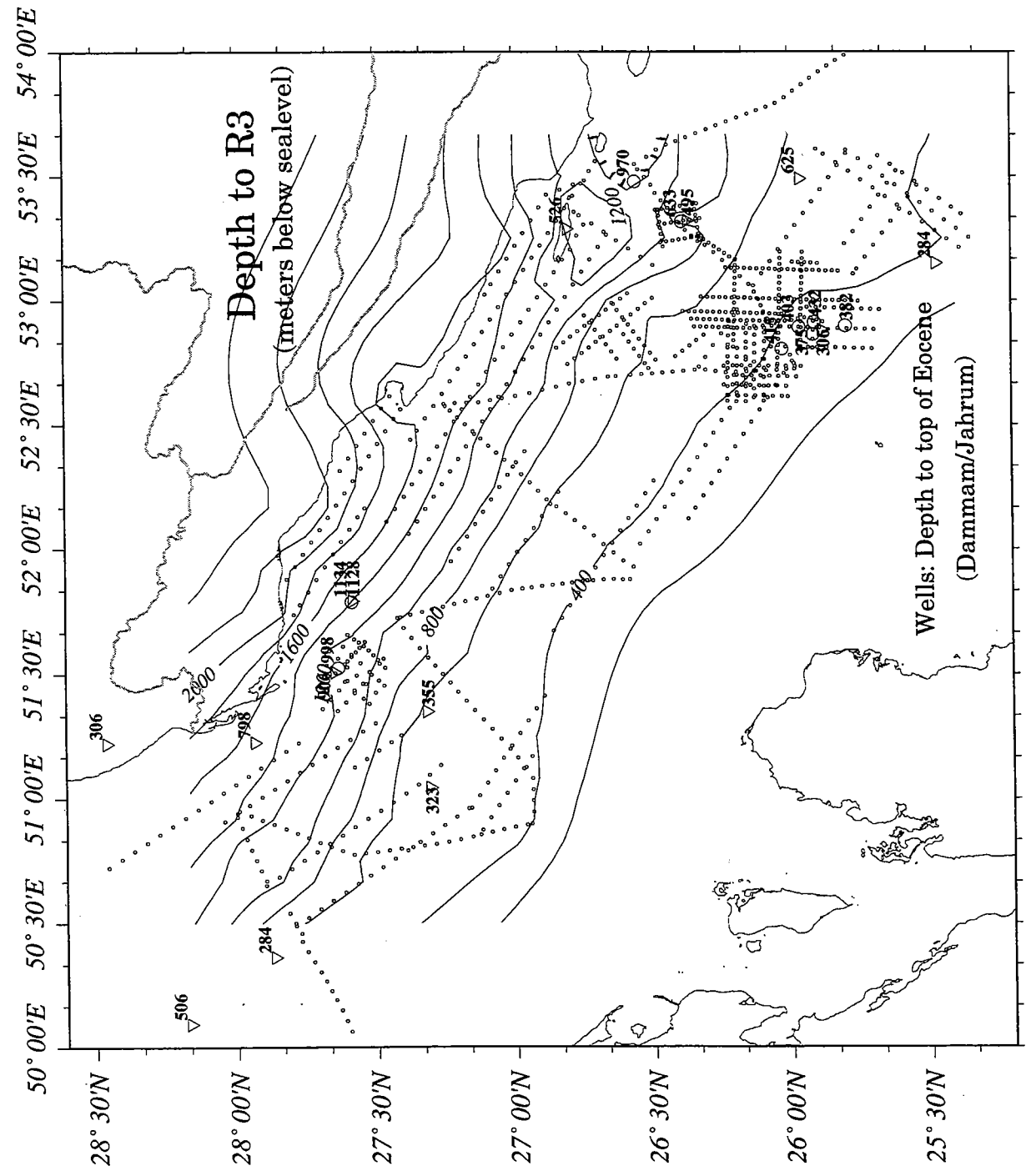

Figure 13. Depth in meters below sealevel to horizon R3, the deeper reflector traced in the seismic profiles. The surface dips monotonically to the northeast and appears to correlate to the top-of-the Eocene/Paleocene interval in seismic profiles (Fig. 4). The wells where geologic data are available are annotated with the depth to the top of the Eocene. Symbols as in Fig. 11. Contour interval is 200 m.

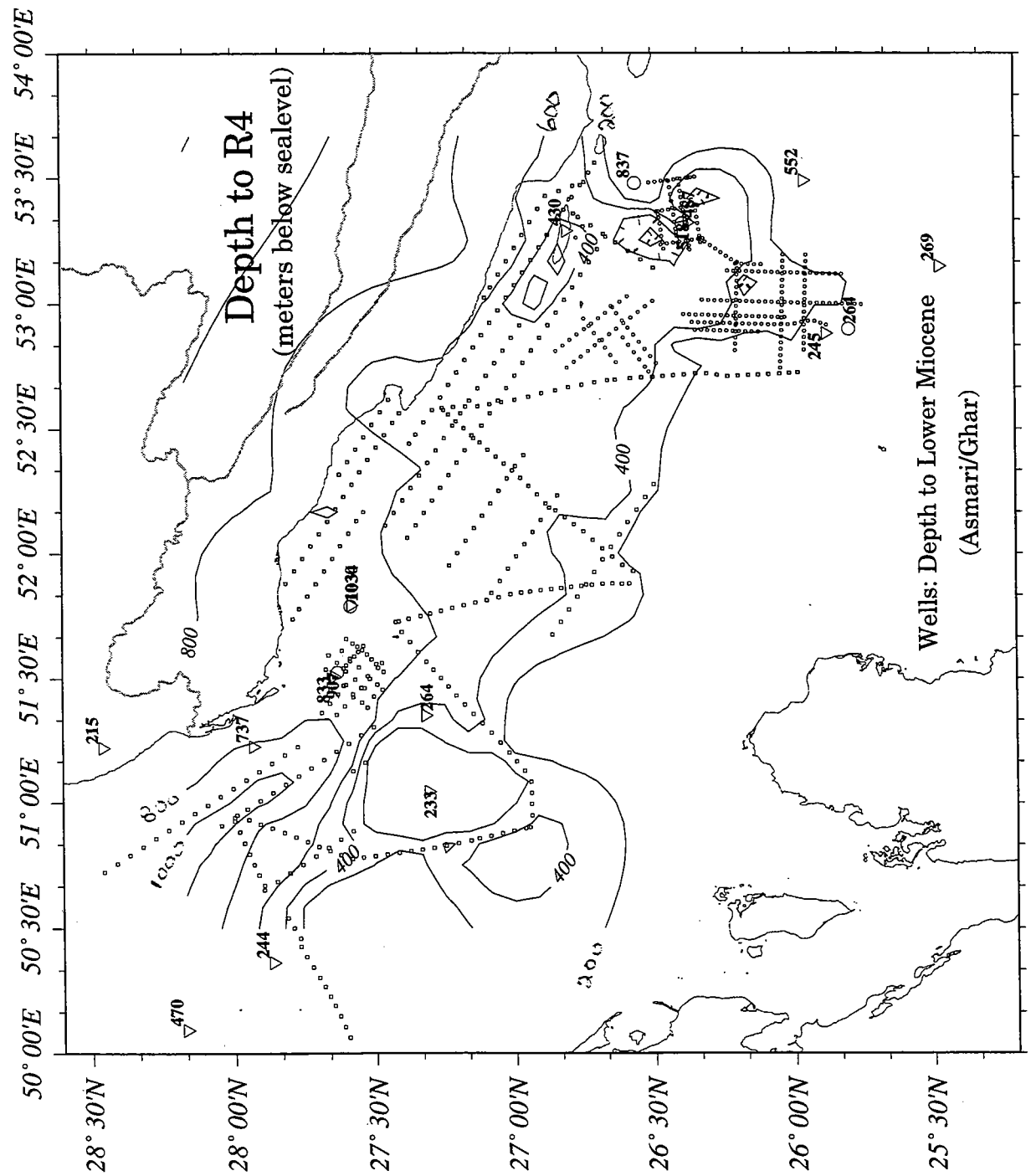

Figure 14. Depth in meters below sealevel to horizon R4, the shallowest feature that could be traced in the seismic profiles throughout the region. The surface dips to the northeast but is much more irregular than R3. R4 appears to correlate to the top-of-the lower Miocene interval in seismic profiles (Fig. 4). The wells where geologic data are available are annotated with the depth to the top of the Asmari/Ghar formations. Symbols as in Fig. 11. Contour interval is 200 m.

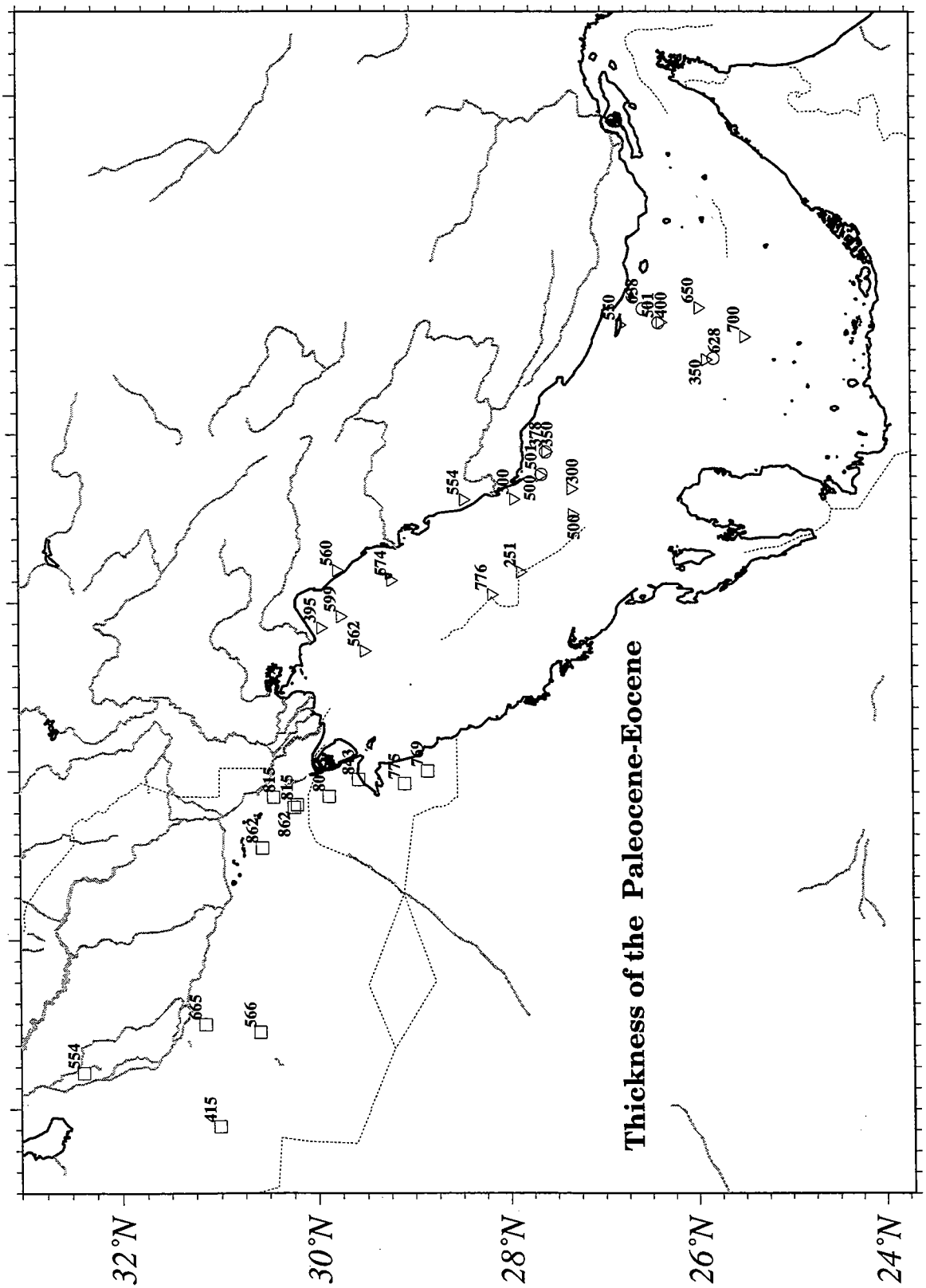

Figure 15. The thickness (meters) of the Paleocene-Eocene formations in wells indicates relatively uniform accumulation during this time. Symbols as in Fig. 11.

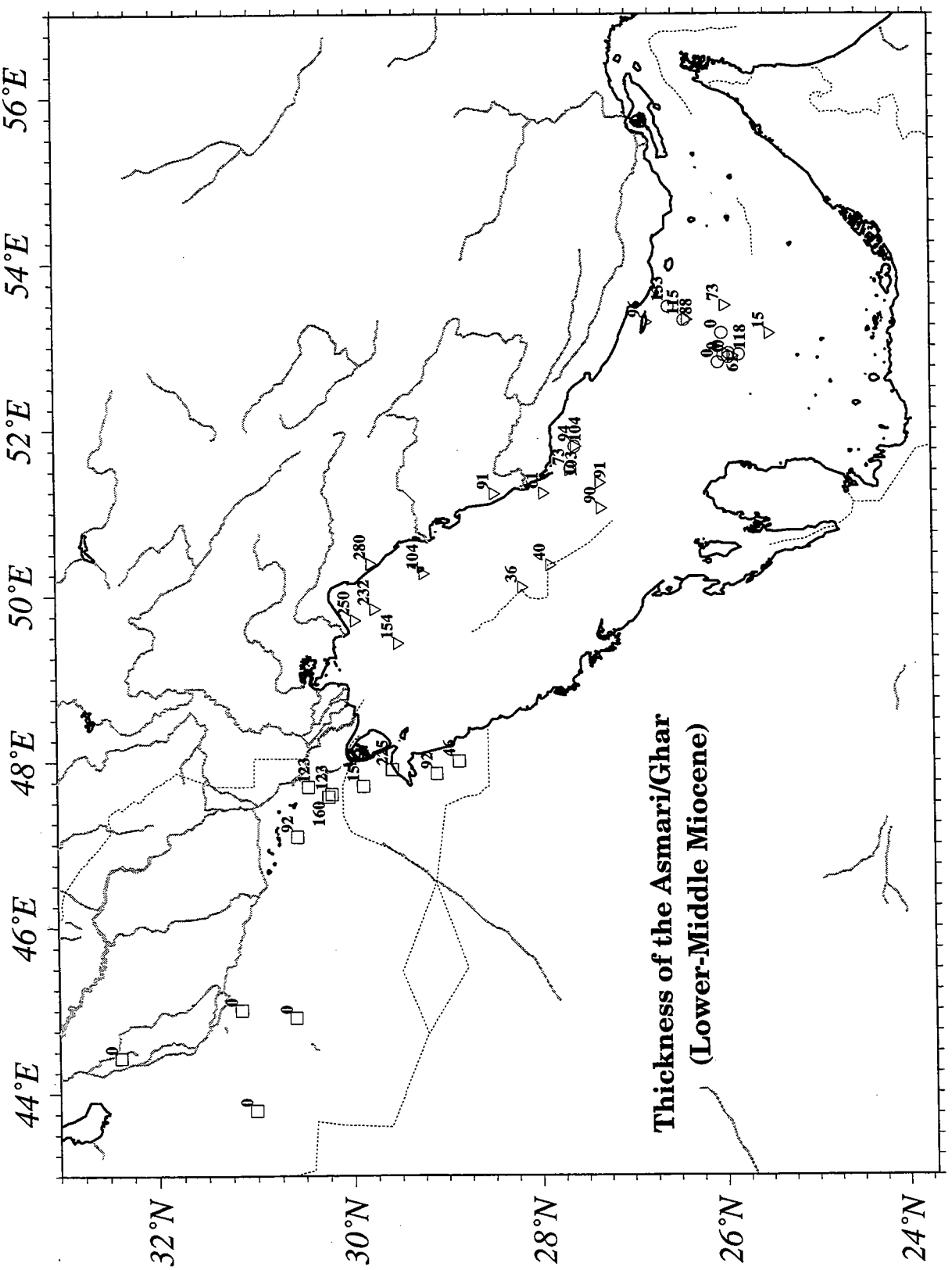

Figure 16. The thickness (meters) of the Asmari-Ghar formations (Oligocene-lower Miocene) in wells indicates relatively uniform accumulation during this time. Symbols as in Fig. 11. Zero values in the northwest indicate removal of the unit by erosion. Zero values in the southeast indicate wells where the stratigraphy is insufficient to resolve the unit.

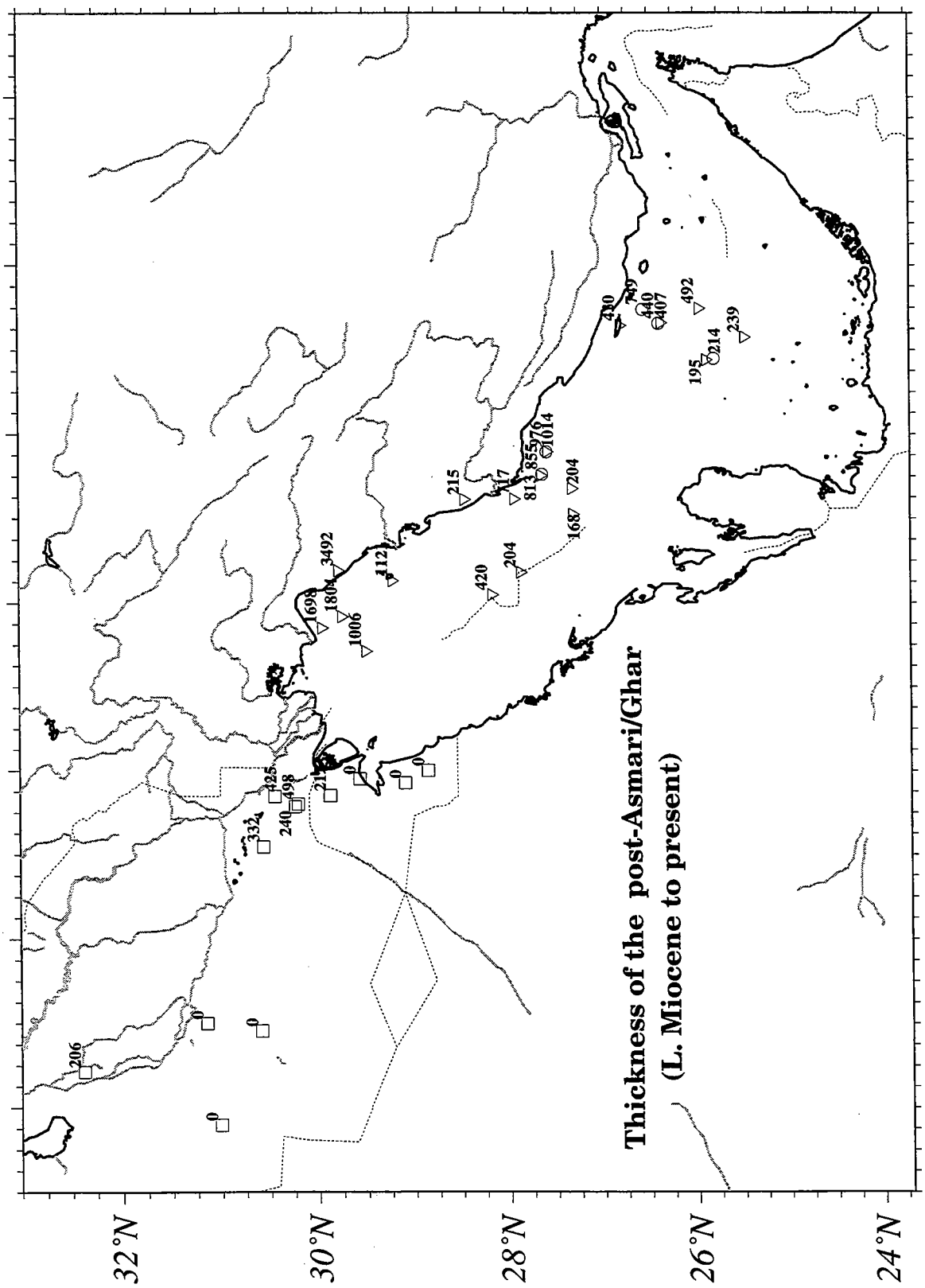

Figure 17. The thickness (meters) of the interval between the Asmari/Ghar (Oligocene-lower Miocene) and the seafloor increases to the northeast reflecting accumulation of clastic sediment transported from the Zagros Mountains that developed during this time. Zero values in the northwest indicate removal of the unit by erosion. Symbols as in Figure 11.

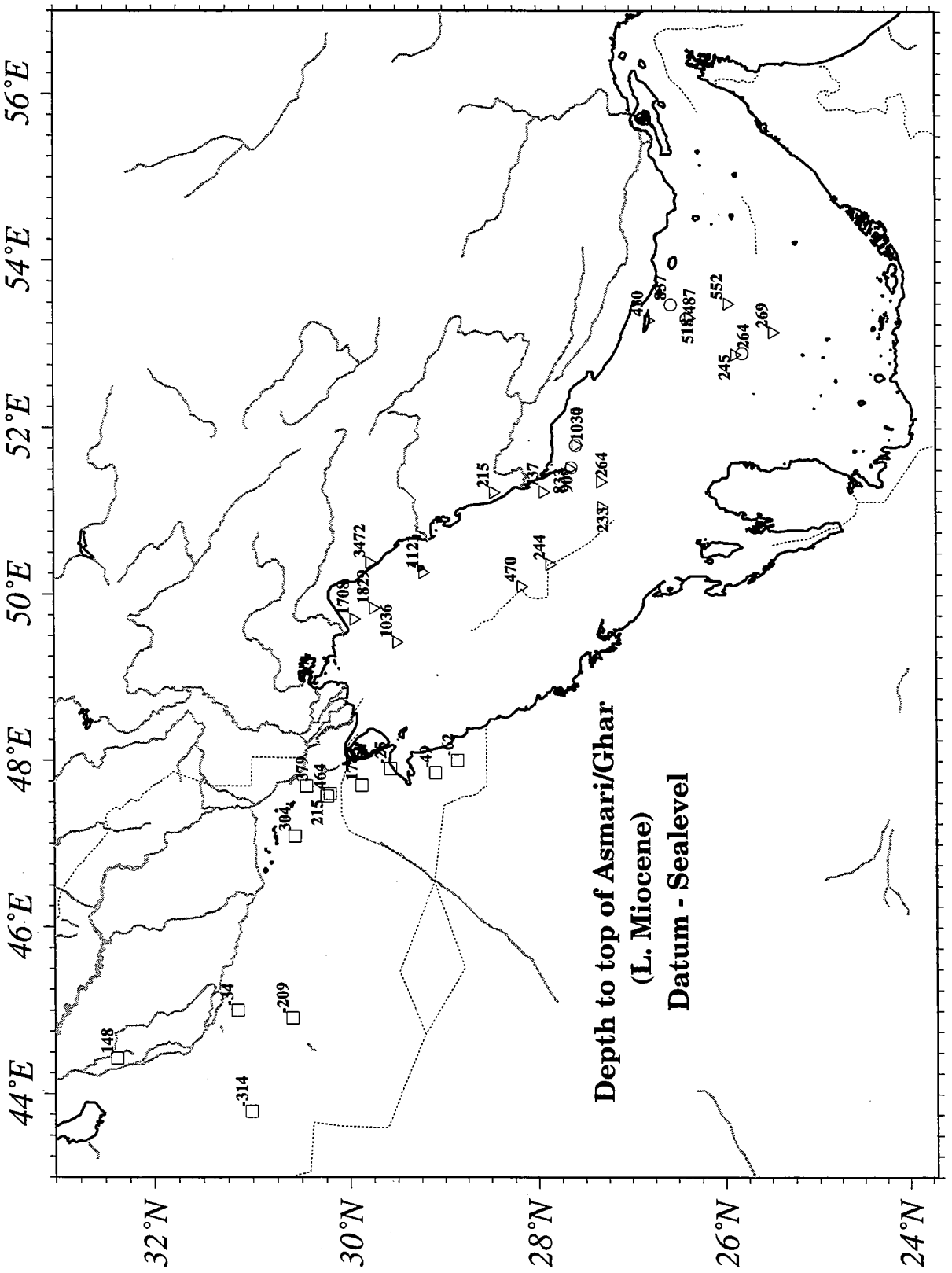

Figure 18. Depth (meters) below sealevel to the top of the Asmari/Ghar formations (lower Miocene) increases to the northeast. Local variations in depth are due to effects of very recent folding near Iran and, probably, to point sources of sediment at the mouths of rivers draining the Zagros Mountains. Negative values indicate that the surface is above sealevel. Symbols as in Figure 11.

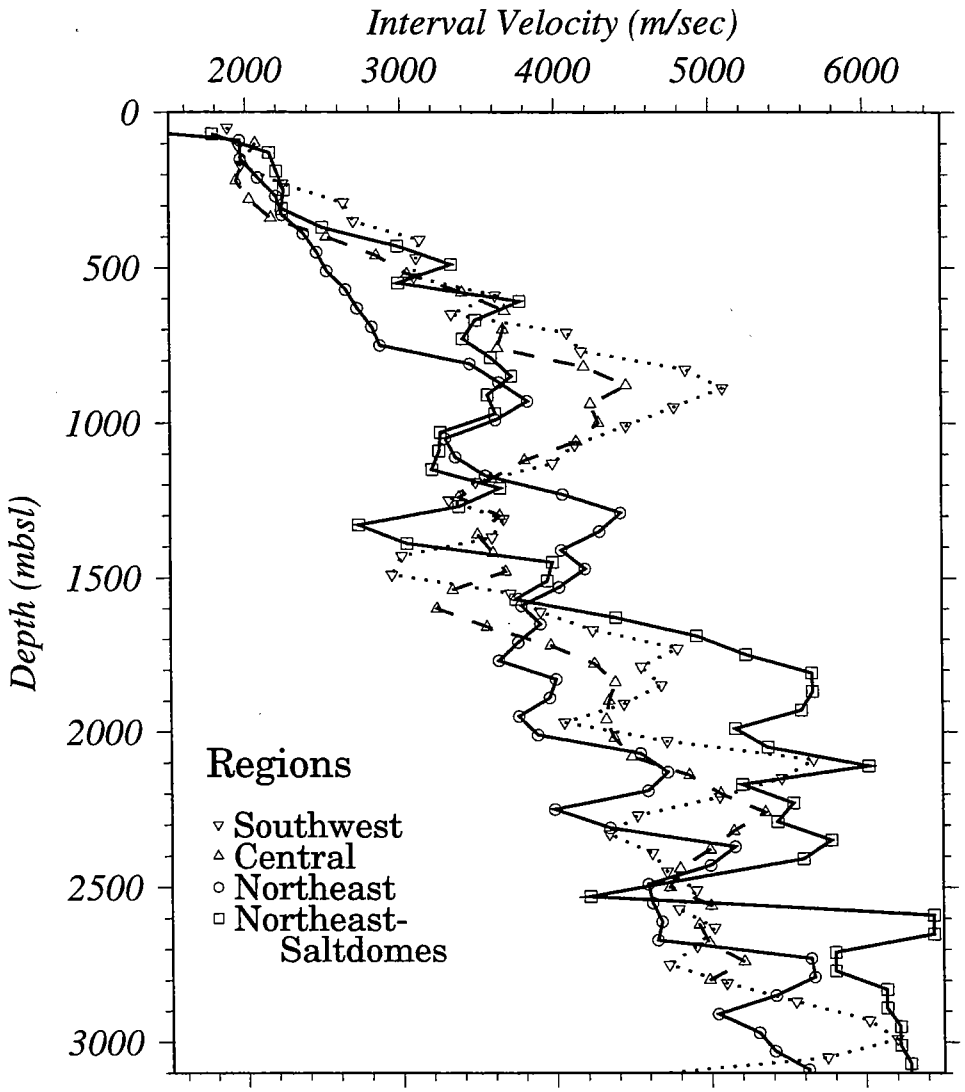

Figure 19. Interval velocities obtained by averaging all the sonic logs in each of the three regions indicate that the vertical velocity gradient in the upper 0.8-1.0 km increases southwestward from Iran towards Arabia. Below about 1 km depth, the velocities in the different regions do not show distinctive trends.